IMAGING ANALYSIS IN RHEUMATOID ARTHRITIS PATIENTS

PERIPHERAL QUANTITATIVE COMPUTED TOMOGRAPHY-DERIVED BONE OUTCOMES AND RELIABILITY IN RHEUMATOID ARTHRITIS PATIENTS AND CONTROLS

BY JESSICA Y. AMIN, B.Sc. (Hons)

A Thesis Submitted to the School of Graduate Studies in Partial Fulfilment of the Requirements for the Degree Master of Science

McMaster University MASTER of SCIENCE (2020)
Faculty of Health Sciences (Medical Sciences)
Hamilton, Ontario

TITLE: Peripheral Quantitative Computed Tomography-Derived Bone Outcomes and Reliability in Rheumatoid Arthritis Patients and Controls

AUTHOR: Jessica Y. Amin, B. Sc. (Hons) (McMaster University)

SUPERVISORS: Dr. Maggie J. Larché MD PhD and Dr. Karen Beattie PhD

NUMBER OF PAGES: xii, 146

Lay abstract

Rheumatoid arthritis (RA) affects joints in the hands and feet. The bones of these joints are affected by periarticular bone loss leading to bone erosions. Magnetic resonance imaging (MRI) and X-ray are used to visualize erosions. Since erosions are characterized by a decrease in bone mineral density (BMD) leading to holes in the bone, we tested the reliability of a peripheral quantitative computed tomography (pQCT) scanner, to measure volumetric BMD (vBMD) in 25 RA patients and compared vBMD to healthy controls. The vBMD measures appeared lower in RA patients than healthy individuals in some joints. As well, there was agreement between bone erosions detected by MRI and reduced vBMD measured by pQCT. Although we could not monitor the change over time, we are hopeful that this scanner will be able to better characterize RA disease activity, with vBMD as a surrogate marker for erosion presence.

Abstract

Introduction

Rheumatoid arthritis (RA) is an inflammatory autoimmune disease that affects the feet in up to 90% of patients, and can result in bone erosions. Little is known about disease activity at the metatarsophalangeal joints (MTPJs). Magnetic resonance imaging is used to visualize erosions, but does not provide quantification. Quantitative computed tomography (QCT) allows for differentiation between bone layers and quantifies volumetric bone mineral density (vBMD). We used a peripheral QCT (pQCT) scanner in MTPJs 2-5 in RA patients to determine reliability of a pQCT protocol, and then we determined the variability in vBMD between RA patients and controls.

Methods

Patients (n=25) diagnosed with RA (2010 ACR criteria) were recruited from an academic Rheumatology clinic. Controls (n=27) were also recruited and matched for sex, age and ethnicity. Baseline MR data demonstrated that 80%, 64%, 40% and 20% of patients had erosions at MTPJs 2-5, respectively. One year later, MTPJs 2-5 were scanned using pQCT (XCT 2000); 2 transaxial slices were acquired per joint. A trained pQCT operator acquired 2 scans per participant with repositioning. Test-retest, intra- and inter-rater reliability were assessed blindly for total and cortical subcortical densities (mg/cm^3). Reliability was reported as root mean square coefficients of variation (%RMSCV) and RMS standard deviation (RMSSD).

Results

The mean (SD) age and disease duration were 57.8 (10.2) years and 5.0 (0.9) years, respectively. Test-retest reliability was better for MTPJs 2 and 3, than MTPJs 4 and 5. Inter- and intra-rater reliability demonstrated high reproducibility. Total and cortical subcortical vBMD appeared lower in RA patients than controls.

Conclusion

We have reliably determined vBMD using pQCT in MTPJs 2 and 3 in RA patients. The lower vBMD in MTPJ 3 suggests that RA patients may have true erosions at this joint. This research is in the early phases, but we hope to explore the correspondence between pQCT and other RA assessment tools.

Acknowledgements

I would like to start by thanking my supervisors, Dr. Maggie Larché and Dr. Karen Beattie, for the opportunity to embark on this research project – I will always be grateful for the lessons that I have learned during this time. Both have helped me achieve independence and helped me gain confidence in my work. Dr. Larché has taught me to think critically and cheered me on for my achievements. Dr. Beattie has always listened, taught me how to communicate my ideas clearly, and provided advice during the challenging times. It has been an absolute pleasure working with both of them, and I am indebted to them for their mentorship, guidance and support.

As well, I'd like to thank Dr. George Ioannidis for his statistics expertise and analysis advice during the course of my Master's. I would also like to thank Dr. Andy Kin On Wong and Dr. Chris Gordon for their continued support in helping me with the pQCT scanner, from helping me learn how to use the scanner to teaching me the analysis methods. This Masters would not have been possible without them.

As well, thank you to Barbara Baker for her help with research ethics and patient recruitment, she has taught me so much about executing a clinical study. Thank you to Christine Fyfe for performing all the MR scans, Hannah Zou for helping me familiarize with the project, Shannon Reitsma for answering my pQCT questions, and Aarabi Thayaparan for her help in pQCT rater analysis.

Lastly, I'd like to express my utmost gratitude to my parents and my brother, Justin, for their unconditional encouragement and support throughout this Masters. They have helped me get through some of the more challenging days of data analysis and thesis writing. In fact, they believed in me at times when I didn't even believe in myself. Part of this degree is theirs because I couldn't have done it without them.

- Jessica Amin

Table of Contents

List of Figures

List of Tables

List of Abbreviations

%RMSCV: root mean square coefficients of variations
µSv: microSieverts
κ: Cohen's kappa
aBMD: areal bone mineral density
ACPA: anti-citrullinated protein antibody
ACR/EULAR: American College of Rheumatology/European League Against Rheumatism
BMC: bone mineral content
BMD: bone mineral density
BME: bone marrow edema
CCP: cyclic citrullinated peptides
CDAI: clinical disease activity index
CM: contour mode
CR: conventional radiography
CRP: C-reactive protein
CT: computed tomography
CTLA: cytotoxic T-lymphocyte antigen
DAS28: disease activity score 28
DMARDs: disease modifying anti-rheumatic drugs
DXA: dual energy X-ray absorptiometry
EDGA: evaluator disease global assessment
ELISA: enzyme-linked immunosorbent assay
ESR: erythrocyte sedimentation rate
FOV: field of view
GSUS: grayscale ultrasound
HA: hydroxyapatite
HAQ-DI: Health Assessment Questionnaire-disability index
HAQ: Health Assessment Questionnaire
HLA: human leukocyte antigen
HR-pQCT: high resolution peripheral quantitative computed tomography
IFNγ: interferon gamma
Ig: immunoglobulin
IL-1Ra: interleukin-1 receptor antagonist
IL: interleukin
JAK: Janus kinase
LFIS: Leeds Foot Impact Scale
MC: metacarpal
MCPJs: metacarpophalangeal joints
MRI: magnetic resonance imaging
mSv: milliSieverts
MT: metatarsal
MTPJs: metatarsophalangeal joints
MTX: methotrexate
NK: natural killer
NSAIDs: nonsteroidal anti-inflammatory drugs
PDGA: patient's disease global assessment
PD: power Doppler
PIPJs: proximal interphalangeal joints
PM: peel mode
pQCT: peripheral quantitative computed tomography
Q1-4: quadrant 1-4
RA: rheumatoid arthritis
RAMRIS: rheumatoid arthritis magnetic resonance imaging scoring system
RANKL: receptor activator of NF-kappa B ligand
RF: rheumatoid factor
RMSSD: root mean square standard deviation
ROI: region of interest
SJC: swollen joint count
ST: synovial thickening
TGFβ: transforming growth factor beta
TJC: tender joint count
TLRs: toll-like receptors
TNFα: tumour necrosis factor alpha
TR: repetition time
Treg: regulatory T-cells
US: ultrasound
VAS: visual analogue scale
vBMD: volumetric bone mineral density
VEGF: vascular endothelial growth factor
WHO: World Health Organization

Declaration of Academic Achievement

My supervisor, Dr. Maggie Larché, designed the foot imaging study. The pQCT scan protocol was designed by Dr. Andy Kin On Wong and me. The pQCT analysis protocol was designed by Dr. Chris Gordon and me. I performed all pQCT scans and analyzed all pQCT data acquired from January 2019 to October 2019; Aarabi Thayaparan assisted in inter-rater analysis (January 2020). I, Jessica Amin, declare that the data presented in this thesis is my own work. Dr. Maggie Larché and Dr. Karen Beattie have provided me with guidance and suggestions on analysis methods. The results from part of this project have previously been presented at research gatherings.

Chapter 1.0: Introduction

1.1 Rheumatoid Arthritis Disease Overview

Rheumatoid arthritis (RA) is a chronic inflammatory, autoimmune disease that affects the small joints of the body, with extreme cases resulting in disability (suboptimal physical function), reduced quality of life and premature death (Aletaha *et al.*, 2010; Rowbotham and Grainger, 2011; Vyas *et al.*, 2016; Malm *et al.*, 2017). The most common clinical features of RA include swollen joints, morning stiffness and myalgia (pain in a group of muscles) (Vyas *et al.*, 2016). The synovial membrane of patients with RA is characterized by swelling, increased vascularity as well as an increase in inflammatory cells (Choy and Panayi, 2001). The disease manifests as chronic inflammation in the synovial joints, bone erosion and joint damage (Yang *et al.*, 2017). RA involves both periarticular and generalized bone loss (Zhu *et al.*, 2012). Patients initially present with periarticular osteopenia near the affected joints, which may then develop structural erosions that can be potentially irreversible (Yang *et al.*, 2017). Periarticular bone loss is associated with the elevation of proinflammatory cytokines such as tumour necrosis factor alpha (TNFα), interleukin (IL) 6 and 1β in the synovium (Fouque-Aubert *et al.*, 2010). Extra-articular features of RA include rheumatoid lung, rheumatoid nodules, keratoconjunctivitis sicca (dryness in the conjunctiva (membrane that lines inner part of the eyelid) and cornea), uveitis (inflammation in uvea), and rheumatoid pericarditis (inflammation of heart membrane) and vasculitis (inflammation of small blood vessels) (Mateen *et al.*, 2016).

Autoantibody indicators in blood, such as rheumatoid factor (RF) and anti-citrullinated protein antibody (ACPA) may be present before RA symptoms appear (Aletaha *et al.*, 2010). Although ACPA has a high specificity and predictive value for RA, it is present in <60% of patients (Majithia and Geraci, 2007).

Genetic studies have shown a strong link between RA and major-histocompatibility complex II antigens human leukocyte antigen (HLA)-DR4 alleles (Choy and Panayi, 2001; Mateen *et al.*, 2016; Firestein and Mcinnes, 2017). The epitope sequence associated with the disease is usually glutamine-leucine-arginine-alanine-alanine, which is present in DR4, DR14 and DR1β chains (Mateen *et al.*, 2016; Firestein and Mcinnes, 2017). Interestingly, a susceptibility epitope was determined in amino acids 70-74 in the third hypervariable region of the DRβ chain (Firestein and Mcinnes, 2017). The epitope primarily faces away from the antigen binding groove that binds processed peptides (Firestein and Mcinnes, 2017). The main role of the HLA class II molecules is to present antigenic peptides to CD4+ T cells (Choy and Panayi, 2001; Firestein and Mcinnes, 2017). More recent research has identified more amino acids at the base of the antigen binding site, which may contribute to the specificity of antigen binding, specifically at amino acid 11 with leucine and alanine variants (Firestein and Mcinnes, 2017). Additionally, past studies have shown that the presence of serine at amino acid 11 reduces the risk of RA (Firestein and Mcinnes, 2017). Thus, variations in amino acids deep within the binding cleft are contributing factors to disease.

1.1.1 Pathophysiology of RA

Established cases of RA lead to progressive structural joint damage. Radiographic imaging of joint space loss and erosions have been used as a surrogate marker for joint damage (Goldring, 2003). Currently, many disease modifying anti-rheumatic drugs (DMARDs) and biologics slow the progression of joint damage in RA patients (Goldring, 2003). These drugs target IL-1 and TNFα, thus providing evidence that these immune markers are involved in joint destruction and inflammatory processes (Goldring, 2003).

1.1.1.1 Bone Physiology

Bone tissue is composed of three main parts: mineral, organic matrix and water (Manhard *et al.*, 2017). The mineral crystals of bone are bound to protein (Department of Health and Human Services, 2004). Specifically, the crystals are composed of calcium, phosphate, and carbonate and hydroxyl substitutions, forming hydroxyapatite (HA) (Department of Health and Human Services, 2004; Manhard *et al.*, 2017). This part of the bone gives it its' strength and stiffness (Manhard *et al.*, 2017). The organic matrix is composed of type 1 collagen, noncollagenous proteins and fats; this part of the bone is important for malleability and flexibility (Manhard *et al.*, 2017). Lastly, the water resides in the porous parts of the bone and is attached to the matrix (Manhard *et al.*, 2017).

The outer dense layer of bone is called cortical bone and accounts for three quarters of an individuals' total skeletal mass (Department of Health and Human Services, 2004). This tough exterior layer is important for strength, protection, and a site of attachment for tendons and muscles (Department of Health and Human Services, 2004). The inner porous component of bone is called trabecular bone. This network of

rods and plates is essential for mineral exchange and provides integrity at weight-bearing sites (Department of Health and Human Services, 2004).

Bone remodeling continuously occurs during an individuals' life. This process is important for replacing damaged bone and brittle older bone (Department of Health and Human Services, 2004). Physiological bone remodeling is initiated by the cells that line the trabecular bone surface (Goldring, 2003). These osteoblast originated cells as well as cells from the bone marrow stroma receive hormonal and cytokine signals that start the cycle of bone remodeling (Goldring, 2003). After activation, these cells release other cytokines and chemokines that play a role in recruitment and induction of osteoclasts. Osteoclasts are the main type of cell involved in bone resorption (Goldring, 2003). Bone resorption is important for providing calcium and phosphorus when these minerals are deficient in the body (Department of Health and Human Services, 2004). In addition, cells from the bone lining are important as they prepare the bone surface to recognize osteoclast precursor cells (Goldring, 2003). Upon completion of the resorption process, the bone surface is occupied by osteoblasts or preosteoblasts (these differentiate into mature osteoblasts) (Goldring, 2003). Bone matrix is laid down and then mineralized to produce a new bone surface (Goldring, 2003). After completion of the cycle, osteoclasts and osteoblasts apoptose (Goldring, 2003). The dynamic balance between the amount of bone removed during resorption and the bone placed down during formation allows for adaptation to the changing environment and repair to microdamage (Goldring, 2003).

Imbalances in the bone remodeling system can lead to bone disease (Department of Health and Human Services, 2004). In RA, bone resorption is increased resulting in

loss of cortical and adjacent trabecular bone, and osteoblastic activity in the osteitis is suppressed preventing repair of bone (Geusens and van den Bergh, 2014). The increased osteoclastic activity induced by autoantibodies and proinflammatory cytokines results in periarticular bone erosion (cortical disruptions), loss of bone mineral density (BMD) and damage to the microstructure (Fig. 1) (Peters *et al.*, 2019). Note that erosions are different

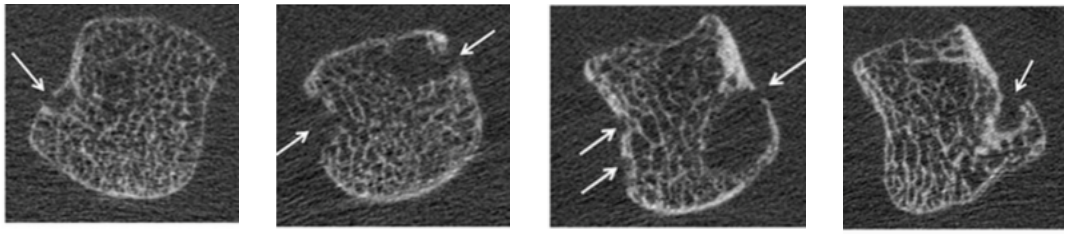

Figure 1. Examples of cortical interruptions as seen on HR-pQCT in the MCPJs of RA patients (white arrows) (Peters et al., 2019).

from bone cysts, which are regions of bone disappearance (osteolysis) in the trabecular bone, but no destruction in the cortical layer (Schett and Gravallese, 2012).

Many published imaging studies utilize cadavers to analyze bone structure and develop protocols. However, there have been controversies regarding how transferable the physiological conditions in cadavers are to living organisms as cadavers may not replicate the dynamic balance between bone formation and resorption as live humans do (Kushdilian *et al.*, 2016). In addition, when originally made, certain modalities such as pQCT were meant for measuring BMD in living bone (Chirchir, 2016). Some researchers have looked into the effects of freezing cadavers and have found a 10% reduction in stiffness in trabecular bone, likely due to the expansion of interstitial fluids (Topp *et al.*, 2012). Others have demonstrated that formalin and formaldehyde embalmed bones may be more brittle and have reduced strength, respectively (Topp *et al.*, 2012). Regardless,

studies have shown stable bone mineral content measures in cadavers, made of 62-65% of dry bone weight; dry bone weight is valid for use as the mineral density is still high (Chirchir, 2016). Thus, it can be concluded that cadaveric bone has the potential to be a model for density measures.

Bone erosions are specific to RA patients, demonstrating the severity of disease activity (Fouque-Aubert *et al.*, 2010). The erosive changes imply that there is an imbalance between the resorption and formation processes, leading to progressive articular bone loss (Goldring, 2003). Erosions generally appear within two years of disease onset, but may continue to develop over the next decade (Fouque-Aubert *et al.*, 2010).

1.1.1.2 Inflammation Processes

Inflammatory arthritis is induced by autoimmune inflammation in joints and can present as spondylo-arthropathies (psoriatic arthritis, reactive arthritis, ankylosing spondylitis) or RA; RA is the most common form (Ledingham *et al.*, 2017). Inflammatory arthritis is diagnosed with the presence of morning stiffness (lasting more than 1 hour), joint pain, and warm, swelling joints (Ledingham *et al.*, 2017). Blood tests which include inflammatory markers (ESR, CRP) and RF also need to be performed in order to confirm suspicions of autoimmunity (Ledingham *et al.*, 2017). However, negative blood results do not necessarily indicate that an individual does not have RA (Ledingham *et al.*, 2017).

1.1.1.2.1 Blood Markers

Serological Indicators

Rheumatoid factor (RF) is an autoantibody. RFs are a class of immunoglobulins (IgM, IgG or IgA) (Ingegnoli *et al.*, 2013). The CH2 and CH3 domains of the Fc segment on the IgG antibody are recognized by RF (Egerer *et al.*, 2009). Rheumatoid factor can be detected by the following standardized methods: enzyme-linked immunosorbent assay (ELISA) and nephelometry (Egerer *et al.*, 2009). Patients who are positive for this factor are considered to have seropositive RA. Rheumatoid factors are not specific to RA patients and can be found in patients with other autoimmune and non-autoimmune diseases, and healthy individuals (normal range: ≤14 U/ml) (Yazdani-Biuki *et al.*, 2005; Ingegnoli *et al.*, 2013).

Anti-citrullinated protein antibodies are an important serological indicator for RA specific disease activity, as normal uninflamed synovium does not have high levels of citrullinated proteins (Szekanecz *et al.*, 2008). Anti-citrullinated protein antibody levels are determined based on their reactivity to cyclic citrullinated peptides (CCP) (van der Woude *et al.*, 2010). Citrullination occurs through an enzymatic process of deaminating the arginine residues, producing a citrulline residue (Egerer *et al.*, 2009). Protein citrullination is a posttranslational modification that results in a change in the charge of the protein (positive amino group is hydrolyzed to a neutral oxygen group), ultimately altering the 3D structure of the protein (van Venrooij *et al.*, 2002; Egerer *et al.*, 2009). The physiological implications of citrullination are a change in cell differentiation and apoptosis (Egerer *et al.*, 2009).

Acute Phase Reactants

C-reactive protein (CRP) is a part of the pentraxin protein family, which has a structure of five 23-kDa subunits, and causes precipitation in the serum (Litao and Kamat, 2014; Kim *et al.*, 2015). C-reactive protein levels can increase 1000 fold or more as a result of infection, inflammation and tissue damage, and is stimulated by IL-6, IL-1β and TNF-α in hepatocytes (Kim *et al.*, 2015). C-reactive proteins remove harmful microorganisms and damaged cells through a complement cascade system, which increases the phagocytic action of neutrophils (Kim *et al.*, 2015). Additionally, it plays a role in inflammation by stimulating the production of proinflammatory cytokines (Kim, 2015). The clinical implications of elevated CRP have been linked to morning stiffness, pain, fatigue and disability (Kim *et al.*, 2015).

Erythrocyte sedimentation rate (ESR) measures the height of red blood cells that settle in a tube of anticoagulated blood in a given time unit (usually an hour) with a quick and inexpensive lab test (Brigden, 1998). The two factors that impact this measurement are the level of red blood cell aggregation and hematocrit levels (Brigden, 1998). The aggregation of red blood cells is dependent on plasma proteins, which decrease the negative electrostatic forces between the cells (Brigden, 1998). This results in aggregation and faster sedimentation (Brigden, 1998). Reduced levels of hematocrit cause the red blood cell aggregates to fall faster, therefore increasing sedimentation rate (Brigden, 1998). Patients with inflammation have higher ESR levels due to the high levels of fibrinogen and stacking of erythrocytes (Litao and Kamat, 2014). In RA, ESR levels can reflect an individuals' morning stiffness and fatigue (Brigden, 1998).

1.1.1.2.2 Inflammatory Markers/Cytokines

Rheumatoid arthritis is characterized by consistent inflammation in the synovitis, with the majority of disease activity in the peripheral joints. B-cells play a crucial role in the pathogenesis of RA and this is evident through reduced symptoms in patients who take pharmacological treatments that target the reduction of B-cells, such as rituximab (anti-CD20 antibody) (Mateen *et al.*, 2016). The following are contributing factors of B-cells to RA disease activity: produce RF (autoantibodies to IgG), secrete proinflammatory cytokines (TNF-α, IL-6), activate T-cells, antigen presentation, respond to chemokines, and assist in forming TNF-α which results in activation of macrophages (Mateen *et al.*, 2016).

Activated B-cells, macrophages, dendritic cells (antigen presenting cells) present RA specific antigens to T-cells. This results in activation of innate immune cells, B-cell activation, osteoclast activation, and secretion of cytokines that are associated with synovial tissue inflammation (Mateen *et al.*, 2016). CD4+ T-cells are prominently found near HLA-DR+ dendritic cells and macrophages, and differentiate into Th1-like effector cells (Mateen *et al.*, 2016). Th1-like effector cells stimulate production of pro-inflammatory cytokines (e.g. IFNγ and TNF-α) (Mateen *et al.*, 2016). CD4+ T-cells differentiate into fewer Th2-like effector cells, which produce anti-inflammatory cytokines (e.g. IL-4, IL-10, IL-13) (Mateen *et al.*, 2016). Th17 cells, another class of CD4+ T-cells, play an important role in synovial inflammation and bone erosions via production of IL-17 and IL-23 (Mateen *et al.*, 2016). Regulatory T-cells (Treg) have inhibitory effects by releasing inhibitory cytokines (e.g. TGFβ and IL-10) and expressing

cytotoxic T-lymphocyte antigen 4 (CTLA-4) to inhibit immune activation (Mateen *et al.*, 2016). CTLA-4 competitively binds to co-stimulatory ligands on T-cells (Mateen *et al.*, 2016). In RA, Treg cells are reduced and Th17 thrive, leading to inflammation (Mateen *et al.*, 2016).

Cytokines play an important role for a functioning body; they are responsible for cell growth, proliferation, differentiation, inflammation, tissue repair, activation status and maintenance of immune responses (Mcinnes *et al.*, 2015; Mateen *et al.*, 2016). They are also involved in the pathogenesis of RA, as they play a role in inflammation and joint damage. Rheumatoid arthritis is characterized by the imbalance between dominating pro-inflammatory cytokines over anti-inflammatory cytokines. (Mateen *et al.*, 2016) The pathophysiology of RA involves many cytokines. For the purposes of this report, the emphasis has been placed on cytokines that appear most frequently in the literature and those that can be targeted with medication.

TNF-α

Tumour necrosis factor plays a role in white blood cell activation, adhesion, migration, endothelial cell activation and programmed cell death, chemokine expression, and osteoclast activation and function (Mcinnes *et al.*, 2015). Tumour necrosis factor-α is one of the main cytokines involved in the inflammation process of RA and is present in elevated amounts in the serum of RA patients. It is produced by macrophages, monocytes, fibroblasts, mast cells and natural killer (NK) cells (Mateen *et al.*, 2016). It has two receptors: TNF-R1 (also known as 55-KD receptor/p55) and TNF-RII (also known as 75-KD receptor/p75) (Mateen *et al.*, 2016). TNF-R1 is present in most tissues and can bind

to membrane bound TNF and soluble forms of TNF, whereas TNF-RII expression is specific to immune cells and can only interact with membrane-bound TNF (Mateen *et al.*, 2016). Tumour necrosis factor-α induces the proliferation and differentiation of B-cells, T-cells and NK cells, as well as production of pro-inflammatory cytokines (e.g. IL-1, IL-6, IL-8) (Mateen *et al.*, 2016).

IL-1

The IL-1 cytokine family primarily consists of the following: IL-1α, IL-1β, IL-18 and IL-33 (Mcinnes *et al.*, 2015; Mateen *et al.*, 2016). IL-1α is expressed on cell surfaces whereas IL-1β elicits its effects by acting on other cells. IL-1 receptor antagonist (IL-1Ra), an endogenous inhibitor, can be used to inhibit the effects of IL-1α and IL-1β. There are two categories of IL-1 receptors: IL-1R1 and IL-1RII (Mateen *et al.*, 2016). The interaction between IL-1 and IL-1RII results in an intracellular signal transduction, which can be enhanced with the IL-1R-AcP accessory protein. On the other hand, binding of IL-1 to IL-1RII results in no signal transduction due to a short cytoplasmic domain (Mateen *et al.*, 2016). In RA patients, there is a discrepancy in the homeostatic levels of IL-1 receptor antagonist and IL-1. There are elevated levels of IL-1β in both plasma and synovial fluid (Mateen *et al.*, 2016).

IL-6

IL-6 is another important cytokine in RA and is targeted by some therapeutics. It is a 22-29 KD glycoprotein which participates in both proinflammation and antiinflammation. It can be produced by B-cells, T-cells, fibroblasts, endothelial cells, monocytes, macrophages, keratinocytes, chondrocytes and some tumour cells (Mateen *et*

al., 2016). The IL-6 receptor has two chains: IL-6 specific receptor (IL-6Ra) and a signal transducer (gp130). In the signaling pathway, IL-6 binds to the receptor, and interacts with gp120 to stimulate downstream activation of cells using Janus Kinase (Mateen *et al.*, 2016). There are higher levels of IL-6 in the blood and synovial fluid of RA patients. It has further implications in acting on neutrophils which release reactive oxygen intermediates and proteases (Mateen *et al.*, 2016). In addition, IL-6 induces osteoclast differentiation using a receptor activator of NF-kappa B ligand (RANKL) pathway or RANKL independent pathway. As well, it can act synergistically with IL-1β and TNF-α to produce vascular endothelial growth factor (VEGF) which plays a role in development of the pannus (Mateen *et al.*, 2016).

1.2 Epidemiology

Approximately 1% of Canadians are affected by RA, with rising incidences in the aging population (Statistics Canada, 2006). The age of peak disease incidence is 50 years, affecting women 3-4 times more than men (Egerer *et al.*, 2009; Mateen *et al.*, 2016). The foot is often affected early on with a prevalence of up to 90% in the metatarsophalangeal joints (MTPJs), while 15% have initial disease manifestation in the forefoot (Muradin and van der Heide, 2016). Based on conventional radiography, early erosive changes are more commonly found in the feet, however, from 3 years and on, both hands and feet are equally affected (Otter *et al.*, 2010; Colebatch *et al.*, 2013; Wilson *et al.*, 2017).

About 80% of patients have reduced functionality within 2 decades of disease onset (Statistics Canada, 2006). Abnormalities such as atrophy, claw toes and dislocation

of the plantar fascia lead to deformities (Muradin and van der Heide, 2016). The number of Ontarians suffering from RA has doubled in the period between 1996 and 2010 (Towheed *et al.*, 2016). The crude number of individuals diagnosed with RA has increased from 5,523 in 1996 to 6,395 in 2010 (Widdifield, Bernatsky, Bombardier, *et al.*, 2015). After standardization of age and gender, the prevalence of RA has steadily increased from 473 per 100,000 in 1996 to 784 per 100,000 in 2010 (Widdifield, Bernatsky, Bombardier, *et al.*, 2015). The annual cost of disease, while considering direct (e.g. medications) and indirect costs (e.g. time lost from paid work), was previously reported to be $9300 for RA patients living in Ontario (Maetzel *et al.*, 2004). Although new interventions have advanced management of RA, there are still 40-50% more deaths in individuals with RA in comparison to the general population (Widdifield, Bernatsky, Paterson, *et al.*, 2015). To add to the problem, RA is associated with increased risk of co-morbidities such as cardiovascular disease, metabolic syndrome, psychiatric disease and certain cancers (Firestein and Mcinnes, 2017). These diseases are attributed to the elevated levels of circulating cytokines and immune molecules (Firestein and Mcinnes, 2017).

1.3 Diagnosis and Criteria for Diagnosis

RA initially presents with polyarthritis, accompanied by pain, swelling and stiffness in a bilateral and symmetrical manner (Majithia and Geraci, 2007). The most commonly involved joints in RA are the metacarpophalangeal joints (MCPJs), proximal interphalangeal joints (PIPJs), wrist and metatarsophalangeal joints (MTPJs) (Majithia

and Geraci, 2007). Preliminary blood tests should include a complete blood cell count with differential RF, and ESR/CRP (Majithia and Geraci, 2007). In addition, baseline renal and hepatic function should be tested to assist in determination of appropriate medication. The American College of Rheumatology (ACR) criteria assists in diagnosis, although does not always provide a definite diagnosis, thus it is suggested that it is used in combination with other available information about the patient (Majithia and Geraci, 2007).

The two initial questions by a primary care physician are: 1. Is diagnosis of RA likely? 2. Does the patient need early treatment or a referral to a rheumatologist? (Majithia and Geraci, 2007). Some of the findings leading to these questions are joint swelling in 3 or more joints, a positive squeeze test (pain while squeezing joints) in the metacarpal (MC) or metatarsal (MT) joints, morning stiffness for more than 30 minutes and increased blood markers (ESR, CRP, RF) (Majithia and Geraci, 2007). Patients are referred to a rheumatologist when the diagnosis is unclear or more than 5 joints are involved in symptoms, or they have unusual laboratory findings (Majithia and Geraci, 2007).

The 2010 ACR/European League Against Rheumatism (ACR/EULAR) classification criteria (*Appendix A1*) is used for patients where clinical swelling is detected in at least 1 joint and for those who do not have another diagnosis (e.g. gout, psoriatic arthritis) (Kay and Upchurch, 2015). There are four main criteria that patients are evaluated on: joint involvement, serology (RF and ACPA), acute-phase reactants (CRP and ESR), and duration of symptoms. A score greater than or equal to 6 classifies

an individual as having RA (Kay and Upchurch, 2015). The amendment of the classification criteria from the 1987 ARA RA classification criteria was to ensure early diagnosis in order to initiate early therapy to reduce the occurrence of structural damage (Kay and Upchurch, 2015). The newer criteria includes circulating ACPAs as well as the higher levels of the serological biomarkers in the overall score (Kay and Upchurch, 2015).

Patients are monitored every 2-3 months for assessment of disease activity, extra-articular manifestations, side effects and overall functionality (Majithia and Geraci, 2007). In addition, yearly hand and foot X-rays are recommended (Majithia and Geraci, 2007).

1.3.1 Measures of Disease Activity

1.3.1.1 Disease Activity Score (DAS)

Disease Activity Score (DAS) and the newer DAS28 are clinical measures that can be used to determine an RA patient's disease activity and progression. Disease Activity Score was first developed in the early 1990s and included the following measures: 44 swollen joint count, ESR levels and patient global assessment on a visual analogue scale (VAS, values from 0 [best]-100 [worst] mm) (Porter *et al.*, 2011). The adjusted DAS28 includes the following: swollen and tender joint count (scored from 0-1; 0 indicates no swelling/tenderness, 1 indicates presence of swelling/tenderness), patient's evaluation of their disease activity (VAS) and ESR levels (Porter *et al.*, 2011). This new version was created to save time and for convenience, and has proven to be valid (Porter

et al., 2011). It can be calculated using the following formula: $DAS28 = 0.56 * \sqrt{TJC28} + 0.28 * \sqrt{SJC28} + 0.70 * \ln(ESR) + 0.014 * (general\ health)$ (Singh *et al.*, 2011; van Riel and Renskers, 2016). The DAS28 score is a continuous variable, that can range from 0 to 9.4; scores >5.1 indicate high disease activity, scores between 3.2 and 5.1 indicate moderate activity, scores <3.2 indicate low disease activity, and scores <2.6 indicate remission (Porter *et al.*, 2011; Singh *et al.*, 2011). The newest DAS28 includes CRP levels rather than ESR levels, although this method is not as well validated as the DAS28-ESR method (Porter *et al.*, 2011).

1.3.1.2 Clinical Disease Activity Index (CDAI)

The Clinical Disease Activity Index (CDAI) is a measure of disease activity that does not account for any acute phase reactants. It accounts for the total swollen and tender joint count (SJC and TJC) from 28 joints, and patient and physician global assessments on the VAS scale (PDGA and EDGA, respectively; 0-10 cm). The CDAI score can range from 0-76. This method is beneficial in clinical settings as it does not require data from acute phase reactants or complex calculations, while easily providing an approximation of the patient's disease state. The CDAI can be calculated using the following formula: $CDAI = TJC + SJC + PDGA + EDGA$ (Singh *et al.*, 2011). Interpretation of CDAI scores are as follows: scores >22 indicate high disease activity, scores between 10 and 22 indicate moderate disease activity, scores <10 indicate low disease activity, and scores <2.8 indicate remission (Singh *et al.*, 2011).

1.3.1.3 Self-Reported Measures of Disease Activity

Leeds Foot Impact Scale (LFIS)

The Leeds Foot Impact Scale (LFIS) was developed in order to better detect the status of the foot in patients with RA. The questionnaire includes two subscales and a total of 51 statements. The first subscale involves questions regarding impairment/shoes (21 items) such as "*My feet hurt me"* and "*I can't get any shoes on"*. The second subscale includes items regarding activities/participation (30 items) such as "*I can't run"* and "*I feel I slow other people down"*. Each item can be given a score of 0 (not true) or 1 (true). The two subscale scores are then added for a total LFIS score, where the maximum score can be 51. (Helliwell *et al.*, 2005)

Health Assessment Questionnaire (HAQ)

The Health Assessment Questionnaire (HAQ) is a patient reported outcomes evaluation. The original full HAQ consists of five sections: disability, pain, medication effects, costs of care, and mortality (Bruce and Fries, 2005). The shorter version (2-page HAQ) only includes the HAQ-disability index (HAQ-DI), patient global VAS and the pain VAS (Bruce and Fries, 2003, 2005; Gonzalez and Gottlieb, 2016). The HAQ-DI measures a patient's overall functionality with questions regarding fine motor skills/locomotor activity in the upper and lower extremities (Bruce and Fries, 2005). A standard scoring system is implemented for any aids or devices that are used while performing tasks (Bruce and Fries, 2005). There is a total of 21 items divided into 8 categories (dressing and grooming, arising, eating, walking, hygiene, reach, grip, activities) (Gonzalez and Gottlieb, 2016). Each category has sub-category questions. Each

item can be scored from 0 to 3, with a higher value indicating greater disability (0=without any difficulty, 1=with some difficulty, 2=with much difficulty, and 3=unable to do) (Bruce and Fries, 2005; Voshaar *et al.*, 2015). Once completed, the highest sub-category value is taken to determine the overall value for that category (Bruce and Fries, 2005). If aids/devices are used, scores of 0 or 1 are increased to 2 (scores that are already at 3 remain the same) (Bruce and Fries, 2005). The categorical scores are then averaged for an overall HAQ-DI score which can range from 0 to 3 (Bruce and Fries, 2005; Voshaar *et al.*, 2015). Scores of 0-1 indicate mild to moderate difficulty, 1-2 indicate moderate to severe disability, and 2-3 represent severe to very severe disability (Bruce and Fries, 2005). The HAQ-DI has repeatedly proven to be a validated assessment, with test-retest correlations ranging from 0.87 to 0.99 (Bruce and Fries, 2005).

1.3.1.4 Prognosis

One of the most crucial aspects of managing RA is predicting prognosis. Typically, the presence of X-ray erosions predicts a poor prognosis. Magnetic resonance imaging has also been shown to be advantageous in determining prognosis due to its ability to visualize soft tissue. In particular, bone marrow edema (BME) has been shown to be a reliable predictor for subsequent X-ray erosions (Tan and Conaghan, 2011). As well, grayscale ultrasound (GSUS) has been shown to be a predictor for MRI erosive damage (Tan and Conaghan, 2011). A systematic review demonstrated that ultrasound was also able to predict flare in varying regions in patients who were power Doppler ultrasound (PDUS)-positive, with ORs between 3.6 and 13 (Cate *et al.*, 2013). As well,

GSUS and PDUS had predictive value in determining if radiological joint damage would occur, with ORs between 1.4 and 12 (Cate *et al.*, 2013).

Strategic treatment plans and pharmacological therapies are able to bring 75-80% of patients to low disease activity or remission, allowing them to continue their daily activities with a normal life expectancy (Aletaha and Smolen, 2018). However, there are still 20-25% of RA patients in developed countries that are not able to achieve low disease activity. Reasons include not being able to access optimal care and resistant disease that does not improve with medication (Aletaha and Smolen, 2018). For such patients, new therapies are needed, such as more selective JAK inhibitors (Aletaha and Smolen, 2018).

1.4 Treatment Options

Although RA is not curable, medications and altered lifestyle choices can help patients gain better control of their disease and potentially achieve remission. Treatment for RA has many layers as it should include patient education, physical/occupational therapy and drug treatment (Majithia and Geraci, 2007). Nonsteroidal anti-inflammatory drugs (NSAIDs) can be used to improve symptoms, but cannot prevent the progression of joint damage (Aletaha and Smolen, 2018). The NSAIDs should only be used during the short window of time when diagnosis of RA is still not confirmed. Second, glucocorticoids can be used (prednisolone) to provide short term relief of symptoms (Mateen *et al.*, 2016). In the last 20 years, the best options for patients diagnosed with RA have included the use of DMARDs, as well as biologic agents (Aletaha *et al.*, 2010).

Disease Modifying Antirheumatic Drugs (DMARDS)

Disease Modifying Antirheumatic Drugs (DMARDs) are a class of drugs that can improve symptoms for RA patients and prevent the progression of joint damage, and thus should be initiated as soon as diagnosis is confirmed (Burmester and Pope, 2017; Aletaha and Smolen, 2018). The DMARDs are divided into two categories: synthetic DMARDs, which are orally administered chemical molecules, and biologic agents, which are non-orally administered proteins (Aletaha and Smolen, 2018). Synthetic DMARDs are further divided into conventional (methotrexate (MTX), sulfasalazine, leflunomide, hydroxychloroquine) and targeted DMARDs (tofacitinib, baricitinib) (Aletaha and Smolen, 2018). To date, targets to conventional DMARDs are unknown, however, targeted DMARDs are known to target Janus kinase (JAK) enzymes (Aletaha and Smolen, 2018). JAKs are involved in the signaling pathway that converts the responses of cytokines into downstream cellular effects (Aletaha and Smolen, 2018).

In patients with mild disease activity (usually involves less than 5 joints) and normal radiographic scans, hydroxychloroquine, sulfasalazine, minocycline and in some cases MTX can be used (Majithia and Geraci, 2007). Methotrexate is typically used as an initial drug therapy for moderate to severe cases (usually the involvement of more than 5 joints) or cases with abnormal radiographic findings (bone erosions) (Majithia and Geraci, 2007; Burmester and Pope, 2017). If this option is not sufficient for patients, leflunomide, azathioprine or combination therapy (MTX with another medication) are recommended (Majithia and Geraci, 2007). Methotrexate is one of the most common RA medications as 25-40% of patients experience improvement with monotherapy, and when

used with a glucocorticoid, ~50% of patients are able to achieve low disease activity/remission (Aletaha and Smolen, 2018). Table 1 has a list of DMARDS and their respective targets (Majithia and Geraci, 2007).

Table 1: DMARDs and their Cellular Targets

Medication	Target
Methotrexate	Interleukin-8, -6
Hydrochloroquine	Toll-like receptors (TLRs), IL-6, IL-17, IL-22
Leflunomide	Dihydroorotate dehydrogenase
Sulfasalazine	Unknown

Biologic Agents

Biological agents use molecular mechanisms to target cytokines, signaling molecules, and cells that are involved in inflammation and joint destruction (Majithia and Geraci, 2007). Biologic agents target TNF, B-cells, and members from the cytokine family (IL-1, IL-6) (Burmester and Pope, 2017; Aletaha and Smolen, 2018). If remission or reduced disease activity is not achieved within 3-6 months, EULAR suggests that other conventional DMARDs are used, or patients begin using a biologic in combination with a conventional DMARD (Burmester and Pope, 2017; Aletaha and Smolen, 2018). Unfortunately, all biologics come with the risk of infection and tuberculosis reactivation (Majithia and Geraci, 2007). Table 2 has a list of biologics and their respective cellular targets (Majithia and Geraci, 2007).

Table 2: Biologics and their Cellular Targets

Medication	Target
Adalimumab, etanercept, infliximab (first line agents)	TNF
Anakinra	IL-1
Tocilizumab	IL-6
Abatacept	T-cell co-stimulation down-regulator
Rituximab	Anti-B cell antibody

1.5 Imaging Modalities

Imaging modalities are important to help rheumatologists confirm their clinical diagnosis of RA (Vyas *et al.*, 2016). Diagnosis is challenging as clinical, imaging and serological evidence of disease may not appear simultaneously (Vyas *et al.*, 2016). Structural changes can occur early on in RA, thus, imaging modalities that are able to detect these variations with high sensitivity in the early stages of disease are crucial to initiate prompt treatment, and prevent bone and joint damage. Imaging modalities can determine the severity and monitor the progression of disease activity in response to treatment (Vyas *et al.*, 2016). During the time period in the early disease stage, termed the "window of opportunity", if the correct treatment is initiated, patients can have long-term improved outcomes and prevent the progression of disease (Vyas *et al.*, 2016). Therefore, early diagnosis and treatment are pivotal to positive health outcomes in RA patients, stressing the importance of accurate imaging in RA. In addition, modalities that are easily accessible and able to monitor drug efficacy in relation to disease progression are ideal (Rowbotham and Grainger, 2011). All in all, the ideal imaging modality would allow for early and accurate diagnosis, have the ability to predict poor prognosis and have the

ability to monitor disease progression in response to drug therapy (Tan and Conaghan, 2011).

1.5.1 Conventional Radiography/X-Ray

Machine and Core Concepts

X-rays provide a two-dimensional projection of three-dimensional anatomical structures (Døhn *et al.*, 2006). Radiographic joint damage is most commonly found in the peripheral joints in early RA (~75% of patients display damage in the first 2 years of disease onset) (Alasaarela *et al.*, 1998). Conventional radiography (CR) uses X-rays, an energy form that is on the higher end of the electromagnetic spectrum. The X-rays are produced in a vacuum tube, when a high voltage is passed across two terminals. This releases high-energy electrons from the cathode, which move towards the anode. It is important to be cautious of the radiation levels (measured in milliSieverts, mSv), as they ionize tissues, allowing electrons to be liberated to form ion pairs, and ultimately lead to generation of free radicals. The energy level of the X-rays can be adjusted by altering the voltage and current in the tube, using filters, and switching the anode material. Different tissues appear differently on X-ray images (due to attenuation), depending on their density, thickness and atomic number. For instance, the air in lungs is transparent and appears black; calcified bone tissues appear white on X-ray images. Soft tissues have characteristics in between the former two examples. Additionally, contrast agents can be used to enhance X-ray attenuation. Positive contrast agents have high radiodensity properties, such as iodine and barium, and appear white on X-ray as the rays are blocked.

Negative agents are low density, such as air and carbon dioxide, and are black in X-rays. (Harvey and Blomley, 2005)

The low cost and easy accessibility make it an attractive choice to clinicians (Vyas *et al.*, 2016). Other advantages of the modality include its reasonable reproducibility, quick scan time, and validated methods for assessing scans (Østergaard *et al.*, 2008; Tan and Conaghan, 2011).

Use in Rheumatoid Arthritis

X-ray is the most commonly used imaging modality for RA and is used as the first-line of imaging for diagnosis, as it is the traditional gold standard (Tan and Conaghan, 2011; Vyas *et al.*, 2016). It is able to detect bony erosions and joint space narrowing in patients with established RA (Vyas *et al.*, 2016). These parameters are assessed using the Sharp van der Heijde scoring system. Erosions in the hands and wrist are examined in 16 joints, scored on a scale of 0-5 per joint (5=more than 50% loss of articular bone) (Boini and Guillemin, 2001; Landewé and van der Heijde, 2005). For the

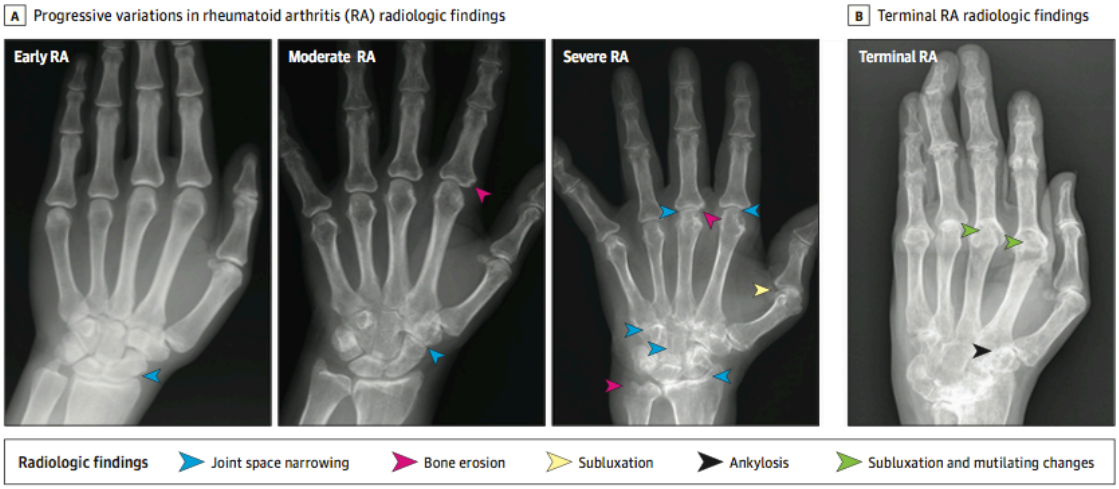

Figure 2. Radiological findings in A) progressive and B) terminal RA. (Aletaha and Smolen, 2018)

feet, 6 joints are assessed and are graded on a scale of 0-10 per joint (Ory, 2003; Landewé and van der Heijde, 2005). Joint space narrowing is assigned a score between 0-4: 0=no narrowing; 1=minimal narrowing; 2=50% loss of joint space; 3=75% loss of joint space; 4=complete loss of joint space (Ory, 2003). For joint space narrowing, 15 joints are assessed in the hands and wrists, and 6 joints in the feet (Landewé and van der Heijde, 2005). The maximum score is 280 and 168 for erosions and joint space narrowing, respectively, for a total Sharp score of 448 (Landewé and van der Heijde, 2005). Radiographic features in an RA hand are shown in Fig. 2.

In RA patients, regular follow-ups are required and repeated exposure to ionizing radiation from X-ray is not preferable with the limited two dimensional data that is provided (Østergaard *et al.*, 2008; Vyas *et al.*, 2016). In addition, it has a low sensitivity in the early stages due to its inability to detect soft tissue changes and early manifestations of bone erosion (Østergaard *et al.*, 2008; Tan and Conaghan, 2011). Its inability to provide information regarding soft tissue edema, tenosynovitis, synovial thickening and bone marrow make it a suboptimal choice for detecting disease activity (Østergaard *et al.*, 2008; Colebatch *et al.*, 2013; Vyas *et al.*, 2016).

Overall, CR is not beneficial for early diagnosis, as erosions may not be seen when they initially appear with X-ray, although are present in 90-95% of patients who have had symptoms for 10 years and on (Vyas *et al.*, 2016). In CR, patients with early RA appear to have “undifferentiated arthritis”, with normal X-ray results (Rowbotham and Grainger, 2011). In addition, evidence based research over the last decade has

demonstrated the strengths of other modalities which are more sensitive at the early stages of disease and can fill the gaps of X-ray (Colebatch *et al.*, 2013).

Previous Studies

Previous studies have demonstrated that the sensitivity of CR for detection of erosions in MTPJs was poorer than US when MRI was used as the reference standard (0.32 versus 0.79), whereas the specificity was similar between the two modalities (Szkudlarek *et al.*, 2004). As well, CR was unable to detect erosions in patients with early RA (<2 years disease duration), whereas MRI and US were able to detect erosive disease (MRI to a greater extent than US). Even though CR was able to detect erosions in patients with established RA (>2 years disease duration), it did so to a lesser extent than MRI and US (Szkudlarek *et al.*, 2004). Other studies agree with the poor sensitivity of CR for detection of erosions when compared to CT as the reference method (14%-24%) (Døhn *et al.*, 2006, 2007, 2008). The lack of detection of some of the earliest anatomical changes in RA urges the need for more sensitive, easily accessible modalities.

1.5.2 Ultrasonography

Machine and Core Concepts

Ultrasound (US) is a relatively inexpensive, patient friendly, fairly accessible imaging modality which does not expose patients to ionizing radiation, and is beneficial for detecting changes in soft tissue structures (Østergaard *et al.*, 2008; Tan and Conaghan, 2011; Vyas *et al.*, 2016). Ultrasound images are generated by detecting reflected sound waves, which are a result of the US energy pulse waves released from the transducer (Li

and Liebling, 2009). A reflected wave/echo is generated when the longitudinal sound waves reach an interface (Li and Liebling, 2009). High resolution imaging of superficial anatomical regions can be achieved with high frequency transducers (10-22 MHz) (Østergaard and Wiell, 2004). The depth of the interface can be determined by timing the return of the echo to the transducer and by determining the speed of sound (Li and Liebling, 2009; Venables, 2011).

Some modes of US that can be used are grayscale (GSUS; also known as B-mode), color Doppler and power Doppler (PD). Grayscale US can be used to assess static anatomy such as joint effusions, erosions, tissue heterogeneity and pannus tissue by detecting the amplitude of the wave; sound waves travel through homogenous mediums such as clear fluid, resulting in anechoic images (Li and Liebling, 2009; Venables, 2011). Color Doppler can be used for detecting blood flow (can detect direction and presence of flow) by assessing the change in frequency of the moving flow (Li and Liebling, 2009). Power Doppler assesses the amplitude of the frequency change and is more sensitive to smaller vessels when compared to color Doppler (Venables, 2011). Ultrasound gels are used to prevent distortion of the image by allowing minimal pressure, and ensure better clarity in the near-field region close to the transducer (Li and Liebling, 2009).

Use in Rheumatoid Arthritis

US is widely used to monitor disease progression changes in follow-up visits and upon the administration of DMARDs as it can provide real-time structural information (Østergaard *et al.*, 2008; Vyas *et al.*, 2016). One of the abnormalities detected is synovial fluid, and according to OMERACT, this is an abnormal hypoechoic US signal (Tan and Conaghan, 2011). Synovial thickening (ST) is assessed semi-quantitatively on a 4-point scale: 0=no ST; 1=minimal ST (angle between periarticular bones filled); 2=moderate ST bulging over the line that connects the top of the periarticular bone (not extending into the diaphysis); 3=severe ST bulging over the line connecting the tops of periarticular bone and reaching to at least one bone diaphyses (Fig. 3) (Szkudlarek *et al.*, 2003). Power Doppler allows for the detection of synovial vascularity, which is graded on a 4-point semi-quantitative grading system: 0=no flow; 1=one or more vessels; 2=<50% of synovium has vessel signals; 3=>50% of synovium has vessel signals (Fig. 3) (Szkudlarek *et al.*, 2003; Tan and Conaghan, 2011). PDUS has been shown to correlate well with histologically detected synovitis in joints with inflammation (Tan and Conaghan, 2011). According to OMERACT, joint erosions are defined as intra-articular discontinuity of the bone surface that is visible in two perpendicular planes (Tan and

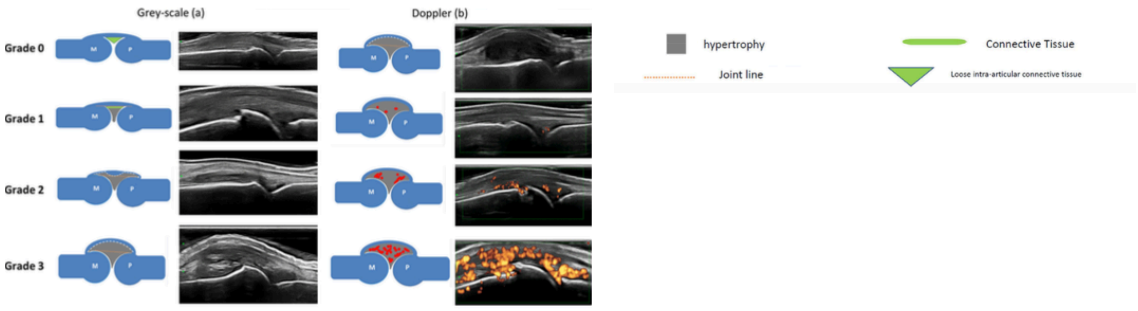

Figure 3. GS and PD scoring, using US. (D'Agostino et al., 2017)

Conaghan, 2011). Erosions are also scored on a 4-point scale: 0=regular surface; 1=irregularity in surface without a discrepancy seen in 2 planes; 2=discrepancy in bone surface visualized in 2 planes; 3=extreme bone destruction (Szkudlarek *et al.*, 2003). Ultrasound has been shown to detect more erosions than CR in early RA (Tan and Conaghan, 2011). There is also a EULAR-OMERACT combined scoring system to assess GS and PD signals simultaneously (D'Agostino *et al.*, 2017). Some studies assign US grades of 0 and 1 for ST and erosions as normal, and grades of 0 for PD as normal in order to better differentiate between arthritic and non-arthritic patients (Szkudlarek *et al.*, 2003; Cate *et al.*, 2013).

Downfalls of this device include the variability between machines as well as the inter-reader variation as a result of the dependence on the expertise of the operator (Østergaard *et al.*, 2008; Li and Liebling, 2009; Vyas *et al.*, 2016). In addition, its sensitivity to bone erosions is dependent on the site of interest (high sensitivity in areas which are easily accessible, e.g. MTPJ 5) as it cannot penetrate bone (Østergaard *et al.*, 2008).

Previous Studies

Past studies have shown the benefits of inclusion of US in routine rheumatology practice, as it can allow site-specific scanning at multiple joints, confirmation of diagnosis, and real time results, all of which reduce clinic time and allow quick decision making (Wakefield *et al.*, 2005; Tan and Conaghan, 2011).

Despite the dependence on operator experience, one study has demonstrated high intra- and inter-rater reliability for assessing synovitis with the use of a reference atlas;

median intra- and inter-rater ICC values were 0.95 and 0.97 for GS and PDUS, respectively (Hammer *et al.*, 2011). Thus, high intra- and inter-rater reliability can be achieved with the help of extensive training, calibration of the scoring system, and reference to the atlas (Hammer *et al.*, 2011). As well, US has been shown to be a reproducible tool in assessing and monitoring tenosynovitis in RA patients; intra-rater reliability was good for GS and PDUS, whereas inter-rater reliability was moderate and good for GS and PDUS, respectively (Naredo *et al.*, 2013).

US has been compared to other RA imaging modalities. In one study, US has been reported to be more sensitive in detecting bone erosions in MCPJs, PIPJs and MTPJs than CR (Østergaard *et al.*, 2008). In another study, US was compared to CR in RA patients, and it was found that GS and PDUS were able to detect 20% more erosions than CR; US sensitivity has been shown to be better than CR in multiple studies (Alasaarela *et al.*, 1998; Weidekamm *et al.*, 2003; Szkudlarek *et al.*, 2004, 2006). Interestingly, even when compared to MRI, US was found to be better at detecting bone erosions at MTPJs 1 and 5, likely because the probe had access to the dorsal, lateral and plantar region in these joints (Szkudlarek *et al.*, 2004).

In a systematic review that compared clinical examination to US, multiple papers demonstrated that US synovitis improved diagnosis in RA patients; US was found to be superior to clinical examination in 75% of patients (Colebatch *et al.*, 2013). In addition, when comparing clinical examination with US for synovitis, US had a 2.18 fold higher mean detection rate in the hands and wrist (Colebatch *et al.*, 2013). Ultrasound is also used for remission evaluation in RA patients. In a systematic review of 11 studies, there

was disagreement between clinical presentation and US results; some joints that did not show swelling/inflammation during the clinical assessment showed US signs (Cate *et al.*, 2013). This is expected, as clinical assessments are often unable to detect mild synovitis (Joshua *et al.*, 2006). As well, PDUS was able to detect signs of inflammation in up to 60% of patients in clinical remission (Cate *et al.*, 2013). The study concluded that PDUS is superior to GSUS in detecting true remission, as it is more specific and has higher predictive value (Cate *et al.*, 2013).

1.5.3 Magnetic Resonance Imaging

Machine and Core Concepts

Magnetic Resonance Imaging (MRI) has become an important tool in the clinical practice of musculoskeletal medicine. It is able to generate multiplanar cross-sectional images without using ionizing radiation (Østergaard *et al.*, 2008). The scan protocol is determined based on the region of interest (ROI), availability of coils and the strength of the magnet (Vyas *et al.*, 2016). Images should be taken from two separate planes and the thickness of slices should be <3 mm; thinner slices are recommended for smaller joints (Vyas *et al.*, 2016).

Magnetic resonance imaging technology uses electromagnetic radiation (magnetic fields) to produce slice images (Katti *et al.*, 2011). Nuclei within body tissues have their own magnetic moment; usually hydrogen nuclei are used in MRI due to the large quantity of water in the body (McMahon *et al.*, 2011). Once an external large magnetic field (B_0; z plane) is applied, the hydrogen nuclei align; some atoms align parallel to the field, and

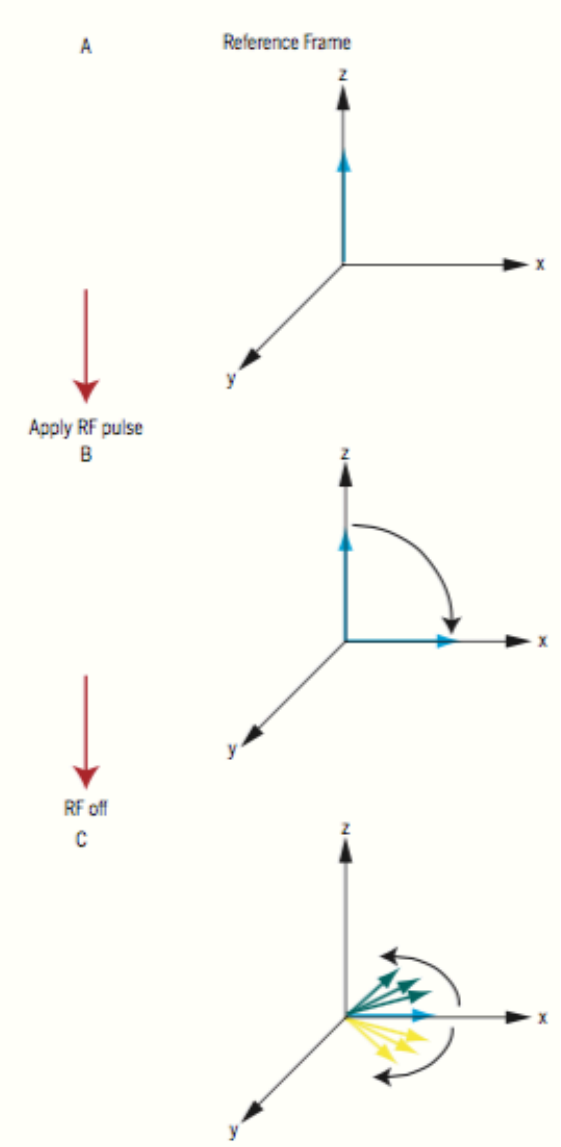

Figure 4. Magnetic moments in MRI. A) Static magnetic field in the z plane (B_0 field) B) Upon administration of a radiofrequency at 90° (B_1 field) C) After removing the radiofrequency; the net magnetization is in the xy plane. (McMahon et al., 2011)

some antiparallel to the field (Katti *et al.*, 2011). The axis of the protons slightly oscillate in the direction of the field, and this is called precession (Katti *et al.*, 2011). Then, a radiofrequency pulse (also known as B_1 field) is applied for a given period of time, aligning the protons in a high-energy state, which eventually moves the net magnetization from the B_0 field (or longitudinal magnetization) to the transverse plane (xy plane) (refer

to Fig. 4) (McMahon *et al.*, 2011). Only net magnetization in the xy plane can be detected by the MR receivers (McMahon *et al.*, 2011).

After reaching the excited phase in the xy plane, the nuclei begin to relax/disappear. There are two types of relaxation: T1 relaxation (longitudinal) and T2 relaxation (transverse). In T1 relaxation (time it takes for magnetic vector to reach resting state), the relaxation occurs along the z plane and the energy from the radiofrequency pulse is spread to the surroundings; it takes seconds for 63% of the original longitudinal

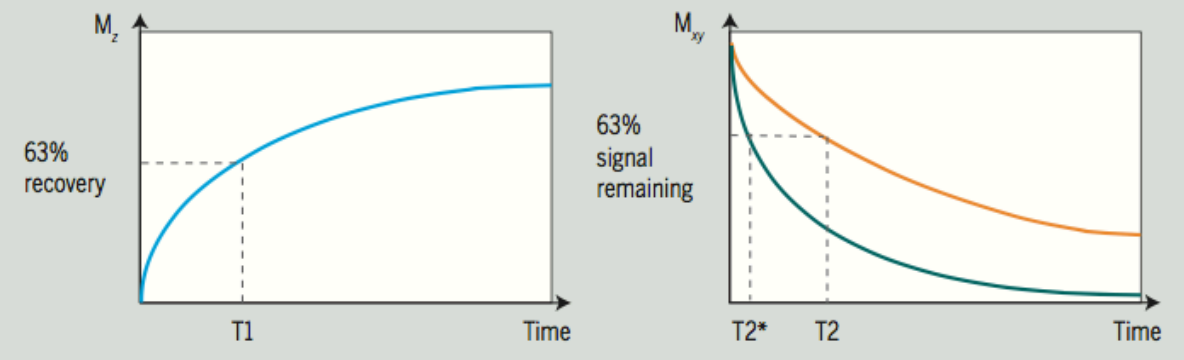

Figure 5. Plots showing T1 and T2 relaxation. T1 (left) shows recovery of the magnetic field to the z plane. T2 (right) shows loss of the transverse signal due to loss of order in the hydrogen nuclei. T2* is a *chemical shift* as a result of disturbances in the magnetic field; may result in quicker loss of order in the hydrogen nuclei. (McMahon et al., 2011)

magnetization to be recovered (Fig. 5) (Berger, 2002; McMahon *et al.*, 2011). A low intensity, dark MR image is seen in tissues with a long T1 relaxation (Katti *et al.*, 2011). In T2 relaxation, the transverse magnetization is lost and the nuclei begin to misalign (i.e. time it takes axial spin to reach resting state); it takes tens to hundreds of milliseconds for 63% of the original transverse magnetization to remain (Fig. 5) (Berger, 2002; McMahon *et al.*, 2011). A high-intensity, bright MR image is seen in tissues with long T2 relaxation times (the opposite is true for short T2 relaxation times) (Katti *et al.*, 2011). Different

tissues have different T1 and T2 rates, thus protocols can be optimized based on the region being scanned. Fast moving molecules (e.g. synovial fluid) or molecules that are far apart will have longer T1 times than solid materials (e.g. bone). T2 relaxation rates are slower in gas phases (e.g. water) and faster in solid phases (e.g. bone) (McMahon *et al.*, 2011). T1-weighted images allow for differentiation between various tissues which have T1 properties (e.g. bone marrow and muscle), by using short repetition times between the radiofrequency pulse excitation (McMahon *et al.*, 2011). This allows tissues with short T1 times to recover the longitudinal magnetization between the pulses and provide a differentiated signal than a tissue with a longer T1 relaxation time; fat has the shortest T1 time and appears bright in the MR image (Katti *et al.*, 2011; McMahon *et al.*, 2011). In T2-weighted images, a longer repetition time results in a greater loss of order in the transverse plane (McMahon *et al.*, 2011). Tissues with longer T2 times will display brighter in T2-weighted images (e.g. synovitis/tissues with water content), and this is often seen in abnormal tissues (Katti *et al.*, 2011; Vyas *et al.*, 2016).

Intravenous contrast agents (i.e. IV gadolinium) can be used to better distinguish synovitis (Tan and Conaghan, 2011). Gadolinium is a heavy metal that has paramagnetic effects on water protons, allowing the protons to quickly relax on T1-weighted sequences (McQueen, 2000). The intensity of the signal, which spreads to vascular tissue, is proportional to the concentration of gadolinium and the relaxation of the surrounding water molecules (McQueen, 2000; Raymond and Pierre, 2005). Therefore, tissues that are highly vascular and have inflamed synovium are enhanced in brightness (McQueen, 2000). Gadolinium allows for the differentiation between joint effusion (excess fluid

accumulation in joint) and synovium as they appear with low intensity on T1-weighted images (McQueen, 2000). Bony erosions usually appear enhanced with gadolinium administration, further confirming the presence of an inflamed synovium (McQueen, 2000).

Use in Rheumatoid Arthritis

Magnetic resonance imaging has been used in RA patients for its ability to detect erosions without using ionizing radiation, in a multiplanar view, while simultaneously detecting changes in soft tissue and fluid at the joint level (McQueen, 2000; Vyas *et al.*, 2016).

Magnetic resonance imaging has been shown to be the most sensitive modality for early diagnosis, as well as for disease monitoring (Tan and Conaghan, 2011; Vyas *et al.*, 2016). Previous MRI studies have observed that the pathological progression of RA begins with synovitis, followed by BME, and finally results in erosions (McQueen, 2000). MRI is superior to CR as it allows for visualization of bone, surrounding soft tissues and fluid within a given joint (McQueen, 2000; Tan and Conaghan, 2011). Magnetic resonance imaging is beneficial in terms of detecting underlying pathological changes that may go undetected in the early phases using CR. For instance, bony erosions present as focal areas in the cortical bone, where the normal signal intensity is decreased in T1-weighted images and increased in T2-weighted images (McQueen, 2000).

In terms of parameters measured by MRI, a reference atlas has been published by the EULAR-OMERACT groups (Conaghan *et al.*, 2005). Synovial inflammation is one of the prominent markers of RA; synovitis detected in MRI has also correlated with histopathological features of inflammation. Synovitis appears on MRI with a thickness greater than the normal synovium, with a high signal intensity on T1-weighted images (Ostergaard *et al.*, 2003). On MRI, it is scored on a scale of 0-3 (0=normal, 1=mild, 2=moderate, 3=severe), and best visualized in a T1-weighted sequence (Fig. 6)

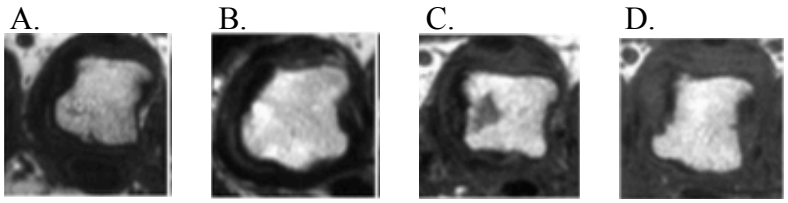

Figure 6. Synovitis scored from 0-3 in figures A-D, respectively, at the MCPJ (Conaghan et al., 2005).

(Østergaard *et al.*, 2017). Bone marrow edema is another parameter that can be measured by MRI, although it is nonspecific to RA. According to OMERACT, BME seen on MRI is a lesion within the trabecular bone with poorly defined margins and MRI signals indicating increased water content. Bone marrow edema appears with a low signal

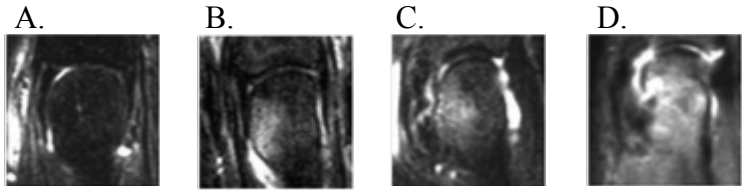

Figure 7. BME scored from 0-3 in figures A-D, respectively, at the MC head (Conaghan et al., 2005).

intensity on T1-weighted images and with a high signal intensity on T2-weighted fat-saturated images (Ostergaard *et al.*, 2003). Bone marrow edema is graded on a scale of 0-

3 (0=no BME, 1=1-33% of bone with edema, 2=34-66% BME, 3=67-100% BME), and optimally visualized as T2-weighted fat-saturated images (Fig. 7) (Østergaard *et al.*, 2017). Bone marrow edema is a strong predictor of subsequent erosion development and has a prevalence of 39-75% in early RA patients (McQueen, 2000; Conaghan *et al.*, 2003; Døhn *et al.*, 2011; Lee *et al.*, 2015). As well, MRI is advantageous as it can determine if the edema is active (detected as enhancing pannus) or inactive (detected as fibrous tissue) (Perry *et al.*, 2005). Lastly, bone erosions, a sharp distinct bone lesion, are also detected by MRI (Ostergaard *et al.*, 2003). Note that due to the low amount of moving protons in bone, cortical bone appears on MRI as signal voids, distinguished from signal releasing bone marrow and periosseous tissues (Døhn *et al.*, 2008). According to OMERACT, bone erosions need to be visible from two different planes, and a cortical break needs to be seen in at least one plane. On T1-weighted images, cortical bone appears abnormally with a high signal intensity, and trabecular bone appears abnormally with a low signal intensity (Ostergaard *et al.*, 2003). Erosions are scored from 0-10 (0=no erosion, 1=1-10% bone is eroded, 10=91-100% bone is eroded, etc.), and best seen in T1-weighted images (Fig. 8)

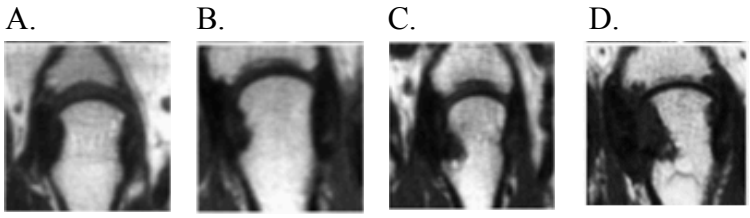

Figure 8. Bone erosions scored from 0-3 in figures A-D, respectively, at the MC head (Conaghan et al., 2005).

(Østergaard *et al.*, 2017). Magnetic resonance imaging is able to better characterize bone erosions due to its ability to visualize tomographic scans which make it easier to see. (Tan and Conaghan, 2011)

Limitations to MRI scanning include high cost, long scan durations, low availability, and the invasive nature and potential side effects of contrast agents (Østergaard *et al.*, 2008; Tan and Conaghan, 2011; Manhard *et al.*, 2017). As well, patients may have contraindications to the scanner due to the strong magnetic field (e.g. metals in the body, pregnancy) (Dill, 2008). Other disadvantages of the system include

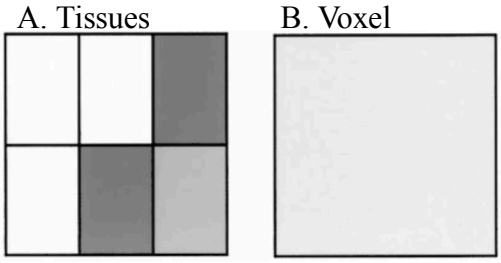

Figure 9. Partial volume artefact. A. Three different tissues are presented in this square. B. Due to the large size of the voxel, the three tissues cannot be differentiated and the average measure for all three tissues is taken. (Kothari et al., 1998)

partial volume artefacts (where the voxel is too large and contains more than one type of tissue, therefore the signal is an average of two tissues; Fig. 9); although this can be resolved by imaging from two planes (axial and coronal) and using thinner slices (Norman *et al.*, 1983; Kothari *et al.*, 1998; Taber *et al.*, 1998; McQueen, 2000; Perry *et al.*, 2005). Lastly, quantitative data cannot be extracted from the images, unless a radiologist analyzes them (e.g. BMD).

Previous Studies

In a systematic review that compared clinical assessment to MRI, MRI was able to detect inflammation with a 2.20 fold mean detection rate in the hands and wrist (Colebatch *et al.*, 2013). As well, MRI results have been compared to histologic data. Jimenez-Boj et al. sought to determine the pathologic nature of erosions and BME in RA joints; in all tested joints, there were changes in the bone marrow, seen on both MRI and histologic sections (2007). Histological analysis revealed that bone damage in RA was due to the replacement of bone marrow fat with inflammatory cells adjacent to the cortical break; correlation was found between MR lesions and localized bone marrow inflammation (due to inflammatory infiltrates) and increased blood vessels (Jimenez-Boj *et al.*, 2007). Thus, MRI can be used as an indicator of the inflammation in adjacent bone marrow, and the correlation between lesions and histologic findings demonstrates that lesions occur due to true inflammatory changes in the bone marrow.

Due to the versatile nature of MRI, it has been compared to other imaging modalities to determine its benefits in RA disease. In one study that compared US and MRI modalities in RA, it was shown that MRI detected erosions better at MTPJs 2-4, when compared to US (Szkudlarek *et al.*, 2004). Magnetic resonance imaging is beneficial in its ability to acquire a 360° view of the ROI. In another study, MRI was able to detect erosions in 45% of scans in comparison to 15% by CR in early RA patients (McQueen *et al.*, 1998). As well, one study demonstrated that after the presentation of MR erosions, X-ray erosions appear 6-12 months later (McQueen, 2000).

In regards to the role of MRI in erosion detection in RA patients, it has been previously found that when comparing RA patients to symptom-free controls, RA patients had 1.20 times the erosion scores of controls, independent of age and gender (Boeters *et al.*, 2018). Although, there was a lot of overlap in erosion scores at the individual level. As well, erosions present with simultaneous BME and synovitis were specific to middle-aged RA patients (<60 years) (Boeters *et al.*, 2018). When comparing to patients with other arthritides, erosions with inflammation were not specific to RA patients anymore, although erosion grades ≥2 were (Boeters *et al.*, 2018).

The MRI outcomes have also been used to monitor the response to therapy in RA patients. One study compared patients taking DMARDs and steroids to those only taking DMARDs. Patients on DMARD and prednisolone therapy experienced a decrease in synovial membrane volume after 3-6 months; those taking DMARDs only displayed a decrease in the synovial volume after 6-12 months (Østergaard *et al.*, 1999). In another study, patients taking MTX and intra-articular corticosteroids and those taking only MTX were compared. A decrease in synovitis was seen in both groups at 0-3 months; patients in the MTX only group developed more erosions than the other group. After 3 months, no differences in synovitis or bone damage were found between the two groups. Thus, in both studies MR was able to demonstrate the anti-inflammatory effects of fast-acting glucocorticoids by imaging the synovium.

1.6 Bone Mineral Density

One of the primary focuses of the next phase of this study is to quantify the volumetric bone mineral density (vBMD) of patients with RA in the MTPJs. To our knowledge, to date, no studies have been published regarding the measurement of vBMD using peripheral quantitative computed tomography (pQCT) in the MTPJs of RA patients. Thus, this portion of the study, when compared to a normal population, will provide a better idea on the presence of erosions.

1.6.1 DXA

Machine and Core Concepts

Areal bone mineral density (aBMD) is most commonly measured by dual energy X-ray absorptiometry (DXA) (Zengin *et al.*, 2015). Two-dimensional aBMD values act as a surrogate marker of bone strength and determination of fracture risk (Zengin *et al.*, 2015). DXA scans are sensitive to the mineral component of the bone (Manhard *et al.*, 2017). An aBMD value is extracted from the difference in X-ray attenuation of photon energy between bone mineral and soft tissues, presented in units of mineral mass per pixel area (Manhard *et al.*, 2017). In terms of clinical use, DXA aBMD values are assessed based on T-scores which determine an individuals' variability from a young healthy populations' BMD (matched for gender and ethnicity), using standard deviations. DXA is most commonly used for detecting risks of fracture at the hip, spine and distal radius. Along these lines, the World Health Organization (WHO) has created the

following criteria for T-scores: <-2.5 = osteoporosis; -1 to -2.5 = osteopenia (Manhard et al., 2017).

Dual energy X-ray absorptiometry is advantageous as it has good precision, low cost and a low radiation dose of 5-20 μSv (Maricic, 2014; Zengin *et al.*, 2015; Manhard *et al.*, 2017). But, the modality is limited by its ability to only measure aBMD (g/cm^2), projectional bone area (cm^2), and bone mineral content (BMC, g) (Zengin *et al.*, 2015). It provides an average value of all bone components (trabecular and cortical BMD) (Zengin *et al.*, 2015). Thus, it does not account for bone structure (shape and size) as it is unable to differentiate bone depth, and does not recognize different components of bone (trabecular and cortical bone) (Zengin *et al.*, 2015). Hence, results from DXA must be interpreted with caution as height and weight of a patient are not considered (Zengin *et al.*, 2015).

Use in Rheumatoid Arthritis

Dual energy X-ray absorptiometry has been previously used in RA patients to determine fracture risk and osteoporotic bone loss using T-scores (Zhu *et al.*, 2012; Maricic, 2014). Assessment of osteoporotic bone loss in RA is important, as osteoporosis in RA has a prevalence of 20-30% and 7-26% in the spine and hip, respectively (Zhu *et al.*, 2012). As well, DXA has compared RA patients to age- and sex-matched controls by using standard deviation calculations (Z-scores) (Jensen *et al.*, 2005). Interestingly, moderate correlations have been found between the hip, spine and radial BMD in DXA, and radial and MC head vBMD in HR-pQCT (Zhu *et al.*, 2012). Although many studies have assessed aBMD using DXA in RA patients, it is limited by its' inability to assess

microstructural changes, and differentiate between trabecular and cortical bone, which are important components to assess in the inevitable periarticular bone loss seen in RA.

Previous Studies

The reliability for measuring BMD in the spine, hand and heel have demonstrated good reproducibility (%CV <5%) (Shibuya *et al.*, 2002; Hoff *et al.*, 2007). As well, past studies have demonstrated high test-retest, intra- and inter-rater reliability in the MCPJs and MTPJs, although variability was higher in MTs 3 and 4 (Jensen *et al.*, 2005; Fuller *et al.*, 2016).

In one study, patients with early and established RA were assessed. Greater reductions in Z-scores were seen in patients with more progressed disease (and erosions) in comparison to those with early disease (and no erosions) (Jensen *et al.*, 2005). In one 2-year follow-up study, significant reductions in spinal and hip DXA-BMD were displayed in RA patients (Hoff *et al.*, 2007). Interestingly, in the same study, hand BMD was only reduced in patients with early disease (≤3 years) and not in those with longer disease duration (>3 years), likely due to the increased inflammation in the peripheral joints in the early years of disease (Hoff *et al.*, 2007). Other studies have also demonstrated the comparatively faster loss of BMD in the hands in comparison to the hip and spine in early RA patients (Devlin *et al.*, 1996; Haugeberg *et al.*, 2006). Studies that have compared RA patients to controls have demonstrated lower hand DXA-BMD in patients in cross-sectional studies (Alenfeld *et al.*, 2000) and further hand bone loss in longitudinal studies (Deodhar *et al.*, 1995). Longitudinal studies with RA patients and patients with other rheumatic diseases have also shown that RA patients have greater

reductions in hand BMD over time (Daragon *et al.*, 2001; Jensen *et al.*, 2004; Haugeberg *et al.*, 2006). Note that although joint level bone loss is of particular interest in RA, measuring whole hand DXA-BMD is more feasible and has higher precision (Hoff and Haugeberg, 2010).

1.6.2 CT Derived 3-D Technologies

Computed tomography (CT) is a tomographic (cross-sectional) radiographic (use of X-rays) imaging modality that is able to visualize calcified tissue (Østergaard *et al.*, 2008). It is a reference standard for damage of calcified tissues, such as bone erosions (Østergaard *et al.*, 2008; Srikhum *et al.*, 2013). Evidence in the literature has demonstrated that CT may be more sensitive to detection of bone erosions than MRI and radiography (Østergaard *et al.*, 2008; Srikhum *et al.*, 2013). However, it is not used often in clinical practice due to exposure to ionizing radiation.

Advances in CT derived three-dimensional technologies such as peripheral quantitative CT (pQCT) and high-resolution pQCT (HR-pQCT) have allowed for quantification of volumetric bone mineral density (vBMD) and bone microarchitecture, respectively (Zengin *et al.*, 2015). These modalities also allow for visualization of the trabecular and cortical bone *in vivo*, providing better measures for bone strength (Zengin *et al.*, 2015). As well, these technologies use less radiation than whole-body CT (e.g. typical abdominal CT has a radiation dose of 5 mSv) (Lee *et al.*, 2015). See Table 3 for a quick comparison between pQCT and HR-pQCT.

Table 3: Key Differences between pQCT and HR-pQCT (Wong, 2016)

Feature	pQCT	HR-pQCT
Resolution/voxel size	200-800 µm	82 µm (standard)
Slice thickness	2.3 mm (non-isotropic)	82 µm (isotropic)
Effective dose	1 µSv/slice	3 µSv/scan (110 slices over 9.02 mm distance)
Detector type	Single cadmium telluride (CdTe) crystals (functional through a variety of temperatures)	CCD metal-oxide silicon (The silicon is sensitive to higher temperatures; therefore, a cooling mechanism is needed on HR-pQCT. This results in a larger and less portable scanner.)
Gantry depth	Unlimited	Limited
Protocols	Not standardized	Highly standardized
Cost	Lower cost	Higher cost

QCT uses the concepts of photoelectric absorption to detect bone. The number of photons passing through an object can be modeled using the Beer-Lambert law (shown below) (Wong, 2016). In this equation, the ratio between the intensity of transmitted photons (I_{out}) and intensity of incident photons (I_{in}) is negatively related to the thickness of the material (d) and the linear attenuation coefficient (µ) (which is affected by the photon energy and material density) (Wong, 2016). A greater number of photons will be captured by detectors if the material is thinner and less dense. Quantitative CT can differentiate between bone, muscle and fat due to the differences in the linear attenuation of these tissues (Wong, 2016).

$$\frac{I_{out}}{I_{in}} = -e^{\mu x d}$$

1.6.2.1 pQCT

Machine and Core Concepts

Peripheral QCT is an imaging modality with the advantage of short scan times, low radiation doses and high reproducibility (Srikhum *et al.*, 2013). It uses a purpose built scanner to scan extremities of the body such as the tibia and radius, while providing valuable information on the mechanical properties of bone (Chaplais *et al.*, 2014; Weatherholt *et al.*, 2016).

Peripheral QCT can be used to evaluate bone geometry, and separately determine vBMD for trabecular and cortical bone in a non-invasive manner with a low radiation dose (1 μSv/single scan) (Binkley and Specker, 2000; Fonseca *et al.*, 2013). Bone parameters such as total cross-sectional area and density, cortical area, thickness, and density, and trabecular area and density can be determined using pQCT (Binkley and Specker, 2000). Since the modality measures transaxial slices (cross-sections), it has the added benefit of not requiring adjustment for body size (Fonseca *et al.*, 2013). Additionally, information regarding bone strength can also be extracted from analysis, providing a better understanding of overall bone health. Scans can be acquired in a relatively short period of time (e.g. 9 mins), making it a feasible imaging modality for RA patients who have undergone various scans in a single day. But, the modality is limited by its accessibility and primary use solely in research studies (Fonseca *et al.*, 2013). In addition, although there is a vast array of data for bone density and geometry yielded by pQCT, a lot of the data is not comparable as there is a lack of standardization of the measurements (Fonseca *et al.*, 2013).

Use in Rheumatoid Arthritis and Past Studies

Currently, there is no standardization in pQCT protocols to assess vBMD in RA patients. Thus, studies have assessed outcomes based on different scan protocols and criteria. The most commonly used bone parameters are total, trabecular and cortical vBMD.

Reproducibility has been assessed using pQCT. The reliability in cadaveric feet (distal and midshaft regions of MTPJ 2) were assessed in one study; %CV values ≤10% were considered good reliability (Chaplais *et al.*, 2014). After repositioning, ICC values were 0.96-1.0, and %CV was 0.8-3.5%; the most reproducible variable was cortical vBMD (Chaplais *et al.*, 2014). All in all, good reproducibility can be achieved with pQCT for joints as small as the MTPJs. Other studies have also explored the reliability of pQCT at various sites of the tibia (Sievanen *et al.*, 1998; Veitch *et al.*, 2004; Shields *et al.*, 2006; Szabo *et al.*, 2011; Duff *et al.*, 2017) and radius (Sievanen *et al.*, 1998; Szabo *et al.*, 2011; Duff *et al.*, 2017), and demonstrated acceptable reproducibility.

Studies have also focused on medication use and the impact that it may have on bone density in RA patients using pQCT. One study assessed the role of corticosteroids in postmenopausal RA patients who were taking prednisolone and those who were oral corticosteroid naïve. There was no significant difference in bone outcome measures between the steroid-users and non-users. Thus, corticosteroids had little negative impact on bone density and RA demonstrated to be associated with significant loss of appendicular bone (e.g. hips, radius) (Martin *et al.*, 1997). In a similar study, the impact of low dose steroids on bone loss in RA was explored in peri- and postmenopausal

women. Trabecular bone loss was higher in the steroid treated group than the non-steroid users (Felder and Ruegsegger, 1991). The modest decrease of trabecular density and no effect on cortical density with steroid treatment suggested that estrogen depletion in postmenopausal women may be a greater contributor to loss of bone (Felder and Ruegsegger, 1991). Thus, pQCT-vBMD in both studies were able to assess the impact of steroid treatment in postmenopausal patients.

The pQCT scanner has previously been used for other bone related health issues, such as the impact of exercise on bone density measures in postmenopausal women (Polidoulis *et al.*, 2012), the effect of impact/nonimpact sports on bone health in premenopausal women (Nikander *et al.*, 2006), the variation in bone density based on menopausal status (Szabo *et al.*, 2011; Stathopoulos *et al.*, 2016), the potential for osteoporotic fracture risk (Siu *et al.*, 2003), and bone health in children (Fonseca *et al.*, 2013; Duff *et al.*, 2017; Vlok *et al.*, 2019). The pQCT scanner is ideal for measuring bone density in growing children as it measures cross-sectional area, independent of bone size, and images can be acquired within a short duration with little radiation (Fonseca *et al.*, 2013).

1.6.2.2 HR-pQCT

Machine and Core Concepts

High-resolution pQCT (HR-pQCT; dose: 3 μSv/single scan) is a modification of the conventional CT modalities. It is a non-invasive modality with the ability to take in vivo measurements of the vBMD (measured in units of mg HA/cm^3) and bone

microarchitecture (Barnabe *et al.*, 2016; Stagi *et al.*, 2016; Peters *et al.*, 2019). Protocols used in RA patients typically use a spatial resolution of 82μm, allowing for a resolution that is ~5 times greater than the pQCT modality (Fouque-Aubert *et al.*, 2010; Fonseca *et al.*, 2013; Zengin *et al.*, 2015). High resolution-pQCT can visualize bone structure and pathological features, such as erosions (Regensburger *et al.*, 2015; Barnabe *et al.*, 2016). The high resolution of this system allows for visualization of very small cortical breaks (Regensburger *et al.*, 2015). The system directly measures trabecular bone and uses this as a surrogate marker for trabecular bone volume, trabecular thickness, trabecular separation and bone strength (Zengin *et al.*, 2015). However, just like pQCT, HR-pQCT is sensitive to movement and results in motion artefacts; microarchitecture measures are more sensitive to motion than geometric and densitometry parameters (Stagi *et al.*, 2016).

Use in Rheumatoid Arthritis and Past Studies

The HR-pQCT scanner has shown to be beneficial in assessing erosion progression in RA patients, due to the smaller voxel sizes which can display better resolution than pQCT. As well, the ability for this modality to measure microstructural properties, such as trabecular separation, trabecular number and cortical porosity allow for better characterization of bone damage and disease progression (Cheung *et al.*, 2013).

Barnabe et al. and the Study group for xtrEme Computed Tomography in Rheumatoid Arthritis (SPECTRA) have previously defined erosions in HR-pQCT in hopes of standardizing erosion detection criteria (2016). The definition for an erosion, as determined by SPECTRA, is the presence of a definite interruption in cortical bone, a cortical break that extends over at least 2 consecutive slices detectable in 2 perpendicular

planes, loss of trabecular bone at the cortical break and a nonlinear shape (Barnabe *et al.*, 2016). The group also quantified erosions: maximal width ranged from 0.16-8.9 mm (mean 1.84 mm) and maximal depth ranged from 0.3-8.0 mm (mean 1.86 mm) (Barnabe *et al.*, 2016)

Previous studies with post-menopausal women have shown a reduction in vBMD and variations in trabecular and cortical bone architectures which were associated with vertebral and non-vertebral fractures (Boutroy *et al.*, 2005; Sornay-Rendu *et al.*, 2007). In another study, bone damage was assessed in early and late RA patients at MCPJs 2 and 3. RA patients had a lower total vBMD at MCP2, and lower trabecular vBMD at both MCPJ 2 and 3 (Fouque-Aubert *et al.*, 2010). Total and trabecular vBMD were negatively correlated with disease characteristics such as DAS28, ESR and CRP levels (Fouque-Aubert *et al.*, 2010). Thus, in both cases, measurements taken by HR-pQCT were associated with other disease outcomes.

1.6.3 Factors Impacting BMD

Bone mineral density is dependent on age, gender and ethnicity. Aging is associated with both intrinsic and extrinsic factors which reduce bone mass over time. Intrinsic factors include genetics, peak bone mass at youth, and biochemical and hormonal changes, whereas extrinsic factors include nutrition, physical activity and medical conditions (Demontiero *et al.*, 2012). Peak bone mass and size occurs at 15-20 years of age for women and later for men (Demontiero *et al.*, 2012). After this, bone turnover occurs at a slower rate due to the reduction in biochemical measures of bone

remodeling. The result of age associated bone loss is cortical thinning, increased cortical porosity, thinning of trabeculae and reduced trabecular connectivity (Demontiero *et al.*, 2012). The overall impact of these series of events results in a decrease in bone quality and strength (Demontiero *et al.*, 2012).

Age-adjusted DXA measures show that men generally have higher BMD than women (Looker *et al.*, 2009). Hip BMD measures have demonstrated that men older than 50 years of age experience BMD loss at a rate of 1.5-2.5% per decade (Papaioannou *et al.*, 2009). Longitudinal studies have demonstrated a crude rate of BMD loss of 0.3-0.5% per year at the hip for men (Papaioannou *et al.*, 2009). Prior to menopause, women experience accelerated bone loss at a yearly rate of ~1-2% (Curtis *et al.*, 2015). When women reach menopause, there is a significant increase in bone resorption, resulting in faster bone loss (Demontiero *et al.*, 2012). In one pQCT study, it was demonstrated that in healthy Japanese women, cortical bone volume and cortical BMD began to decrease after 40 years of age (Fujii *et al.*, 1995). In another study, men and women were divided into three groups: 50-60 years old, 60-70 years old and 70+ years old. Data showed that rate of bone loss was similar for all groups of men, however for women, there was greater loss of BMD in the 60-70 and 70+ groups (Daly *et al.*, 2013). Other studies have shown that women lose more trabecular bone than men and that cortical bone in men stays fairly constant whereas in women there is a reduction (Roschger *et al.*, 2003).

Ethnicity factors that may affect bone health include geography, diet, sunlight exposure, ancestry and physical features linked with race (e.g. height) (Zengin *et al.*, 2015). In terms of ethnicity, past studies have demonstrated that individuals of African

origin have the highest BMD, whereas Asian individuals have the lowest BMD (Barrett-Connor *et al.*, 2005). Hispanics and Caucasians have similar bone mass, which is an intermediate between the two extremes (Barrett-Connor *et al.*, 2005). Interestingly, a study reported that both Asians and individuals with African origin had the lowest fracture rates, whereas Caucasians and Hispanics had the highest fracture rates (Barrett-Connor *et al.*, 2005). The lower fracture risk in individuals with African origin can be attributed to the thicker cortices and higher connectivity within the trabecular microarchitecture (Zengin *et al.*, 2015). This is not an uncommon finding, as global age-matched data has demonstrated that white-American or British/European populations have higher incidences of fracture than other ethnic groups (Zengin *et al.*, 2015).

1.7 Initial Study Phase

This study is an extension of an initial observational study that involved patients who were newly diagnosed with RA and were treatment naïve (symptoms <2 years). Patients were diagnosed using the 2010 ACR/EULAR classification criteria (Aletaha *et al.*, 2010) and were excluded if they had any other arthritic diseases (e.g. gout). The MTPJs 2-5 were assessed clinically, and with US and peripheral MRI. The main results of the study demonstrated that US was able to detect subclinical inflammation, and suggested that US should be used alongside clinical examination in patients who do not display joint swelling.

During the preliminary phases of the foot imaging study, there have been discordances when it came to comparing the presence of erosions in MRI and US,

specifically for erosions that were grade ≤1. Thus, this study extension was undertaken to answer underlying questions from the last phase and to better characterize erosions seen in RA patients.

1.8 Objectives

To our knowledge, there have been no publications on pQCT-derived measures of vBMD in the MTPJs of patients with RA. Our study introduces a novel protocol which analyzes vBMD in the feet of RA patients, with aims of better characterizing periarticular bone in patients with inflammatory disease. To do so, we established 3 objectives:

1. Develop a reliable protocol for quantifying vBMD in MTPJs 2-5 by dividing MTPJs into two regions of interest;
2. Compare vBMD in patients with RA to vBMD of age, sex and ethnicity-matched individuals;
3. Assess the possible associations between vBMD and US parameters and MR erosions in RA patients.

The cortical subcortical region is the region of most interest as established cases of RA may be characterized by erosions, and therefore vBMD loss in the outer regions. We are hopeful that our results will allow more definite characterization on the presence/absence of the smaller erosions in the feet, as well as help us draw associations between the quantified vBMD and US parameters and MR erosion scores.

Chapter 2.0 Methods

2.1 Study Objectives

As a continuation of the previous study, one of the main goals of this project was to quantify vBMD as a potential surrogate marker of bone erosions. To accomplish this, three objectives were established. The first was to determine test-retest and rater reliability of a novel pQCT protocol for scanning the MTPJs. The second objective was to compare quantitative vBMD values between controls and RA patients as measured by the pQCT scanner. The last objective was to determine if there was an association between vBMD and clinical measures, US parameters and MR parameters.

2.2 Study Design

This is a longitudinal observational clinical study. Patients have completed up to 6 visits prior to this study appointment which were scheduled at baseline, 6 weeks, 3 months, 6 months, 1 year and ≥2 years. A clinical examination and US were performed at all time points. X-rays and MR scans were performed at baseline, 1 year and ≥2 years. Data for this thesis were acquired at the ≥3 year follow-up. The appointment included a clinical examination and US of the MCPJs and MTPJs, bilateral X-ray of the hands and feet, MR scan of the most symptomatic foot, and two pQCT scans of the most symptomatic foot.

Patient Recruitment

Patients with RA were recruited from an academic Rheumatology clinic. Patients were diagnosed based on the 2010 ACR/EULAR classification criteria. At baseline, patients were within ≤1 year of diagnosis, and were between 18 and 85 years of age. If they had been previously treated with a disease modifying agent, corticosteroid treatment (within the last 3 months) or had a significant arthritic disease, they were excluded from participating. At the baseline visit, data collection included demographic information (e.g. age, sex, occupation, etc.), clinical symptoms, the DAS28 score, HAQ score, VAS pain, antibody status (RF, ACPA), inflammatory markers (ESR, CRP), and medication history. A total of 42 patients were recruited.

In the current study, RA patients were recruited from the original cohort by telephone. Patient recruitment began in January 2019, upon approval by the Hamilton Integrated Research Ethics Board. A total of 25 RA patients agreed to return for a follow-up visit.

Control Recruitment

The pQCT segment of the study was designed to compare vBMD data between those with and without RA. Thus, healthy controls were recruited in a 1:1 ratio for normative comparison with RA patients matched for age, gender and ethnicity. Healthy controls included individuals who did not have inflammatory arthritis (osteoarthritis was acceptable) and were recruited through word of mouth, an online advertisement on Kijiji, and posters in the Charlton Medical building (25 Charlton Ave E). Based on the annual 1-

2% rate of BMD loss, age matched controls who were ±2 years were acceptable (Nilas and Christiansen, 1988; Curtis *et al.*, 2015). Given the majority of the patient population was Caucasian, mostly Caucasian controls were recruited. For the three non-Caucasians, patients were matched with controls from the same continent.

Study Population

Each individual enrolled in the study was provided with information about the purpose of the study, and potential risks and benefits. Consent forms were signed by each participant prior to beginning study protocol. In order to keep patient and control identities confidential, an ID number was assigned to each individual. To allow follow-up with patients, identifiers such as name and telephone number were collected at baseline.

Inclusion Criteria

Since patients were being recruited from the original cohort, new inclusion criteria were not defined. However, this time patients had to have had RA for ≥3 years rather than ≤1 year. In addition, most patients who participated in the study were on disease modifying agents (DMARDs and biologics) as this is the standard of care for RA.

Exclusion Criteria

Rheumatoid arthritis patients were excluded if they had any new contra-indications to MRI including in vivo/implanted metal (e.g. pacemaker, defibrillator,

metal/wire mesh implants, metal rods/pins/plates, tattoos), pregnancy or surgery (e.g. brain, vascular, bone, eye, head).

2.3 Clinical Examination

During the clinical examination, an update on clinical symptoms and medications was noted. The weight and height of patients were recorded. Based on any changes, an adjusted healthcare plan may have been suggested, such as change in medications or doses. Metatarsophalangeal joints 1-5 were assessed for swelling and tenderness (0=absent, 1=present) by an experienced rheumatologist (ML), forming a total swollen joint count (SJC) and tender joint count (TJC), respectively. However, MTPJ 1 will be excluded for purposes of analysis due to the overlap with other arthritic diseases in this region, such as gout. In addition, examination of MCPJs 1-5 and PIPJs 2 and 3 were determined for all patients. The most recent CRP lab values were noted, and if unavailable, bloodwork was ordered as recommended standard of care. ESR values were not reported in newer blood test reports.

Questionnaires

Prior to the clinic visit, patients were asked to complete the following questionnaires based on their current health status and lifestyle: LFIS and HAQ.

2.4 Scanning Protocol for Ultrasonography

The rheumatologist that performed all prior clinical examinations and US scans also performed all US scans in the current phase (ML). An US (Esoate MyLab70) with a 6-18 MHz linear array probe was used, at a frequency of 18 MHz. The US determined synovial thickening (ST), Power Doppler (PD) and erosions in MTPJs 2-5 in both feet, MCPJs 2 and 3 in both hands, PIPJs 2 and 3 in both hands, as well as in both wrists. For MTPJs 2-5, scans were taken for the dorsal and plantar side, and for MTPJ 5, the lateral side was also scanned. Synovial thickening and PD were scored semi-quantitatively (0-3; 0=absent, 3=marked/severe) for each joint, yielding a maximum score of 12 for each feature of the foot (Kawashiri *et al.*, 2014; do Prado *et al.*, 2018). Erosion was described as being absent or present based on the visualization of a cortical break seen in two perpendicular planes (Kawashiri *et al.*, 2014).

2.5 Scanning protocol for MRI

The MRI protocol was performed using the OrthoOne 1.0-T extremity scanner (GE Medical). The protocol acquired scans from the most symptomatic foot, as determined from previous phases of the study. Patients were comfortably seated on a reclining chair, with the base of their foot positioned in the scanner bore, allowing the legs to bend. The foot was stabilized with cushions inside the coil to reduce movement. The other foot was placed on a stool for comfort and ease. The same scanning sequences from the previous phases were used (based on the OMERACT RA MRI scoring system

(RAMRIS) protocol), although there was a minor adjustment – an extra axial sequence was added in order to better visualize and improve clarity for MTPJ 5.

Each scan began with an axial scout view to determine the positioning of the foot in the coil. All scans had a T1-weighted spin echo sequence to optimize the scan for the forefoot region. There were two sequences for the sagittal plane (repetition time (TR) 900 and 4800 ms, field of view (FOV) 150 mm, slice thickness 3 mm), two sequences for the coronal plane (TR 700 and 3600 ms, FOV 150 mm, slice thickness 3.5 mm), and three sequences for the axial plane (TR 950 and 5000 ms, FOV 120 mm, slice thickness 3mm) to determine synovitis, BME and erosions in the patient population.

For the current phase, images from the ≥3 year follow-up were not analyzed. For purposes of analyses, the results from the previous phase (≥2 year study visit) were used for comparison with the new bone density data.

Previously, MTPJs were divided into dorsal, plantar, medial and lateral regions; we have similarly divided pQCT bone slices this way as this analysis is beneficial for better identification of variations in densities and will continue to help in further elucidating the relation between erosions and pQCT results.

2.6 pQCT Scanning Protocol

A trained pQCT operator (JA) acquired all scans using a Stratec XCT 2000 device (Stratec Medizintechnik GmbH, software version 6.20). A cone phantom was scanned at the beginning of each study day for quality assurance and machine calibration. The cone phantom is composed of water and bone-equivalent solid materials, and is normalized for

testing of peripheral bone density parameters (Chaplais *et al.*, 2014). The effective dose of radiation for this protocol was 1 μSv per transaxial slice scan. There was a total of 16 slice scans (8 slice scans per protocol), resulting in a total radiation dose of 16 μSv.

For a thorough review of the protocol, please refer to the "SOP for pQCT MTPJ protocol" in *Appendix A2*. Briefly, MTPJs 2-5 were marked on the most symptomatic foot

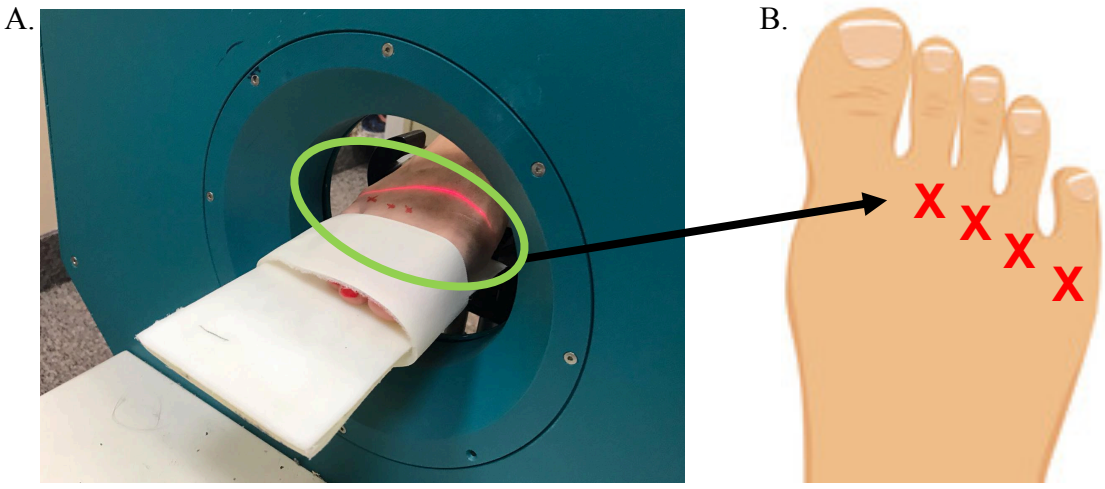

Figure 10. A. Forefoot centered in the middle of the pQCT gantry. B. Exterior coloured marker guides of MT heads 2-5.

of each RA patient, or the dominant foot of each healthy control. The foot was positioned on the custom-made plate, allowing for the foot to be positioned in the centre of the pQCT gantry (Fig. 10A). Correct positioning of the foot was ensured using the exterior coloured marker guides (Fig. 10B). A scout view scan of MTPJs 2-5 was performed prior to running the protocol to gage the positioning of the foot relative to the scanner, and to provide an anatomic reference line (locate scan range) (Fig. 11) (Stagi *et al.*, 2016). The

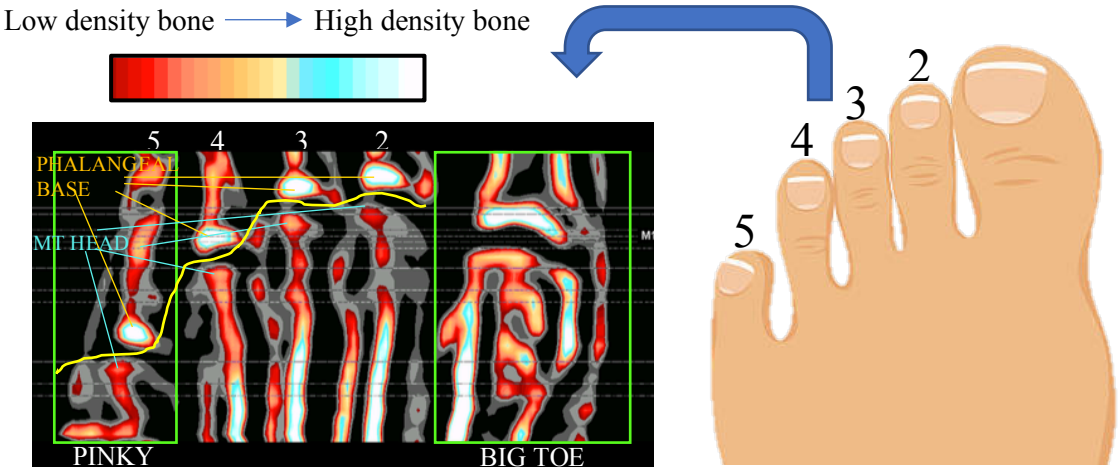

Figure 11. Scout view image of the left foot. The white circular figures represent the phalangeal bases (orange lines) and the red circular figures below that represent the MT heads (blue lines). The green boxes represent the major anatomical markers – the big toe and the pinky toe. Above the scout view image is a BMD scale, with red representing low density bone (e.g. trabecular bone) and white representing higher density bone (e.g. cortical bone).

protocol was set up with 4 reference lines, each consisting of 2 transaxial scans, for a total of 8 slice scans (Fig. 12). Slices 1 and 2 pertained to MTPJ 2, slices 3 and 4 to MTPJ 3, slices 5 and 6 to MTPJ 4, and slices 7 and 8 to MTPJ 5 (Table 4). Any analyses that were performed at the joint level used the average of the two slices for vBMD parameters. For each joint, one transaxial scan was placed 3.5 mm from the reference line and the other was placed 5.0 mm from the reference line. These distances were determined based on previous analyses of MR images which demonstrated that erosions were most prevalent in the region between 2.35 mm and 6.15 mm relative to the MT head. Each reference line

was placed at the distal end of the MT head of MTPJs 2, 3, 4 and 5.

Table 4: Slice Allocations for MTPJs 2-5	
MTPJ	**Average of:**
2	Slice 1 + 2
3	Slice 3 + 4
4	Slice 5 + 6
5	Slice 7 + 8

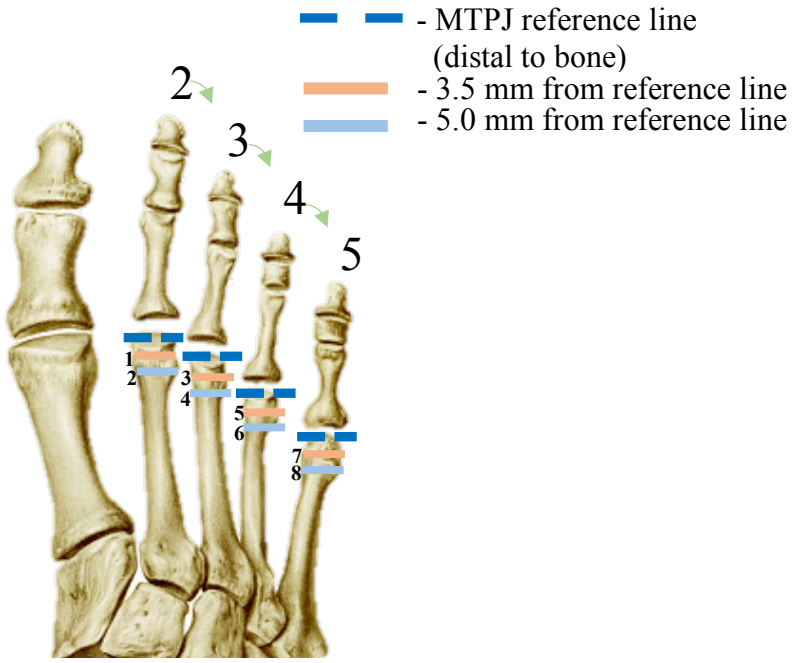

Figure 12. Slice assignment in the pQCT MTPJ protocol. After the scout view image was performed, reference lines were placed at the distal region/tip of the MT heads for MTPJs 2-5. Each MTPJ has two transaxial slice scans – the first at 3.5 mm from the reference line and the second at 5.0 mm from the reference line. The scan protocol began at slice 1 in MTPJ 2 and ended at slice 8 in MTPJ 5.

For RA patients the most symptomatic foot was scanned twice, with repositioning to allow for measurement of test-retest reliability. For controls, the dominant foot was scanned. The sampling resolution (voxel size) and scan speed were 0.40 mm and 40.00 mm/sec, respectively.

2.7 pQCT Analysis

For a thorough review of the analysis protocol, please refer to the "SOP for pQCT MTPJ analysis" in *Appendix A3*. Some vocabulary to familiarize with: Contour Mode -

detection of outer bone layer by separating bone from soft tissue, Peel Mode - separation of cortical from trabecular bone (Veitch *et al.*, 2004). These analysis parameters can be appropriately selected based on the judgement of the images by the rater. In addition, a threshold density is set by the operator, allowing voxels with lower density (e.g. noise) to be removed for analysis purposes. (Binkley and Specker, 2000)

Trabecular Percentage %

Trabecular percentage is a pre-determined value which is allocated to the trabecular region of bone within a MT, or the inner portion of the ROI. This represents the proportion of the bone comprised of trabecular bone.

Contour mode

There are three types of contour modes (CM): CM1, CM2 and CM3. CM1 differentiates bone from soft tissue based on the threshold that is manually set by the rater (e.g. 150 mg/cm^3). CM2 uses automatic detection to find the outer edge of the bone by evaluating the profile of the individual densities of the pixels. Then, the middle of the steepest gradient is used as the threshold. CM3 is similar to CM2 in the aspect that it is automatic, but allows the rater to adjust the threshold. It is important to note that CM2 and CM3 are not feasible to use in the MTPJs due to the thin cortical layer in this region. (Veitch *et al.*, 2004)

Peel mode

There are eight types of peel modes (PM): PM1-7 and PM20. For the purposes of this study, we have explored PM1-2. PM1 allocates the outer bone region based on the CM and peels off the cortical bone. The remains are the pre-determined trabecular percentage. Peel mode 2 detects voxels lower than the threshold and examines the neighbouring pixels to differentiate between the cortical and trabecular bone. Peel mode 1 was used for whole bone analyses and PM2 was used for quadrant analyses.

2.8 Study Analyses

For these analyses, PM1 was selected with a threshold of 150 mg/cm^3. The threshold was set based on the amount of visible trabecular bone. The percentage of peel (trabecular area %) was set to 49% based on the size of erosions determined by HR-pQCT, published by Barnabe et al., 2016 (calculation shown below) (Fig. 13). Thus, the inner 49% of bone was marked as trabecular bone, while the outer region was treated as cortical subcortical bone. For the purposes of our research question, we have chosen to use the cortical subcortical region rather than the cortical bone, as there is little cortical bone in the region that we are scanning in the MTPJs (~0.25 mm width), and it does not scan reliably on the pQCT machine due to the relatively large slice thickness (2.3 mm) used by the pQCT scanner (Jimenez-Boj *et al.*, 2007). In addition, choosing a percentage-driven analysis method ensures that the erosions/loss of BMD will be detected, if present.

Calculation of Trabecular Area Percentage

Equations

$Total\ area = \pi {R_2}^2$

$Trabecular\ area = \pi {R_1}^2$

$Average\ width\ of\ erosion = R_2 - R_1 = 1.84\ mm$

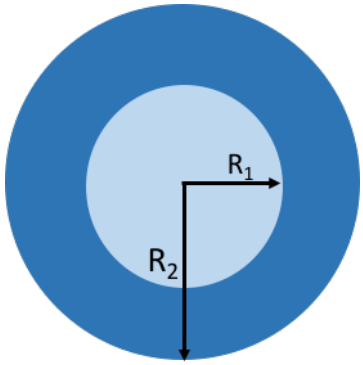

Figure 13. Radius of the total and trabecular areas (R_2 and R_1, respectively).

Calculations

1. $Total\ area = \pi {R_2}^2$

$$\therefore R_2 = \sqrt{\frac{total\ area}{\pi}} = \sqrt{\frac{116.45}{\pi}} = 6.09\ mm$$

2. $Average\ width\ of\ erosion = R_2 - R_1$

$$R_1 = R_2 - 1.84\ mm = 6.09\ mm - 1.84\ mm = 4.25\ mm$$

3. $Trabecular\ area = \pi {R_1}^2 = \pi(4.25)^2 = 56.70\ mm^2$

4. $$Trabecular\ \% = \frac{56.70\ mm^2}{116.45\ mm^2} * 100\% = 48.69\%$$

pQCT Bone Outcome Measures

The 6 bone outcomes that are determined by the XCT software are total density and area, trabecular density and area, and cortical subcortical density and area. Each image slice is composed of voxels. Voxels are similar to the pixels on an image, however each one is three-dimensional (Fig. 14). The quantitative value of each slice is the average density of a 2.3 mm wide slice. Total density considers the average density of the entire area (trabecular and cortical bone) (Fig. 15). The total area is simply the cross-sectional area of this. The trabecular density only accounts for voxels based on either the trabecular % (e.g. 49%) or the dictated density used to differentiate between cortical and trabecular bone. The trabecular area is the cross-sectional area of only the trabecular region. The cortical subcortical region is the outer region of the image slice. The voxels that compose the density of the cortical subcortical region are those that remain after the trabecular % has been removed (e.g. 51%). The same cross-sectional region is being accounted for in the cortical subcortical area (Fig. 16). For the purposes of this study, we have focused on total and cortical subcortical density due to their acceptable

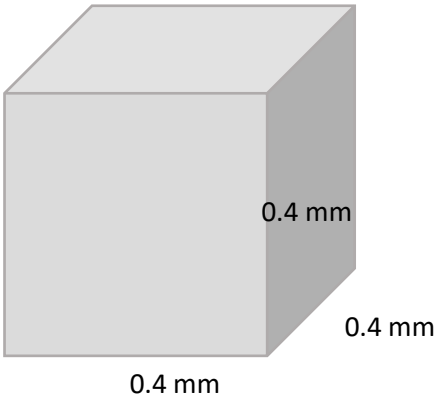

Figure 14. Image of a 3D voxel with the dimensions of 0.4*0.4*0.4mm.

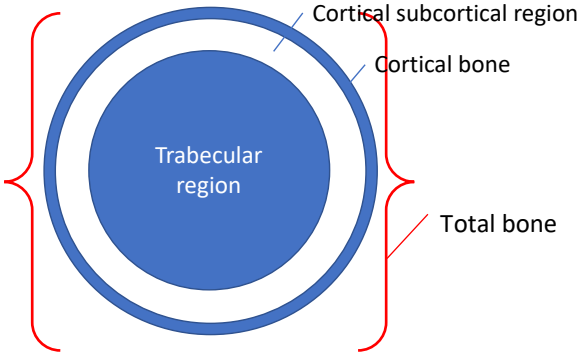

Figure 15. Bone areas of interest.

scanning and measurement reliability. Hereafter, they will be collectively referred to as bone parameters.

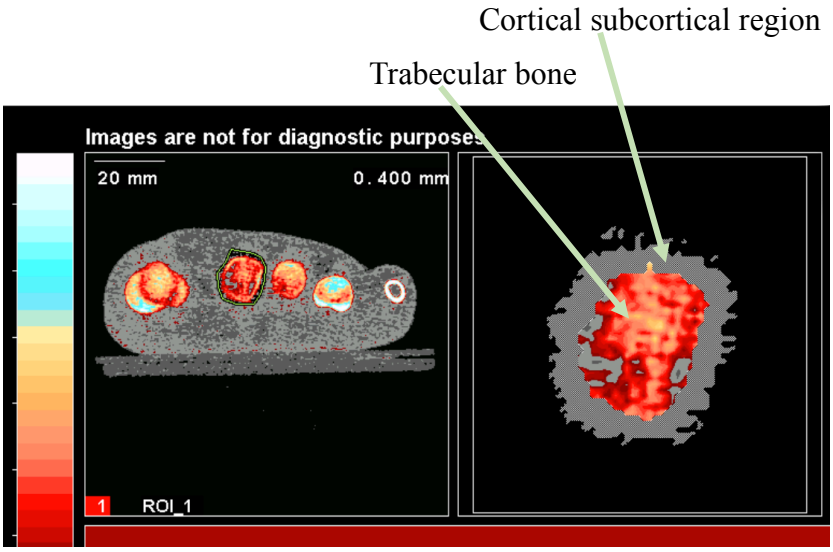

Figure 16. Software mediated division of the cortical subcortical region from the trabecular region.

Quadrants

In addition to analyzing the whole bone cross-section, we have subdivided the bone slices into 4 quadrants in order to compare these results to previous MR (≥2 year

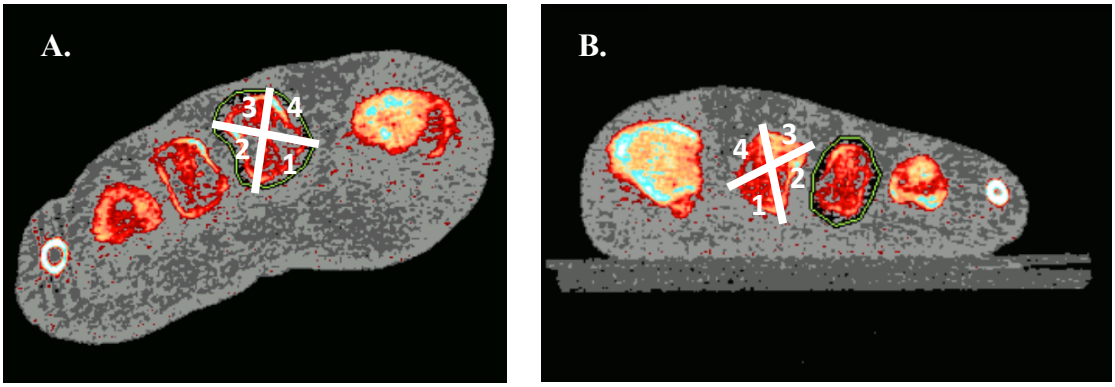

Figure 17. Quadrant assignment in A. the left foot and B. the right foot. Q1=plantar, Q2=lateral, Q3=dorsal, Q4=medial. Note that the lateral and medial regions are switched between the two feet as the medial region is assigned relative to the center of the body.

phase) images showing bone erosions. Quadrants (Q1-Q4) were analyzed for slices 1-4 only (Fig. 17).

Reliability

Since this pQCT protocol is the first of its kind, we have determined test-retest reliability, intra-rater reliability and inter-rater reliability. Additionally, to our knowledge, this modality has not been used to scan the MTPJs in an RA population. Thus, it is important to determine the reproducibility of positioning in the device, as well as the operator and rater reliability.

Test-retest reliability was determined using short-term precision error by acquiring two scans from each participant, and repositioning each person in between scans. This measure was used to determine the operator's reproducibility in positioning the foot in the same position each time, as well as marking the reference line in the same location using the XCT scanning software. As well, the variation in measurements taken by the modality are also reflected with this measure (Koo and Li, 2016).

Intra-rater reliability was determined by blindly selecting the ROI for each slice by a single rater (JA) on two occasions with the reader blinded to initial results. This measure allowed us to determine the variation in analysis when a single rater analysed the same image more than once. For whole bone and quadrant intra-rater reliability, the ROI was re-drawn twice at two different time points.

Lastly, for inter-rater reliability, two blinded raters (JA and AT) selected the whole bone ROI at two different times. This measure allowed us to determine the variation in analysis methods when two different individuals analyzed the same image.

2.9 Statistics

For all measures of pQCT reliability (test-retest, intra-rater, inter-rater), relative and absolute measures were reported with root mean square coefficients of variations (%RMSCV) and RMS standard deviation (RMSSD), respectively (refer to calculation below (Duff *et al.*, 2017)), and the MedCalc software (version 19.2.6) was used to report the 95% CI of %RMSCV. These measures are typically used for precision error analysis of pQCT and HR-pQCT protocols. According to previous densitometry studies and the International Society of Clinical Densitometry (ISCD), the generally acceptable benchmark for reproducibility using %RMSCV is <5% (Wong *et al.*, 2014). One pQCT study that assessed reproducibility in the MT bone used the criteria that %CV ≤10% was considered "good" reliability, thus we are being fairly conservative with the <5% threshold in our study (Chaplais *et al.*, 2014). Gluer et al. demonstrated that 27 degrees of freedom would be sufficient to report precision error, and suggested taking 3 measurements from 14 study participants or 2 measurements from 27 study participants to achieve this; our study used the latter recommendation (Gluer *et al.*, 1995).

$$\textit{Calculation for \%RMSCV} = 100 * \frac{\sqrt{\Sigma(\frac{d}{m})^2}}{2n}$$

Where d=difference between the two paired measures, m=mean of the paired measures, n=number of data pairs

The remaining analyses were performed using SPSS Statistics (version 24). For pQCT reliability, intraclass correlation coefficient (ICC) was reported. This method provided us with valuable information as it included both the degree of correlation and the agreement between measures (Koo and Li, 2016). ICC values <0.5 were considered poor, 0.5-0.75 were moderate, 0.75-0.9 were good, and values greater than 0.90 were considered excellent reliability (Koo and Li, 2016). There are multiple models that can be used for ICC depending on the nature of the analysis. For the purposes of our research question, we used a 2-way mixed effects model.

An independent t-test was run in order to determine if a statistically significant difference existed between total and cortical subcortical vBMD of RA patients and controls ($p<0.05$). Different approaches were taken to determine if there was a difference between the groups, including running an independent t-test between the populations for quadrants.

Lastly, the relationship between total and cortical subcortical vBMD measures were compared to clinical and imaging findings. Relationships between vBMD and each of the clinical findings (SJC and TJC) and US parameters (ST and PD) were presented using bar graphs (95% CI error bars reported). Pearson and Spearman correlation analyses were performed for patient reported symptoms and vBMD measures (interpretation: 0.00-0.30 (negligible correlation), 0.30-0.50 (low correlation), 0.50-0.70 (moderate correlation), 0.70-0.90 (high correlation), 0.90-1.00 (very high correlation)) (Mukaka, 2012). MR erosion data was presented with descriptive statistics due to the low

number of erosions in the cohort. As well, quadrant vBMD and bone erosion data were compared in patients with more severe disease (an MR erosion score ≥2).

Chapter 3.0 Results

3.1 Patients

Twenty-five patients between the ages of 23-72 years (mean (SD) age, 57.8 (10.2) years; 88% female) were recruited. The average (SD) disease duration was 5.0 (0.9) years. Patients received medications as per standard of care. Twenty patients (80%) were on DMARDs, 10 patients (40%) were on biologics, and 2 patients (8%) were taking neither; some patients were on more than one medication. Further details on patient characteristics and medications are below (Table 5).

Table 5: Clinical Findings in RA Patients		
SJC, mean (SD)*		2.2 (2.3)
TJC, mean (SD)*		2.6 (4.0)
CRP (mg/L), mean (SD)		3.91 (4.65)
HAQ, mean (SD)		0.64 (0.63)
Patient global, mean (SD)		2.5 (2.4)
CDAI calculated, mean (SD)		9.8 (8.5)
DAS28-CRP, mean (SD)		2.64 (1.20)
Morning stiffness (mins), mean (SD)		30.88 (63.42)
DMARD, n		
	Methotrexate (Trexall)	10
	Leflunomide (Arava)	4
	Hydroxychloroquine (Plaquenil)	4
	Sulfasalazine (Azulfidine)	2
Biologics, n		
	Adalimumab (Humira)	1
	Etanercept (Enbrel)	1
	Tofacitinib (Xeljanz)	4
	Rituximab (Rituxan)	1
	Abatacept (Orencia)	2
	Tocilizumab (Actemra)	1

*Note that the mean SJC and TJC listed here are those used for the CDAI calculation (includes MCPJs 1-5, PIPJs 1-5, shoulders, elbows, wrists, knees)

3.2 Test-Retest Reliability

RA Patients

Test-retest reliability demonstrates better precision for some slices than others. In RA patients, reproducibility is most optimal for slices 1 and 2 in total density, as the %RMSCV lies below the 5% benchmark. Precision in total density for slices 3 and 4, and cortical subcortical density for slices 1-4 is close to the 5% threshold. The %RMSCV is worse for slices 5-8 and thus, demonstrates more variability. The %RMSCV corresponds to the RMSSD values, with higher RMSSD values agreeing with the lower reliability in slices 5-8. (Table 6)

In terms of ICC, both total and cortical subcortical density show excellent reliability for slices 1-4 (except slice 4 for total density). However, in accordance with Table 6, the reliability appears to worsen in slices 5-8, with ICC scores in the range of poor, moderate and good, and with relatively wide confidence intervals. (Table 7)

Table 6: Test-Retest Reliability in RA Patients Using %RMSCV, n=25

Slice	Total Density			Cortical subcortical Density		
	%RMSCV	RMSSD (mg/cm^3)	95% CI	%RMSCV	RMSSD (mg/cm^3)	95% CI
1	4.21	13.00	2.29-5.49	5.48	14.68	0.00-8.13
2	3.16	8.63	1.92-4.04	6.46	18.06	3.79-8.32
3	5.57	15.16	3.16-7.22	5.32	13.27	3.46-6.68
4	5.78	16.67	0.00-8.24	5.60	15.70	3.51-7.10
5	11.52	32.89	2.43-16.11	12.02	37.27	0.00-18.00
6	14.40	45.11	0.00-21.45	12.40	32.18	4.95-16.82
7	11.74	35.89	7.50-14.81	9.45	30.90	5.24-12.29
8	9.31	29.23	5.03-12.17	9.62	28.50	5.99-12.22

Table 7: Test-Retest Reliability in RA Patients Using ICC, n=25

Slice	Total Density		Cortical subcortical Density	
	ICC	95% CI	ICC	95% CI
1	0.96	0.91-0.98	0.96	0.90-0.98
2	0.98	0.95-0.99	0.93	0.84-0.97
3	0.91	0.80-0.96	0.95	0.89-0.98
4	0.90	0.74-0.95	0.93	0.78-0.97
5	0.65	0.20-0.85	0.57	0.05-0.81
6	0.40	-0.33-0.73	0.61	0.14-0.83
7	0.69	0.29-0.86	0.83	0.60-0.92
8	0.85	0.66-0.93	0.90	0.77-0.95

Controls

Scan-rescan reliability appears better in healthy participants than RA patients. There is less variability between scans for slices 1-6 in both density outcomes of interest, with %RMSCV values below the 5% benchmark in most cases. The variability increases in slices 7 and 8. The agreement between %RMSCV and RMSSD remains in controls as it did in RA patients. (Table 8)

ICC values for both total and cortical subcortical density demonstrate excellent reliability in most cases. The only exceptions are slice 8 for total density, and slices 7 and 8 for cortical subcortical density, both of which demonstrate good reliability. (Table 9)

Table 8: Test-Retest Reliability in Controls Using %RMSCV, n=27

Slice	Total Density			Cortical subcortical Density		
	%RMSCV	RMSSD (mg/cm^3)	95% CI	%RMSCV	RMSSD (mg/cm^3)	95% CI
1	2.23	6.69	0.91-3.02	3.09	9.08	1.74-4.01
2	1.81	5.22	0.00-2.55	2.51	8.61	0.74-3.47
3	4.11	11.46	0.00-6.41	3.30	9.72	1.81-4.31
4	3.33	8.47	0.00-4.96	4.69	13.15	0.53-6.60
5	3.93	10.33	1.83-5.25	3.60	9.50	2.12-4.62
6	4.40	11.95	2.69-5.61	5.65	16.26	3.29-7.28
7	6.19	16.89	2.84-8.27	8.42	23.66	4.08-11.18
8	7.95	22.80	1.12-11.19	10.37	31.53	3.46-14.25

Table 9: Test-Retest Reliability in Controls Using ICC, n=27

Slice	Total Density		Cortical subcortical Density	
	ICC	95% CI	ICC	95% CI
1	0.99	0.97-0.99	0.98	0.96-0.99
2	0.99	0.98-1.00	0.98	0.97-0.99
3	0.93	0.85-0.97	0.96	0.91-0.98
4	0.97	0.92-0.98	0.92	0.83-0.96
5	0.95	0.89-0.98	0.96	0.92-0.98
6	0.95	0.89-0.98	0.92	0.82-0.96
7	0.92	0.83-0.97	0.89	0.75-0.95
8	0.89	0.75-0.95	0.87	0.72-0.94

3.3 Intra-Rater Reliability

3.3.1 Whole Bone Slices

RA Patients

Intra-rater reliability is well below the 5% benchmark for %RMSCV values. In all cases, the values are within 1-2%, demonstrating high reliability. RMSSD also demonstrates agreement with %RMSCV, with lower RMSSD for slices that have higher reliability and higher RMSSD for slices that have lower reliability. When comparing between the two parameters, total density has less variability than cortical subcortical density. (Table 10)

In addition, ICC values all demonstrate excellent reliability. Interestingly, the ICC values for total density are slightly stronger than those of cortical subcortical density. (Table 11)

Table 10: Whole Bone Intra-Rater Reliability in RA Patients Using %RMSCV, n=25

Slice	Total Density			Cortical subcortical Density		
	%RMSCV	RMSSD (mg/cm^3)	95% CI	%RMSCV	RMSSD (mg/cm^3)	95% CI
1	0.75	2.26	0.48-0.94	1.66	4.93	0.99-2.13
2	1.03	2.98	0.00-1.47	2.48	7.86	0.00-3.91
3	0.94	2.61	0.42-1.25	2.06	6.28	0.00-2.92
4	0.94	2.45	0.49-1.23	1.79	5.04	1.04-2.31
5	1.28	2.81	0.07-1.81	2.19	5.27	0.90-2.96
6	0.85	2.17	0.37-1.15	1.60	4.59	0.59-2.19
7	1.19	3.10	0.31-1.65	2.38	6.59	0.32-3.35
8	0.83	2.44	0.52-1.05	1.55	4.84	1.07-1.92

Table 11: Whole Bone Intra-Rater Reliability in RA Patients Using ICC, n=25

Slice	Total Density		Cortical subcortical Density	
	ICC	95% CI	ICC	95% CI
1	1.00	1.00	1.00	0.99-1.00
2	1.00	0.99-1.00	0.99	0.96-1.00
3	1.00	0.99-1.00	0.99	0.97-0.99
4	1.00	0.99-1.00	0.99	0.98-1.00
5	1.00	0.98-1.00	0.99	0.96-1.00
6	1.00	0.99-1.00	0.99	0.98-1.00
7	1.00	0.99-1.00	0.99	0.97-1.00
8	1.00	1.00	1.00	0.99-1.00

Controls

Similar to RA patients, the density measures are highly reproducible with %RMSCV below 2% in all cases when a single rater analyzes the images. RMSSD demonstrates agreement with %RMSCV. As seen with RA patients, the reproducibility is higher in total density than cortical subcortical density. (Table 12)

To add, ICC values for all slices in both parameters of interest are >0.9, demonstrating excellent reliability. It appears that ICC values for both parameters of interest are very similar to each other. (Table 13)

Table 12: Whole Bone Intra-Rater Reliability in Controls Using %RMSCV, n=27

Slice	Total Density			Cortical subcortical Density		
	%RMSCV	RMSSD (mg/cm^3)	95% CI	%RMSCV	RMSSD (mg/cm^3)	95% CI
1	0.55	1.73	0.37-0.68	1.08	3.40	0.75-1.33
2	0.40	1.20	0.30-0.48	0.81	2.70	0.66-0.93
3	0.43	1.19	0.24-0.56	0.88	2.44	0.48-1.14
4	0.47	1.31	0.33-0.57	0.66	1.95	0.47-0.81
5	0.37	0.91	0.22-0.48	0.78	1.91	0.31-1.05
6	0.49	1.29	0.21-0.67	1.03	2.62	0.00-1.47
7	0.70	2.28	0.32-0.94	1.17	4.16	0.47-1.58
8	0.73	2.43	0.30-0.98	1.60	5.68	0.21-2.26

Table 13: Whole Bone Intra-Rater Reliability in Controls Using ICC, n=27

Slice	Total Density		Cortical subcortical Density	
	ICC	95% CI	ICC	95% CI
1	1.00	1.00	1.00	1.00
2	1.00	1.00	1.00	1.00
3	1.00	1.00	1.00	1.00
4	1.00	1.00	1.00	1.00
5	1.00	1.00	1.00	1.00
6	1.00	1.00	1.00	1.00
7	1.00	1.00	1.00	0.99-1.00
8	1.00	1.00	1.00	0.99-1.00

3.3.2 Quadrants

RA Patients

In terms of quadrant divisions, the reproducibility of manual selection of quarter ROIs was determined. All quadrants, aside from Q4 in slice 4, demonstrate acceptable reliability for both total and cortical subcortical density, with %RMSCV values below 5%. For both parameters of interest, Q4 consistently has the highest variability across all slices, with high %RMSCV and RMSSD values. As well, Q3 has the lowest variability in most cases. (Table 14)

Similar to intra-rater reliability in whole bone analysis, ICC for quadrants demonstrates excellent reliability across all measures. Quadrant 4 had poorer reproducibility, but ICC values were not far from the other quadrants. (Table 15)

Table 14: Quadrant Intra-Rater Reliability in RA Patients Using %RMSCV, n=25

Slice	Quadrant (Q)	Total Density			Cortical subcortical Density		
		%RMSCV	RMSSD (mg/cm^3)	95% CI	%RMSCV	RMSSD (mg/cm^3)	95% CI
1	Q1	2.01	6.06	1.20-2.58	2.94	8.26	2.18-3.54
	Q2	2.33	6.78	1.26-3.05	3.69	12.21	2.06-4.80
	Q3	1.48	4.87	0.84-1.91	2.14	7.33	1.36-2.70
	Q4	3.78	9.11	1.98-4.96	5.53	14.25	3.42-7.03
2	Q1	2.83	7.15	0.00-4.01	4.00	10.53	1.41-5.48
	Q2	3.85	11.08	2.33-4.93	4.55	14.77	3.22-5.57
	Q3	2.42	8.07	1.37-3.13	2.65	9.28	0.47-3.72
	Q4	4.69	11.90	0.00-6.78	4.73	12.73	1.60-6.49
3	Q1	1.84	4.67	1.40-2.20	3.64	9.11	2.68-4.39
	Q2	3.47	8.24	0.57-4.88	3.97	9.73	2.46-5.06
	Q3	1.94	6.03	0.99-2.56	2.64	8.80	1.45-3.44
	Q4	4.57	11.30	2.80-5.82	4.66	12.13	2.70-6.01
4	Q1	2.32	5.80	1.25-3.03	3.76	9.16	2.18-4.85
	Q2	4.78	12.02	2.49-6.28	5.27	13.73	3.02-6.81
	Q3	1.73	5.14	1.24-2.11	2.99	9.12	1.80-3.83
	Q4	6.05	15.20	3.93-7.61	6.42	17.17	4.43-7.92

Table 15: Quadrant Intra-Rater Reliability in RA Patients Using ICC, n=25

Slice	Quadrant (Q)	Total Density		Cortical subcortical Density	
		ICC	95% CI	ICC	95% CI
1	Q1	0.99	0.98-1.00	0.99	0.97-1.00
	Q2	0.99	0.97-1.00	0.97	0.94-0.99
	Q3	1.00	0.99-1.00	0.99	0.99-1.00
	Q4	0.99	0.97-1.00	0.97	0.94-0.99
2	Q1	0.99	0.93-1.00	0.98	0.93-0.99
	Q2	0.95	0.90-0.98	0.94	0.85-0.98
	Q3	0.99	0.97-1.00	0.99	0.97-1.00
	Q4	0.97	0.93-0.99	0.97	0.94-0.99
3	Q1	0.99	0.97-0.99	0.95	0.89-0.98
	Q2	0.98	0.94-0.99	0.97	0.93-0.99
	Q3	0.99	0.98-1.00	0.99	0.97-1.00
	Q4	0.95	0.89-0.98	0.96	0.92-0.98

4	Q1	0.98	0.90-0.99	0.95	0.86-0.98
	Q2	0.94	0.86-0.98	0.93	0.82-0.97
	Q3	1.00	0.98-1.00	0.99	0.98-1.00
	Q4	0.88	0.69-0.95	0.91	0.79-0.96

Controls

Quadrant data for controls demonstrates that all vBMD outcomes are reproducible, with %RMSCV values below 5%. In all cases (except slice 4 cortical subcortical density), the variability in Q4 is the highest. Similar to RA patients, controls also have the highest reliability in Q3. (Table 16)

ICC values for quadrant precision in healthy subjects are all in the range of excellent reliability. There appears to be little variability between quadrants of the same slice. (Table 17)

Table 16: Quadrant Intra-Rater Reliability in Controls Using %RMSCV, n=27

Slice	Quadrant	Total Density			Cortical subcortical Density		
		%RMSCV	RMSSD (mg/cm^3)	95% CI	%RMSCV	RMSSD (mg/cm^3)	95% CI
1	Q1	2.16	6.49	1.35-2.74	2.74	7.87	2.14-3.22
	Q2	2.44	6.74	1.23-3.22	2.99	9.08	1.78-3.84
	Q3	1.81	6.10	1.07-2.32	2.39	8.34	1.72-2.90
	Q4	4.19	10.64	1.57-5.72	4.48	11.78	2.66-5.75
2	Q1	2.25	6.39	1.23-2.93	3.12	9.39	1.86-4.01
	Q2	2.45	6.99	0.90-3.34	3.05	9.86	2.11-3.76
	Q3	1.65	5.19	0.51-2.28	2.60	8.09	0.97-3.54
	Q4	4.80	12.72	2.26-6.40	3.73	10.78	2.33-4.73
3	Q1	2.23	5.97	1.22-2.92	3.99	10.76	1.64-5.40
	Q2	2.57	6.47	1.68-3.23	3.42	9.52	1.80-4.48
	Q3	1.78	5.77	1.28-2.18	2.27	7.54	1.42-2.87
	Q4	4.86	12.33	2.53-6.39	6.00	15.87	3.69-7.64
4	Q1	2.52	6.17	0.00-3.58	3.90	9.98	2.14-5.09
	Q2	2.52	6.61	0.92-3.44	2.60	7.24	1.63-3.30
	Q3	1.25	3.92	0.84-1.55	2.25	6.27	1.01-3.02
	Q4	5.20	12.87	2.78-6.81	3.58	9.49	1.47-4.84

Table 17: Quadrant Intra-Rater Reliability in Controls Using ICC, n=27

Slice	Quadrant	Total Density		Cortical subcortical Density	
		ICC	95% CI	ICC	95% CI
1	Q1	0.98	0.90-0.99	0.98	0.94-0.99
	Q2	0.99	0.97-0.99	0.99	0.97-0.99
	Q3	0.99	0.99-1.00	0.99	0.98-1.00
	Q4	0.98	0.95-0.99	0.98	0.96-0.99
2	Q1	0.98	0.93-0.99	0.97	0.92-0.99
	Q2	0.98	0.96-0.99	0.98	0.96-0.99
	Q3	1.00	0.99-1.00	0.99	0.99-1.00
	Q4	0.97	0.94-0.99	0.98	0.96-0.99
3	Q1	0.98	0.93-0.99	0.92	0.80-0.97
	Q2	0.98	0.96-0.99	0.97	0.92-0.99
	Q3	0.99	0.98-1.00	0.99	0.98-1.00
	Q4	0.95	0.90-0.98	0.94	0.87-0.97
4	Q1	0.98	0.91-0.99	0.95	0.79-0.98
	Q2	0.98	0.95-0.99	0.98	0.96-0.99
	Q3	1.00	0.99-1.00	0.99	0.98-1.00
	Q4	0.95	0.88-0.98	0.98	0.95-0.99

3.4 Inter-Rater Reliability

RA Patients

For RA patients, inter-rater data demonstrates good reliability, with %RMSCV values <3%. Cortical subcortical density has higher variability than total density at each slice, with RMSSD showing agreement with this trend when comparing between the two parameters. (Table 18)

As well, ICC demonstrates excellent reliability. The ICC values for total density are slightly stronger than cortical subcortical density, although values are very close. (Table 19)

Table 18: Whole Bone Inter-Rater Reliability in RA Patients Using %RMSCV, n=25

Slice	Total Density			Cortical subcortical Density		
	%RMSCV	RMSSD (mg/cm^3)	95% CI	%RMSCV	RMSSD (mg/cm^3)	95% CI
1	1.54	4.33	0.00-2.23	2.95	8.62	0.65-4.12
2	0.63	1.84	0.45-0.77	1.79	5.66	0.81-2.40
3	1.29	3.50	0.00-1.88	2.97	9.11	0.00-4.54
4	1.13	2.97	0.62-1.48	1.96	5.60	1.02-2.58
5	1.00	2.34	0.00-1.47	1.36	3.46	0.86-1.72
6	0.53	1.21	0.26-0.70	1.45	3.49	0.00-2.30
7	2.19	5.53	0.00-3.39	2.47	7.12	1.43-3.19
8	1.87	4.52	0.00-3.16	2.48	6.61	0.00-3.97

Table 19: Whole Bone Inter-Rater Reliability in RA Patients Using ICC, n=25

Slice	Total Density		Cortical subcortical Density	
	ICC	95% CI	ICC	95% CI
1	1.00	0.99-1.00	0.99	0.97-0.99
2	1.00	1.00	0.99	0.99-1.00
3	1.00	0.99-1.00	0.97	0.94-0.99
4	1.00	0.99-1.00	0.99	0.98-1.00
5	1.00	1.00	1.00	0.99-1.00
6	1.00	1.00	1.00	0.99-1.00
7	0.99	0.98-1.00	0.99	0.98-1.00
8	1.00	0.99-1.00	1.00	0.99-1.00

Controls

For controls, %RMSCV values are well below 5% and are generally within the range of 1-2%. Similar to RA patients, the variability in rater measurements is higher in cortical subcortical density than total density. (Table 20)

ICC also demonstrates excellent reliability. Total density ICC values demonstrate stronger resemblance of measurements taken by the two raters, in comparison to those taken for cortical subcortical density. (Table 21)

Table 20: Whole Bone Inter-Rater Reliability in Controls Using %RMSCV, n=27

Slice	Total Density			Cortical subcortical Density		
	%RMSCV	RMSSD (mg/cm^3)	95% CI	%RMSCV	RMSSD (mg/cm^3)	95% CI
1	0.89	2.86	0.44-1.19	1.90	5.81	0.80-2.57
2	0.83	2.49	0.39-1.11	1.71	5.53	0.86-2.26
3	0.86	2.43	0.55-1.08	1.78	5.19	0.88-2.36
4	0.76	2.22	0.52-0.94	1.23	3.68	0.86-1.51
5	0.72	1.78	0.35-0.96	1.37	3.60	0.72-1.80
6	0.86	2.43	0.54-1.09	1.66	4.89	1.00-2.12
7	1.02	3.35	0.00-1.47	1.92	6.49	0.73-2.61
8	1.06	3.66	0.19-1.48	2.17	7.83	0.32-3.05

Table 21: Whole Bone Inter-Rater Reliability in Controls Using ICC, n=27

Slice	Total Density		Cortical subcortical Density	
	ICC	95% CI	ICC	95% CI
1	1.00	1.00	1.00	0.99-1.00
2	1.00	1.00	1.00	0.99-1.00
3	1.00	1.00	0.99	0.98-1.00
4	1.00	1.00	1.00	0.99-1.00
5	1.00	1.00	1.00	0.99-1.00
6	1.00	1.00	0.99	0.99-1.00
7	1.00	1.00	1.00	0.99-1.00
8	1.00	0.99-1.00	0.99	0.99-1.00

3.5 Bone Outcome Measures

Whole Bone Data

We explored the potential differences in density between RA patients and healthy subjects. Both total and cortical subcortical density appear to be higher in controls than RA patients at each respective slice. There is a statistically significant difference between measures at slices 3, 5 and 6 for both parameters. Standard deviation values in all cases appear larger in the most lateral and medial joints (slices 1, 2, 7, 8) than the inner joints (slices 3-6). As well, in most cases for both parameters, the minimum density value for RA patients is lower than that of controls for a given slice, while the maximum density value for controls is higher than that of RA patients for a given slice. Thus, the range for RA patients is on the lower end when compared to controls. (Table 22 and 23)

Table 22: Mean Total Density in RA patients and Controls

Slice	Total Density (mg/cm^3)							
	RA Patients				Controls			
	Mean	SD	Min.	Max.	Mean	SD	Min.	Max.
1	285.54	43.88	204.90	372.70	299.74	42.77	216.10	379.60
2	274.06	41.01	195.30	344.30	291.57	43.83	200.40	366.20
3	251.45*	33.25	185.10	317.10	272.52*	32.83	226.20	338.90
4	247.43	34.27	176.50	307.40	264.94	31.28	221.60	334.90
5	227.37*	35.37	140.40	288.90	254.63*	33.10	207.40	329.00
6	231.15*	37.14	148.70	318.60	253.67*	39.61	185.80	345.10
7	261.62	45.83	172.90	365.10	285.33	49.33	180.40	385.20
8	277.38	55.29	184.80	393.30	285.38	51.46	192.50	394.20

*statistically significant difference between the two populations ($p<0.05$)

Table 23: Mean Cortical Subcortical Density in RA patients and Controls

Slice	Cortical Subcortical Density (mg/cm^3)							
	RA Patients				Controls			
	Mean	SD	Min.	Max.	Mean	SD	Min.	Max.
1	289.78	47.83	208.90	390.70	305.06	49.47	224.20	392.10
2	288.31	49.51	208.20	405.20	311.16	51.24	220.90	425.60
3	260.28*	40.30	195.30	360.40	281.43*	34.28	225.60	353.50

4	261.74	45.44	193.90	364.90	277.54	33.88	222.70	344.40
5	237.24*	35.57	163.40	299.50	268.92*	35.46	198.10	354.90
6	246.16*	39.19	172.50	341.60	274.00*	43.43	200.70	400.50
7	270.74	49.51	193.10	357.20	295.38	57.40	190.90	430.40
8	295.91	65.84	192.10	444.40	303.78	68.54	195.50	486.00

*statistically significant difference between the two populations ($p<0.05$)

Quadrant Data

Based on the high prevalence of erosions in MTPJs 2 and 3 as well as the acceptable test-retest reliability in these joints from Chapter 3.2 (Table 6 and 8), we have opted to further explore quadrant data only for slices 1-4 (Naumann *et al.*, 2012; Albrecht *et al.*, 2013; Kong *et al.*, 2018).

When comparing quadrants between RA patients and healthy subjects, the average total density appears to be higher in controls than patients at each quadrant across all slices. However, there is only a statistically significant difference between the populations at Q3 of slice 3. In all slices for both populations, total vBMD is highest at Q3. In slices 1 and 2, the vBMD in both populations is lowest in Q4. In most cases, the SD appears to be lower in Q1 and Q2, in comparison to Q3 and Q4. Interestingly, in slices 2-4, the minimum vBMD in RA patients appears to be lower than in controls for Q1-Q3, but at Q4, RA patients appear to have a higher vBMD than controls. There is no consistent trend seen for maximum values. (Table 24)

In terms of cortical subcortical density, mean vBMD measures generally appear higher for controls than RA patients at the quadrant level of each slice. There is a statistically significant difference between the two populations for Q1 of slice 4. In both populations, Q3 has the highest density at all slices. Between quadrants of the same slice, the vBMD in Q1 is the lowest among both of the populations. Similar to the trend seen in

total density, the SD appears to be higher in Q3 and Q4 compared to Q1 and Q2 in both populations. As seen with total density, RA patients appear to have a lower minimum density than controls for Q1-Q3, except in Q4, where the vBMD appears to be higher in RA patients (consistent for all slices except slice 2). (Table 25)

Table 24: Mean Quadrant Total Density in RA patients and Controls

Slice	Quadrant	Total Density (mg/cm^3)							
		RA Patients				Controls			
		Mean	SD	Min.	Max.	Mean	SD	Min.	Max.
1	1	275.25	48.07	202.50	391.10	278.66	30.81	229.00	334.20
	2	286.90	44.05	198.70	374.90	288.32	42.25	223.10	396.90
	3	332.56	55.18	213.30	411.20	351.14	58.39	272.00	468.30
	4	268.45	57.10	184.90	404.50	278.66	54.44	194.50	391.40
2	1	265.30	42.46	190.40	363.50	275.66	29.17	218.80	348.40
	2	287.80	37.72	201.40	380.80	294.44	37.81	228.90	363.40
	3	322.42	53.05	224.70	405.60	345.60	60.94	240.90	453.40
	4	257.07	47.83	182.40	385.20	273.79	56.93	165.70	396.10
3	1	249.02	29.59	193.00	313.00	259.37	30.10	212.90	304.30
	2	244.30	37.54	172.00	342.10	256.31	35.24	212.20	333.30
	3	293.10*	46.71	204.40	389.00	323.54*	39.39	263.70	414.30
	4	253.06	37.79	191.20	341.30	261.32	40.61	187.30	368.60
4	1	241.83	25.16	193.40	288.60	255.14	28.66	197.60	309.10
	2	253.84	35.16	203.70	364.30	261.18	33.54	211.10	358.10
	3	290.34	50.19	211.00	392.30	309.70	40.03	252.60	397.60
	4	257.56	30.43	218.50	321.80	254.76	39.76	186.70	344.10

*statistically significant difference between the two populations ($p<0.05$)

Table 25: Mean Quadrant Cortical Subcortical Density in RA patients and Controls

Slice	Quadrant	Cortical Subcortical Density (mg/cm^3)							
		RA Patients				Controls			
		Mean	SD	Min.	Max.	Mean	SD	Min.	Max.
1	1	274.38	55.43	208.10	410.10	274.91	39.47	222.20	351.90
	2	302.01	51.86	200.10	406.80	304.33	51.27	230.60	423.50
	3	355.20	70.84	196.70	475.00	370.74	72.80	266.00	508.10
	4	279.22	61.58	216.50	424.00	298.61	65.29	199.20	431.20
2	1	272.56	49.84	205.00	388.20	284.41	36.36	225.90	367.40
	2	304.05	41.98	208.90	431.00	324.62	52.64	229.20	411.10
	3	347.22	73.61	208.40	488.50	367.00	75.06	232.20	498.50
	4	276.72	55.96	186.20	424.30	296.80	60.88	202.60	442.30

3	1	245.91	30.41	197.10	315.20	258.20	26.34	212.20	301.80
	2	252.67	41.18	169.20	353.20	267.35	38.88	220.20	361.20
	3	313.89	62.97	213.10	440.10	336.31	51.87	256.40	438.20
	4	266.90	46.76	211.60	366.30	273.69	46.16	199.70	397.30
4	1	243.33*	27.66	200.00	308.00	260.50*	31.04	213.90	328.80
	2	264.08	37.16	208.20	368.60	277.97	37.42	214.20	371.40
	3	315.0	80.81	205.30	473.20	330.04	55.22	231.80	430.10
	4	264.18	40.84	221.90	372.90	266.83	44.40	193.70	384.80

*statistically significant difference between the two populations ($p<0.05$)

Ranking

In order to better characterize the vBMD quantitative measures, we have ranked the quadrants in slices 1-4 in order of lowest to highest vBMD. After ranking the quadrants, the total number of patients with each rank were determined (e.g. in how many patients did Q1 have the lowest density, in how many patients did Q1 have the second highest density, etc.). Lastly, to determine the proportion of patients at each rank (%), the total number of patients within the given rank were divided by the total number of patients in the study (n=25). For RA patients, the data consistently demonstrates that Q3 (dorsal region) has the highest vBMD relative to the other quadrants. In terms of the lowest ranked quadrant, there is agreement in slices 1 and 2 (MTPJ 2), that the density is lowest in Q4 (medial region). (Table 26)

As for controls, results are similar to those of RA patients as Q3 consistently has the highest density value and Q4 has the lowest density in MTPJ 2. There are no obvious trends for quadrants that are ranked with the second highest and third highest density. (Table 26)

Table 26: Overall Rank of Quadrants in RA Patients and Controls

Slice	Quadrant	Ranking (%)							
		RA Patients				Controls			
		Lowest	2nd	3rd	Highest	Lowest	2nd	3rd	Highest
1	Q1	28	44	24	4	33	41	26	0
	Q2	16	24	44	16	26	26	48	0
	Q3	0	20	8	72	0	0	11	89
	Q4	56	12	24	8	41	33	15	11
2	Q1	24	40	36	0	26	56	11	7
	Q2	16	20	40	24	11	30	52	7
	Q3	0	16	16	68	4	4	11	81
	Q4	60	24	8	8	59	11	26	4
3	Q1	32	28	24	16	22	48	30	0
	Q2	44	32	12	12	41	22	37	0
	Q3	4	4	32	60	0	0	11	89
	Q4	20	36	32	12	37	30	22	11
4	Q1	52	20	20	8	26	37	37	0
	Q2	32	20	28	20	22	41	30	7
	Q3	4	12	20	64	0	0	15	85
	Q4	12	48	32	8	52	22	19	7

Ratios

Another method that we used to better understand the quadrant data was to determine the relative measure of each quadrant in relation to the mean density of the whole slice. This was achieved by determining a relative ratio using total density parameters. A ratio <1 indicates that the quadrant has a vBMD less than the total density, and a ratio ≥1 indicates that the quadrant has a vBMD greater than the total density. After summarizing the number of patients and controls with the given ratios, a proportion was determined by dividing the number of patients with each ratio by the total number of patients in the study (n=25) (shown in tables below).

For RA patients, Q3 consistently has a higher density than the whole bone total density. For slices 2 and 4, this was in 100% of cases, and for slices 1 and 3, this was

evident in >90% of cases. Interestingly, for Q1, the proportion of individuals with quadrant ratios <1 and ≥1 are fairly evenly distributed. The ratios are distributed disproportionately in Q2 and Q4, and do not have any obvious trends. (Table 27)

For controls, Q3 consistently has a density that is greater than the total density. This is evident in all cases for slices 1, 3 and 4. For slice 2, this trend is seen in >90% of cases. In Q1, a majority of patients have a ratio <1 across all slices. There are no obvious trends for Q2 and Q4. All in all, some slice quadrants appear to favor one ratio more than the other. (Table 28)

Table 27: Relative Density Ratio of Quadrants in RA Patients When Compared to Whole Bone vBMD

	RA Patients, n=25				
		Slice 1	Slice 2	Slice 3	Slice 4
Quadrant	Q1	≥1 = 11 = 44%	≥1 = 11 = 44%	≥1 = 13 = 52%	≥1 = 12 = 48%
		<1 = 14 = 56%	<1 = 14 = 56%	<1 = 12 = 48%	<1 = 13 = 52%
	Q2	≥1 = 12 = 48%	≥1 = 16 = 64%	≥1 = 10 = 40%	≥1 = 15 = 60%
		<1 = 13 = 52%	<1 = 9 = 36%	<1 = 15 = 60%	<1 = 10 = 40%
	Q3	≥1 = 23 = 92%	≥1 = 25 = 100%	≥1 = 24 = 96%	≥1 = 25 = 100%
		<1 = 2 = 8%	<1 = 0 = 0%	<1 = 1 = 4%	<1 = 0 = 0%
	Q4	≥1 = 7 = 28%	≥1 = 6 = 24%	≥1 = 11 = 44%	≥1 = 19 = 76%
		<1 = 18 = 72%	<1 = 19 = 76%	<1 = 14 = 56%	<1 = 6 = 24%

Table 28: Relative Density Ratio of Quadrants in Controls When Compared to Whole Bone vBMD

	Controls, n=27				
		Slice 1	Slice 2	Slice 3	Slice 4
Quadrant	Q1	≥1 = 4 = 15%	≥1 = 6 = 22%	≥1 = 9 = 33%	≥1 = 10 = 37%
		<1 = 23 = 85%	<1 = 21 = 78%	<1 = 18 = 67%	<1 = 17 = 63%
	Q2	≥1 = 9 = 33%	≥1 = 14 = 52%	≥1 = 9 = 33%	≥1 = 14 = 52%
		<1 = 18 = 67%	<1 = 13 = 48%	<1 = 18 = 67%	<1 = 13 = 48%
	Q3	≥1 = 27 = 100%	≥1 = 25 = 93%	≥1 = 27 = 100%	≥1 = 27 = 100%
		<1 = 0 = 0%	<1 = 2 = 7%	<1 = 0 = 0%	<1 = 0 = 0%
	Q4	≥1 = 7 = 26%	≥1 = 10 = 37%	≥1 = 9 = 33%	≥1 = 11 = 41%
		<1 = 20 = 74%	<1 = 17 = 63%	<1 = 18 = 67%	<1 = 16 = 59%

3.6 Association between vBMD & Clinical and Imaging Signs of Inflammation and Bone Damage

3.6.1 Clinical Findings

Based on the understanding that active inflammation affects bone density negatively, we examined the association between vBMD measures and total SJC and TJC at the joint level, even if bone health may have an indirect relation with clinical symptoms.

Swollen joint count and TJC status (no SJC/TJC, only SJC, only TJC, both SJC and TJC) was determined in MTPJs 2 and 3 separately (25 patients; 50 joints). For the analysis we combined results from MTPJs 2 and 3 given that the impact of swelling and tenderness on the bone is likely not different between these joints. We then compared mean total and cortical subcortical vBMD between these 4 categories.

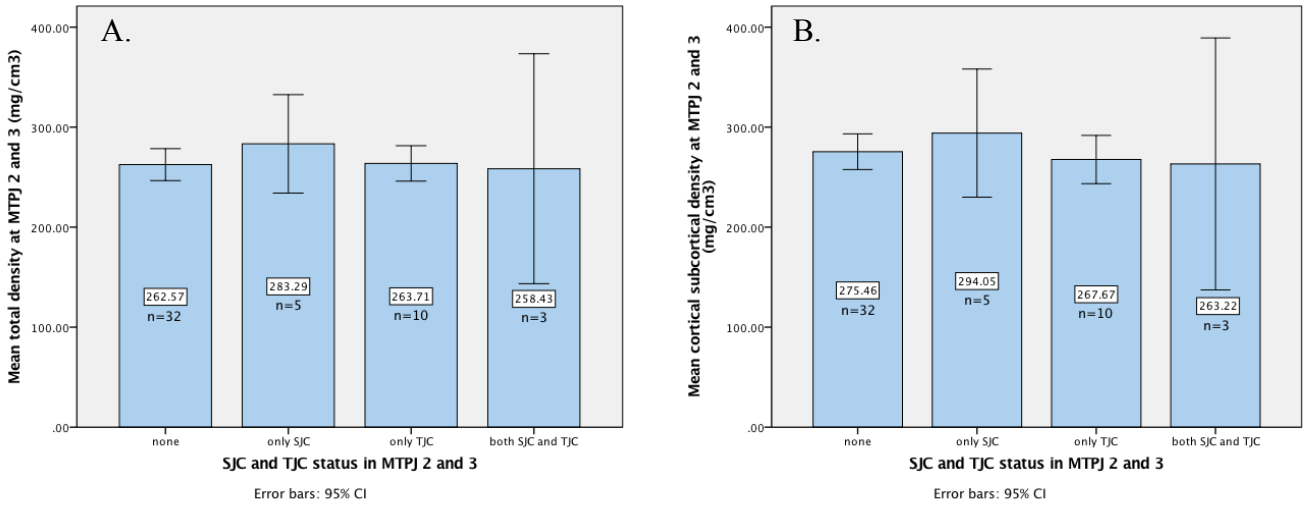

Figure 18. Bar graphs plotting the mean vBMD measures and clinical parameters at MTPJs 2 and 3 (n=50). A. Summary of TJC and SJC vs. mean total vBMD B. Summary of TJC and SJC vs. mean cortical subcortical vBMD

In the bar graphs for both total and cortical subcortical density, it is evident that there is a lot of overlap between the bone parameters in the 4 categories. As well, there are very few joints that are only swollen and that are swollen and tender. (Fig. 18)

Self-reported questionnaires were another aspect of the study which were reflective of the impact of the disease on patients around the time period of the appointment (within days). For each patient, a single representative vBMD measure was calculated for each bone density parameter by taking the average of total and cortical subcortical densities at MTPJs 2 and 3, as questionnaire results are not reflective of symptoms at the joint level. The association between mean vBMD and LFIS scores and patient reported symptoms were analyzed. No significant correlations were found between total or cortical subcortical vBMD and patient reported outcomes, subcategories of LFIS and the total LFIS score (*Appendix A4*).

3.6.2 Imaging Results

In terms of analyzing the quantitative vBMD measures in relation to other imaging modalities, we have focused on US and MR results at the joint level.

US Parameters

Based on the literature (Shimizu *et al.*, 1985; Ozgocmen *et al.*, 2004), the two US parameters of greatest interest are ST and PD due to their biological relevance to erosions. US ST and PD were graded on a scale of 0-3 (0=none; 3=severe ST and vascularization, respectively). Synovial thickening and PD scores of MTPJs 2 and 3 at the dominant foot were used for analysis. Metatarsophalangeal joints 4 and 5 were removed

from the analysis due to the low reliability in vBMD measures, and because PD and ST scores were 0 at MTPJ 5.

There appears to be very little variation in total and cortical subcortical density between the ST scores (Fig. 19A and 19B). While total and cortical subcortical density appear to increase with increasing PD, note that there is only 1 joint with PD scores of 1 and 2 (Fig. 19C and 19D). An ANOVA could not be run due to the unequal distribution in the categories and the small cohort.

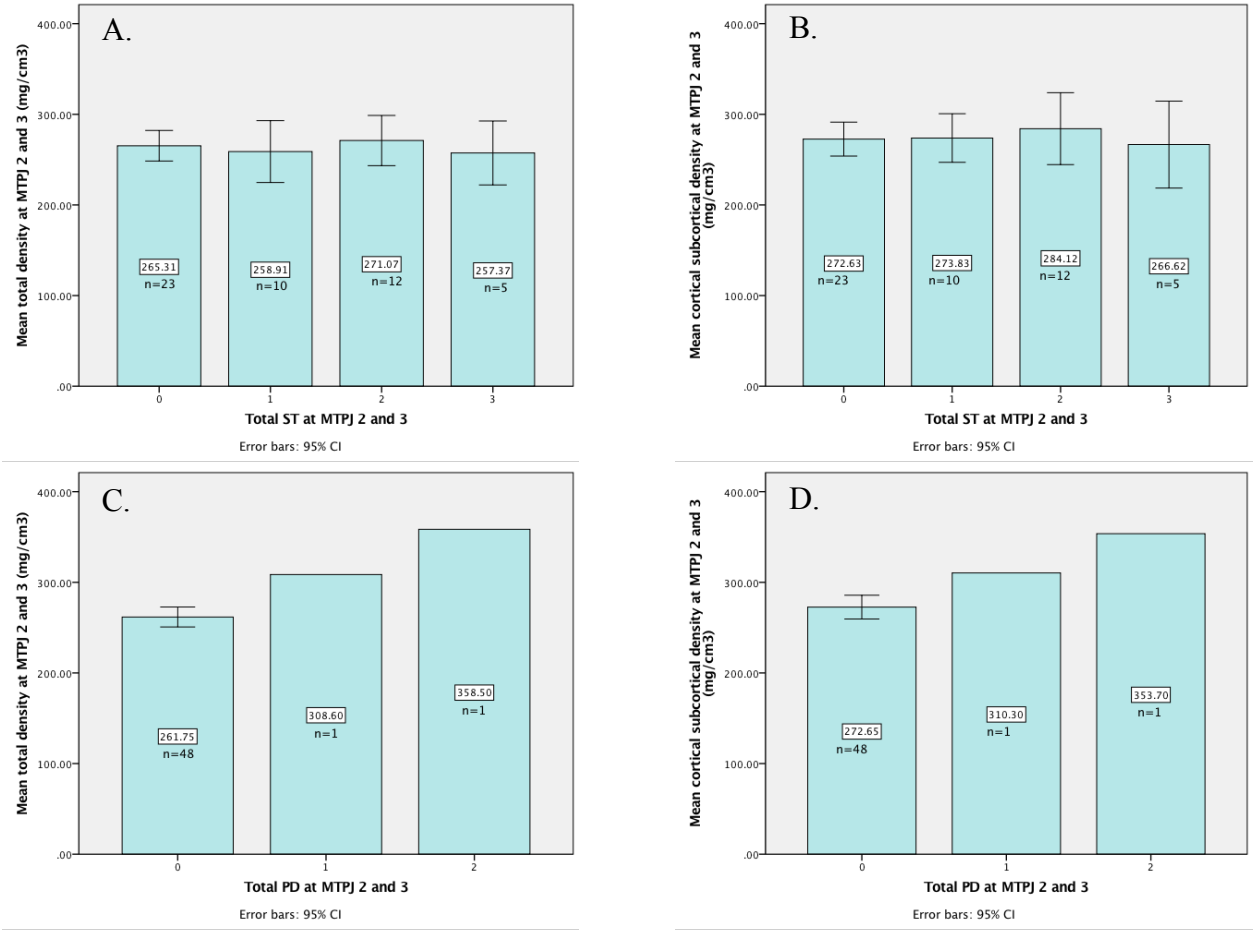

Figure 19. Bar graphs plotting the mean vBMD measures and US parameters at MTPJs 2 and 3 (n=50). A. Total ST score at MTPJs 2 and 3 vs. mean total vBMD B. Total ST score at MTPJs 2 and 3 vs. mean cortical subcortical vBMD C. Total PD score at MTPJs 2 and 3 vs. mean total vBMD D. Total PD score at MTPJs 2 and 3 vs. mean cortical subcortical vBMD

MR Erosions

Given the very small number of MR erosions, descriptive statistics were used to determine if a relationship was present between mean vBMD for those who had erosions and those who did not have erosions at MTPJs 2-4 (binary method). Metatarsophalangeal joint 5 was excluded due to the lack of clarity of this joint on MR imaging.

We expected that an increased prevalence of erosions at a given joint would result in a lower average total and cortical subcortical density. In MTPJ 2, the total and cortical subcortical density appear higher in those patients that do not have an erosion in comparison to those who do, however the number of individuals without an erosion is small. At MTPJs 3 and 4, those without an erosion appear to have a lower vBMD than those who do have an erosion at these joints at first glance. However, there is significant overlap in the confidence intervals of these results suggesting there is no actual difference. A t-test was not performed for this analysis, as the cohort was too small to provide viable results. (Table 29)

Table 29: Descriptive analysis of MR erosions and vBMD at MTPJs 2-4

MTPJ#	# of patients with presence/absence of erosion (n=23)		Total Density (mg/cm^3)			Cortical Subcortical Density (mg/cm^3)		
			Mean	SD	Range	Mean	SD	Range
2	Present	20	275.69	43.65	200.10-358.50	284.70	47.49	215.40-397.95
	Absent	3	298.97	38.03	257.05-331.25	309.20	41.81	266.85-350.45
3	Present	16	249.03	30.94	180.80-293.40	260.13	38.06	194.60-348.90
	Absent	7	243.72	36.95	191.75-293.65	256.20	40.83	206.10-330.10
4	Present	10	239.70	28.71	210.10-294.55	256.30	33.18	202.95-311.55
	Absent	13	220.30	38.96	144.55-287.10	227.83	31.16	167.95-279.55

Lastly, to better elucidate the nature of bone erosions at the quadrant level, we compared the highest and lowest quadrant pQCT vBMD to quadrant MRI bone erosion data from the previous phase. We explored a subset of 4 patients who had displayed MR erosion scores ≥2. Based on the pQCT data, it appears that the plantar region and medial region are most affected by reduced vBMD. These results agree with the bone erosion data, demonstrating that the plantar region is consistently affected across all 4 patients. As well, the lateral and dorsal regions generally appear to have the highest densities across the pQCT slices. Absence of bone erosions at the dorsal region suggest that the bone is preserved in this region and therefore, there is agreement with the pQCT results. (Table 30)

Table 30: Comparison of quadrant pQCT-vBMD and MRI quadrant level erosions at MT heads 2 and 3, n=4*

ID	Metatarsal head #**	MR erosion score	pQCT vBMD highest and lowest quadrant rank***		MR quadrants affected by bone erosion
			Total density	Cortical subcortical density	
18	2	2	S1 lateral S2 lateral	S1 lateral S2 lateral	Plantar, medial, lateral
			S1 medial S2 medial	S1 medial S2 medial	
	3	2	S3 dorsal S4 dorsal	S3 dorsal S4 dorsal	Plantar, medial, lateral
			S3 lateral S4 plantar	S3 lateral S4 plantar	
24	2	2	S1 lateral S2 dorsal	S1 plantar S2 dorsal	Plantar, medial, lateral
			S1 medial S2 medial	S1 medial S2 medial	
	3	3	S3 lateral S4 lateral	S3 dorsal S4 lateral	Plantar, medial, lateral
			S3 plantar S4 plantar	S3 plantar S4 plantar	

34	2	2	S1 dorsal S2 dorsal	S1 dorsal S2 dorsal	Plantar, medial, lateral
			S1 plantar S2 plantar	S1 plantar S2 plantar	
	3	2	S3 lateral S4 lateral	S3 dorsal S4 dorsal	Plantar, lateral
			S3 plantar S4 plantar	S3 plantar S4 plantar	
38	2	1	S1 lateral S2 dorsal	S1 dorsal S2 dorsal	Plantar, lateral
			S1 medial S2 medial	S1 medial S2 medial	
	3	2	S3 lateral S4 dorsal	S3 medial S4 dorsal	Plantar, lateral
			S3 plantar S4 medial	S3 plantar S4 plantar	

**Refer to Figure 17 in Methods for details on the location of the quadrants*
***Refer to Table 4 in Methods for details on slice allocation at MTPJs 2 and 3*
****For the *pQCT vBMD highest and lowest quadrant rank* column, the grey cells represent the highest rank and the white cells represent the lowest rank. S1=slice 1, S2=slice 2, S3=slice 3, S4=slice 4.

Chapter 4.0 Discussion

To our knowledge, this is the first study to measure vBMD in the MTPJs of an RA population using a pQCT scanner. In this study, we have reliably determined vBMD in MTPJs 2 and 3 of healthy controls and RA patients. Secondly, we have determined the variability in vBMD parameters in both of these populations, and demonstrated that both total and cortical subcortical density appear higher in MTPJ 3 of controls than RA patients. Lastly, we have compared quantitative vBMD measures in the MTPJs of RA patients to clinical and imaging signs of inflammation and bone erosions, and shown that there is little agreement between vBMD and clinical and US parameters, but some agreement with MR erosions.

4.1 Test-retest reliability

Test-retest reliability in both RA patients and controls was determined. As expected, reliability was better for controls than RA patients. This is likely due to the fact that healthy controls had little anatomical variations (e.g. joint space narrowing, misalignment of phalangeal base and MT heads) compared to RA patients, making it easier to palpate the MT head, place markings and position the foot. This also made visualizing the distinct difference between the phalangeal base and MT head on the scout view image easier in controls. This is in agreement with an HR-pQCT study that found that the minimum joint space width was significantly smaller in MCPJ 2 of RA patients when compared to controls, and joint asymmetry was significantly higher and more variable in RA patients than controls (Burghardt *et al.*, 2013). As well, perhaps due to the

discomfort in RA patients, they may have been prone to more motion artefacts, inconsistencies when repositioning between scans and less clarity in images. In both populations, reliability was highest and most optimal in slices 1-4 (MTPJs 2 and 3).

In a similar study to ours, Chaplais et al., 2014 scanned the same region (MTPJ), used the same modality (XCT 2000), and used the same voxel size (0.40 mm) as our MTPJ pQCT protocol. The scan-rescan reproducibility in cadaver legs was determined with repositioning. The variability at the 15% distal site and 50% midshaft region of MT 2 was reported. The %CV (ICC) for cortical density and trabecular density in all scans was 0.8% (0.98) and 2.8% (0.98), respectively (Chaplais *et al.*, 2014). The test-retest reproducibility in the present study is poorer than the aforementioned study likely because cadavers were used and the study did not have to account for motion. As well, the site of scanning was different between the two studies, particularly when comparing the distal scan region in the present study to the midshaft region (which has thicker cortical bone than the distal region) of the aforementioned study. To this end, the variability in the cortical region is expected to be lower since it is less porous than the total and trabecular bone, and therefore has a higher absolute BMD. Lastly, the disease status of the specimens was not revealed, which may imply that the cadavers were healthy and perhaps for this reason their variability was similar to that of MTPJ 2 in controls from the present study.

Multiple studies using HR-pQCT have reported test-retest reliability in patients with inflammatory arthritis. In one such study by Fouque-Aubert et al., three scans were performed with repositioning in between. Precision in MC heads 2 and 3 of advanced RA

patients and controls was determined using %CV. In RA patients, variability for MC head 2 and 3 for total and cortical vBMD were 1.3% and 1.8%, and 0.7% and 1.4%, respectively (Fouque-Aubert *et al.*, 2010). In controls, the variability in MC head 2 and 3 for the same parameters was 0.6% and 1.0%, and 0.8% and 1.4%, respectively (Fouque-Aubert *et al.*, 2010). In another study, patients with early inflammatory arthritis (symptoms <1 year) were scanned twice using HR-pQCT. Variability in vBMD at MCPJs 2 and 3 was reported using %RMSCV (RMSSD). Precision for total vBMD was 3.6% (11 mg/cm^3) (Brunet *et al.*, 2019). Our results for precision in total vBMD at MTPJs 2 and 3 are comparable to those of the aforementioned studies (3.16-5.78% (8.63-16.67 mg/cm^3)), although the variability in our study is slightly higher. The variability in the first study may have been lower as one more scan was included in test-retest reliability, in comparison to two scans in our study. Similar to the first study, our RA patients also had higher variability than controls. Since the MTPJs are comparatively smaller than other joints of the body (e.g. radius, tibia), this may be the reason why our %RMSCV and RMSSD are on the higher end of the acceptable threshold. As expected, our test-retest %RMSCV (3.16-14.40%) for measurement of total and cortical subcortical density at the MTPJs was higher than %CV (0.38-1.03%) for measurement of cortical and trabecular vBMD in the distal radius of male RA patients using HR-pQCT (Zhu *et al.*, 2014). The better reproducibility with HR-pQCT is likely due to the comparatively larger size of the radius and higher resolution of the modality.

Other studies that measured aBMD in RA patients using DXA also reported test-retest reliability. In a study by Naumann et al., the radiocarpal and carpoulnar joints of the

wrists were measured (2012). Variability was reported using %CV. The precision for the radiocarpal and carpoulnar joints were 0.89% and 1.72%, respectively, for ROIs with a height of 10 mm, and 0.86% and 1.49%, respectively, for ROIs with a height of 12 mm; reproducibility was best for the average of the two joints (whole wrist) (Naumann *et al.*, 2012). The same study also reported reliability (%CV (ICC)) in MCPJs 2, 3, 4 and 5 to be 1.23% (0.98), 1.71% (0.98), 2.33% (0.97) and 2.48% (0.96), respectively (Naumann *et al.*, 2012). In another similar DXA study, the short-term precision error was reported in the hand and MCPJs 1-5 using %CV. The reliability was higher in the whole hand in comparison to the MCPJs (0.8-0.9% versus 3.2%) (Ozgocmen *et al.*, 2004). In regards to the wrist/hand, the anatomically larger bones (e.g. radiocarpal) and larger ROIs resulted in less variability. This is likely because small absolute differences in BMD between scans made less of a difference in both of these cases. In terms of the MCPJs, the first study demonstrated that the variability in MCPJs 4 and 5 was larger than MCPJs 2 and 3 and these results are in line with the higher variability in MTPJs 4 and 5 in our study. It is understandable that the variability in MTPJs 4 and 5 are high as these toes have less dexterity and therefore positioning between scans can vary greatly, however it is interesting that MCPJs 4 and 5 also demonstrate poorer reliability than the rest of the fingers. In the DXA studies, this may be because MCPJs 4 and 5 are slightly smaller than the other fingers and the resolution of the machine is not high enough to accurately detect BMD in these joints between scans. Overall, DXA demonstrates better reliability than our study at peripheral joints, likely because pQCT is highly sensitive to motion and positioning.

4.2 Intra-rater reliability

Whole Bone Slices

Intra-rater reliability is a crucial reliability parameter to test when developing a protocol, to ensure that a single evaluator can achieve consistent results between measurements. Our intra-rater reliability results for whole bone analyses demonstrated high reproducibility in both populations for total and cortical subcortical density, with %RMSCV values <2%. These values agreed with their respective ICC values, demonstrating excellent reliability.

In one study, the intra-rater reliability in the L2 vertebral body was determined from cadaver vertebrae using pQCT (XCT 3000). Analysis was performed by manually selecting rectangular ROIs and then measuring vBMD using a Matlab-derived programme; a total of 7 ROIs were selected (the whole L2 vertebral body, 3 sagittal subregions (into equal thirds), and 3 transverse subregions (into equal thirds)) (Briggs *et al.*, 2010). Intra-rater reliability was reported for 2 different investigators and demonstrated moderate to high reproducibility, with an average %CV (range) of 1.65% (0.34-3.36%) in one rater and 1.90% (0.56-4.92%) in another (Briggs *et al.*, 2010). The %RMSCV range for whole bone intra-rater reliability between both populations in the present study is 0.37-2.48%. Thus, our results are comparable to those of the aforementioned study. The variability in the aforementioned study may have been due to segmentation of the vertebral cross-sectional slices into thirds, which may have been difficult to allocate visually. Although, they used rectangular ROIs to evenly divide the

regions, it may have been difficult to reproduce between measures. In contrast, we used custom ROIs, but selected the whole bone, thus it was easier to reproduce.

Quadrant Reliability

Quadrant intra-rater reliability in our study for both populations for both total and cortical subcortical density was <5% in a majority of the cases. This is surprising as it was challenging to consistently divide bone slices into 4 equal quarters manually with anatomical markers as guides, as these guides were not present in all bone slices. As well, since the ROIs were composed of ¼ of the area of the total bone, smaller absolute vBMD variations would have led to greater variations. To add, slight angle variations relative to the center of the bone between measures would result in higher variability. Interestingly, in both populations, the medial region (Q4) had the highest variability and the dorsal region (Q3) had the lowest variability. Based on the anticipated variability of absolute values, these data suggest that this is likely because the medial region has the lowest density (regardless of disease status) and the dorsal region has the highest density.

In one pQCT study (XCT 3000), athletic premenopausal women were scanned at the midshaft of the tibia. Similar to the present study, cross-sectional bone slices were split into 4 90° sections; repeat measures were taken 1 week apart. The %RMSCV for intra-rater reliability in quadrants was reported to be 0.3-1.4% (Rantalainen *et al.*, 2011). This patient population is most comparable to controls in the present study, who had a %RMSCV of 1.25-6.00%. Although the reliability in our quadrant data is generally acceptable, the higher variability in the present study is likely due to the smaller size of

the MTPJs in comparison to the tibia, and the comparatively smaller sample size (n=25 versus 221).

High resolution-pQCT studies have explored different aspects of quadrant intra-rater reliability in the hands of RA patients and controls; bone slices were divided into the dorsal, palmar, ulnar and radial regions. In one such study, the reliability in assessing cortical interruptions in MCPJs and PIPJs 2 and 3 was determined. Variability in cortical interruption status at the quadrants was reported using Cohen's kappa (κ), and intra-rater variability in reporting the total number of cortical interruptions at the quadrants was reported using ICC; two experienced raters assessed the bone slices. The scoring system used visual assessment of cortical breaks (e.g. division of bone into quadrants; cortical interruption seen in at least 1 slice and in 2 consecutive slices of another plane or interruption seen in more than 1 consecutive slice in 1 plane and in more than 1 slice in another plane; measurement of maximum diameter of interruption in the transverse/coronal/sagittal plane) (Scharmga *et al.*, 2018). The intra-rater reliability for both raters was moderate (κ=0.63-0.67) for identifying the presence of an interruption, and moderate (ICC=0.69-0.76) for reporting the number of cortical interruptions at the quadrants (Scharmga *et al.*, 2018). In another study, reliability in scoring bone lesions at MCPJs 2-4 was assessed. Intra-rater variability was reported using κ; duplicate measures were assessed 1 month apart by a rheumatologist. The scoring system was semi-quantitative (bone erosions, osteophytes and cortical bone changes were considered when scoring lesions), with a scale of 0-3 (0=no lesion; 3=severe lesion) (Stach *et al.*, 2010). The intra-rater reliability was good, with a κ=0.82 (Stach *et al.*, 2010). Both studies

reported moderate to good agreement between quadrant measures taken by the same rater when assessing bone defects in RA patients. The κ agreement in the second study may have been better than the first because of the differences in raters; the raters in the first study had extensive experience in image analysis on HR-pQCT, whereas the rater in the second study was a rheumatologist. The rheumatologist may have had more relevant clinical experience and exposure to the structural features of bone erosions which allowed them to detect bone defects with greater accuracy between measures. Another reason for the higher κ agreement in the second study compared to the first may be differences in disease duration of populations; the mean disease duration in the first study was 9.8 years and 6.5 years in the second. Patients with advanced disease likely have larger erosions, thus, it may have been difficult to distinguish quadrant bone defects between measures due to the destruction of the normal joint anatomy. As well the differences in criteria for assessing bone defects may have also contributed to the variability in κ between studies. Although we have not reported κ, our ICC values for intra-rater reliability at the quadrants of MTPJs 2 and 3 demonstrate excellent reliability (ICC>0.90). Our reliability is likely better than the first study because we analyzed the vBMD at all 4 quadrants in all 4 slices, whereas the HR-pQCT study assessed the number of cortical interruptions in the quadrants of 550 slices which may have introduced more variability between measures as the rater's judgment had to be considered. In addition, the paper addressed that including smaller cortical interruptions in the scoring system introduced more variability (due to less agreement between measures, thinner cortex which made cortical breaks difficult to

see, and discrepancies in categorizing the smaller cortical breaks (grouping many together or counting each one individually)).

4.3 Inter-rater reliability

Inter-rater reliability in both RA patients and controls was <3%, demonstrating high reproducibility. Our results suggest that training and using the Standard Operating Procedure manual as a guide for analyses can provide good reproducibility between raters.

In one pQCT study (XCT 3000), the inter-rater reliability of vBMD in the L2 vertebral body in cadaveric vertebrae was determined. As previously mentioned, rectangular ROIs were manually selected by two raters and vBMD was measured using a Matlab-derived programme; 7 different ROIs were selected (the whole L2 vertebral body, 3 sagittal subregions, and 3 transverse subregions) (Briggs *et al.*, 2010). Among the 7 ROIs, moderate to high reliability was reported, with a mean %CV of 3.25% (0.82-9.12%) (Briggs *et al.*, 2010). The inter-rater precision in the present study is slightly better than the aforementioned study, with a %RMSCV of 0.53-2.97%. However, if we compare the inter-rater reliability at the ROI that is most similar to our study, the *whole* L2 vertebral body, the results are more in line (2.61%) (Briggs *et al.*, 2010).

In one study, the inter-rater reliability for agreement in erosion detection and erosion dimension measurements using HR-pQCT in MCPJs 2 and 3 of RA patients was assessed in 11 readers with varying experience. There was agreement in 90.2% of cases for the presence/absence of erosions, with a κ agreement of 0.52 (Barnabe *et al.*, 2016).

When only experienced raters were considered, a κ value of 0.75 was reported (Barnabe *et al.*, 2016). In terms of inter-rater reliability for manual measurements of erosion dimension, %RMSCV (ICC) for perpendicular width was 12.3% (0.21), perpendicular depth was 24.0% (0.78), axial width was 20.6% (0.67), and axial depth was 22.2% (0.87) (Barnabe *et al.*, 2016). When only experienced raters were considered (>5 years of experience), excellent reliability was demonstrated (ICC >0.90) (Barnabe *et al.*, 2016). A major strength of the aforementioned study is the high number of raters that were assessed, and that rater reliability was reported based on experience level, which has been shown to be a contributing factor to the variability. Our inter-rater reliability data is generally better than this study, likely because rater judgement plays less of a role when measuring vBMD in pQCT bone slices; the rater draws the ROI by selecting the perimeter of the cross-sectional slice, but the density parameters are calculated by the software. As well, since our protocol only included 8 slices, it was feasible for both raters to analyze all slices. In contrast, HR-pQCT scanners produce 100s of slices, which may introduce some subjectivity between raters in terms of selecting common erosions to measure. The variability in our study is lower than the HR-pQCT study as the dimensional analysis (drawing straight lines) for erosions was more intricate than our study, which selected the whole bone cross-section. Minor variations in the angle of the straight line may have introduced variability between raters.

Although we have not explored inter-rater reliability of quadrant data in our study, HR-pQCT studies in RA patients assessed variability in detection of bone defects between raters. In one study, the radial and ulnar region of phalangeal bases and MC

heads 2-4 were assessed; a Pearson correlation of 0.98 was determined between raters. Agreement between raters was better with CT versus MRI (r=0.93) (Albrecht *et al.*, 2013). In another study, reliability in assessing cortical interruptions in MCPJs and PIPJs 2 and 3 was determined; controls were included. As previously mentioned, variability in cortical interruption status at the quadrants was reported using κ, and variability in reporting the total number of cortical interruptions was reported using ICC; two experienced raters assessed the bone slices (Scharmga *et al.*, 2018). The inter-rater reliability was moderate, with a κ agreement of 0.53 and ICC of 0.56 (Scharmga *et al.*, 2018). Interestingly, this paper also reported joint level inter-rater reliabilities, which were poorer than quadrant level analyses (κ=0.37 and ICC=0.48) (Scharmga *et al.*, 2018). Lastly, reliability in scoring bone lesions in MCPJs 2-4 was assessed using κ for two trained rheumatologists; controls were included. As previously mentioned the scoring system was semi-quantitative (0-3) (Stach *et al.*, 2010). The inter-rater reliability was good, with a κ agreement of 0.75 (Stach *et al.*, 2010). Overall, the aforementioned studies demonstrated good reliability for quadrant analyses between raters, as long as raters were trained.

4.4 Bone Outcome Measures

Mean Total and Cortical Subcortical Density in RA Patients and Controls (Whole Bone)

When analyzing whole bone slices, our data suggested that RA patients had a lower total and cortical subcortical density than controls at all slices; there were significant differences in slices 3, 5 and 6, which pertained to MTPJs 3 and 4, although results for slices 5 and 6 should be interpreted with caution as the reliability for vBMD measures was suboptimal at this joint.

In one pQCT study (XCT 3000), female RA patients and controls were assessed for bone geometry and BMD at MCPJ 3 (epiphysis (4% site) and shaft (30% and 50% site)), the radius and the tibia (4% and 66% site). Trabecular and total vBMD were measured at the distal sites (4% site), and cortical BMD and thickness were measured at the shaft region. Erosive damage was also assessed in RA patients using a Ratingen score (joint destruction scale from 0-5 in 20% increments). Trabecular vBMD was significantly lower at all distal sites in RA patients compared to controls (by 13-19%) (Aeberli *et al.*, 2010). As well, total BMD was lower at the distal MCPJ and tibia by 9% and 10%, respectively (Aeberli *et al.*, 2010). Rheumatoid arthritis patients had a lower cortical vBMD than controls at all sites except the 66% site of the tibia (although it is suspected that this is because of partial volume effect rather than true differences); the cortical layer was significantly thinner at all shaft sites (by 7-16%) (Aeberli *et al.*, 2010). Lastly, a significant negative correlation was found between Ratingen scores and total and trabecular BMD at the distal sites, and for cortical thickness at all shafts (Aeberli *et al.*, 2010). This study is comparable to our population as our study was mostly representative

of females, although the patients in this study had more advanced disease (mean duration: 11.4 years). The present study could not demonstrate significant differences for total and cortical subcortical vBMD for the most part, potentially due to the small sample size, although the general trend is in line with the aforementioned study. As well, perhaps our patients had small changes in vBMD that were not large enough to detect significant differences from controls due to the resolution of the pQCT scanner and the fairly early disease status of the patients. We could not report cortical vBMD due to the thin cortex in the MTPJs, as the reference lines in our protocol were placed in distal regions. Interestingly, even though the aforementioned study reported cortical BMD in the shaft region which is considered to have the thickest cortex, the authors mentioned that partial volume effect was still a concern due to the thinner cortices. As well, the fact that only total and trabecular BMD were measured in the distal sites is in line with our protocol which only measured total and cortical subcortical vBMD at the distal site. To add, in the aforementioned study, it is not surprising that total and trabecular BMD demonstrated a negative relation with the joint destruction scale, as bone erosions begin with a loss of trabecular bone in the adjacent region to the cortical break, and the total BMD considers trabecular BMD in the measurement (Barnabe *et al.*, 2016). These results are in line with what we had expected when setting up the analysis protocol – that if an erosion is present, RA patients would have a reduced total and cortical subcortical density compared to controls, and therefore, these density parameters would be surrogate markers for the presence of erosions.

High resolution-pQCT studies have also compared vBMD and microstructural properties in RA patients and controls. In one such study, the distal and ultradistal radius were assessed in Caucasian populations. Average, trabecular and cortical BMD at the distal radius were significantly lower in RA patients compared to controls (Δ=14.8-16.6%, 16.9-24%, 8.2-11.7%, respectively); trabecular BMD was significantly lower in the ultradistal radius (14.7-17.5%) (Kocijan *et al.*, 2014). In terms of bone microstructure at the distal radius, the trabecular number and thickness, and cortical thickness were reduced in RA patients compared to controls; RA patients had more inhomogeneity in the trabecular network than controls; male RA patients had significantly more cortical porosity than controls (Kocijan *et al.*, 2014). In terms of bone microstructure at the ultradistal radius, male and female RA patients had significantly reduced trabecular thickness and trabecular numbers, respectively, than respective controls (Kocijan *et al.*, 2014). In another HR-pQCT study, vBMD at the distal radius was examined in male Chinese populations. Total, trabecular and cortical vBMD were significantly lower in RA patients versus controls (by -13.4%, -23.2%, -3.9%, respectively) (Zhu *et al.*, 2014). Cortical porosity was significantly higher in RA patients than controls, as well, larger diameters in the cortical pores were more often seen in RA patients (Zhu *et al.*, 2014). Patients in both of these studies had more advanced disease (mean duration: 9.5 and 12.3 years, respectively), thus it is possible that this is why significant differences were found in all BMD measures, in comparison to our study where significance was not reached for most cases (mean duration: 5.0 years). As well, in both studies, trabecular BMD and trabecular structural properties generally demonstrated the greatest differences between

patients and controls. The cohort in the first study is more comparable to the present study, as most of our population was Caucasian. Regardless of the ethnicities of the cohorts, similar trends in BMD were found between both studies (trabecular BMD demonstrating greater loss than total/cortical BMD), and this is comparable to our study, as cortical subcortical density generally appeared to demonstrate greater differences in BMD than total density between the two populations (data not shown). A strength of the second study is the all-male cohort, as most BMD studies in the literature either focus on both genders or just females, although the results from our cohort are comparable to this study, regardless of the primarily female population. Lastly, it is important to note that the aforementioned studies and the present study scanned different regions; the distal radius is larger and likely easier to scan in comparison to the MTPJs, which are smaller and prone to more error.

Lastly, DXA studies have also compared BMD in RA patients and controls. In one study, the whole hand (software detected BMD; additional 10 selected ROIs at the whole hand: MCPJs 2-5, PIPJs 2-5, radiocarpal joint, carpoulnar joint), femoral neck and spine were scanned. There was a significant reduction in BMD at the whole hand, femoral neck and spine in RA patients, compared to controls (Naumann *et al.*, 2012). The BMD at the 10 ROIs in the hand were significantly different from the whole hand BMD; BMD in the MCPJs and PIPJs were lower than the net average of the 10 ROIs – the greatest differences were seen in MCPJ and PIPJ 5 (Naumann *et al.*, 2012). In another DXA study, pQCT (XCT 2000) was also used to measure BMD in female populations. The lumbar spine and hip BMD were measured by DXA, and the ultradistal radius vBMD

(4% site) was measured by pQCT. Additional measures included T-scores for DXA and attenuation for pQCT. The DXA BMD measures and T-scores at all sites were significantly lower in RA patients when compared to controls (Juhász *et al.*, 2017). As well, all pQCT BMD measures (total (mean±SD: 310.4±79.7 vs. 354.0±54.1 mg/cm^3), trabecular (157.6±57.0 vs. 193.8±48.7 mg/cm^3), cortical (434.3±115.8 vs. 492.5±64.0 mg/cm^3)), and attenuation measures were significantly lower in RA patients when compared to controls (Juhász *et al.*, 2017). In a similar study, DXA and pQCT (XCT 960) were both used to determine the patterns of bone loss in osteoporosis associated with RA in postmenopausal females; BMD was compared to osteoarthritis and postmenopausal osteoporosis patients. The RA patients were also assessed based on their radiographic stage (scale of I-IV; I=minimal deformity, IV=severe deformity). Spinal, radial and calcaneal (heel) BMD were measured by DXA, and the ultradistal radius (4% site) vBMD (total, trabecular, cortical) was measured by pQCT. RA patients had significantly lower bone parameters at all sites except the spine when compared to osteoarthritis patients, and significantly higher spinal BMD but no difference in the other sites when compared to the osteoporosis patients (Shibuya *et al.*, 2002). The pQCT total and cortical vBMD were significantly lower in patients in stages III and IV than in stages I and II of radiographic damage (Shibuya *et al.*, 2002). In terms of DXA BMD measures, all three studies have measured the spinal BMD, and the first two studies have measured hip BMD; the first two studies have demonstrated a reduced density at both sites in RA patients. However, in the last study, RA patients did not display a lower spinal BMD than the other disease groups, likely because the spinal BMD is less affected in RA patients and marked

changes in BMD are mostly seen in the peripheral bones (e.g. radius, calcaneus bone); periarticular osteoporosis is common but all patients may not experience generalized osteoporosis (Shibuya *et al.*, 2002). In the second study, while using pQCT, total BMD at the radius was lower in RA patients than controls. Although the radius has larger mean BMD measures than the MTPJs, the trend between RA patients and controls is comparable to that at the MTPJs. As well, not surprisingly, the third study demonstrated that patients with more destructive radiographic changes had lower vBMD. Although we did not report cortical vBMD, the trend for this is comparable to cortical subcortical density in the present study. The second study also assessed inter-modality agreement between DXA and pQCT – pQCT total and trabecular vBMD measures significantly correlated with DXA lumbar BMD (r=0.280 and 0.335, respectively) and hip BMD (r=0.362 and 0.342, respectively), whereas pQCT cortical vBMD only significantly correlated with DXA hip BMD (r=0.329) (Juhász *et al.*, 2017). Although we did not scan the hip and spine of our RA patients, the correlations between DXA measures at these sites and pQCT bone density parameters at the hands suggests that potential associations may be present between the hip/spine and the feet.

Mean Total and Cortical Subcortical Density in RA Patients and Controls (Quadrants)

Our study explored quadrants to better locate regions of lower density and erosions in the dorsal, medial, plantar and lateral regions of the MTPJs. There was a statistically significant difference between the two populations in the dorsal region of slice 3 for total density, and the plantar region of slice 4 for cortical subcortical density.

The quantitative values for quadrants were not very different than that of the whole bone slices. This is likely because the whole bone ROIs account for the average of the 2.3 mm width bone cross-section and selection of ¼ of that ROI, although smaller in size, may have excluded regions that were pulling the density down in the whole bone ROI (i.e. low-density material/lost bone).

Two HR-pQCT studies have assessed erosions in quadrants of MCPJs 2-4 in RA patients and controls. In one study, as previously mentioned, the MCPJ bone slices were divided into the dorsal, palmar, ulnar and radial region in the MC heads and phalangeal bases (Stach *et al.*, 2010). The radial quadrant had the highest prevalence of bone erosions (particularly at MCPJs 2 and 3, with a lower frequency at MCPJ 4), and the palmar quadrant had the lowest number of erosions (Stach *et al.*, 2010). Interestingly, controls demonstrated a similar trend (Stach *et al.*, 2010). In another HR-pQCT study, HR-US was included to determine the presence of erosive lesions in patients with inflammatory arthritis (RA and psoriatic arthritis patients). Since US was included, only regions that were accessible by US were analyzed – the radial, palmar and dorsal region at MCPJ 2; palmar and dorsal region at MCPJ 3 and 4. Among the three joints, both modalities demonstrated that MCPJs 2 and 3 had the most erosive lesions; MCPJ 2 had the most severe erosive lesions and MCPJ 4 had the least severely affected lesions (Finzel *et al.*, 2011). Erosions were most prevalent in the radial region, and for controls, smaller lesions were most prevalent in the radial region, as detected by both modalities (Finzel *et al.*, 2011). In terms of the palmar and dorsal regions, HR-pQCT demonstrated that both of these regions were equally affected by erosions, and US demonstrated that the palmar

region was more affected than the dorsal region (Finzel *et al.*, 2011). As well, the MC heads were most severely affected by lesions than the phalangeal bases on US (Finzel *et al.*, 2011). The study also demonstrated good inter-modality agreement for the severity of erosions with a Spearman's ρ of 0.46 (Finzel *et al.*, 2011). In both studies, the radial quadrant was most affected by bone damage. Interestingly, the radial quadrant was also most affected in controls, and although the lesions were smaller in healthy individuals, this suggests that this region is prone to damage regardless of disease status. This is likely because the radial site is next to the insertion region of the collateral ligament (McGonagle *et al.*, 2009; Stach *et al.*, 2010). In the present study, our mean quadrant total vBMD at MTPJ 2 (slices 1 and 2) for both RA patients and controls agrees with the aforementioned studies, as the medial region appears to have the lowest vBMD, suggesting that bone damage may be present at this quadrant, regardless of disease status. As well, the high prevalence of erosions in MCPJ 2 seen in both studies is in line with our MR erosion data, which demonstrated the most erosions in MTPJ 2. Contrary to the present study, the first study demonstrated that the palmar region in the MCPJs had the lowest number of erosions, suggesting that mean BMD would be highest in this region, however, in the present study, the plantar region appears to have the lowest cortical subcortical density in both populations, which would imply that the most bone damage is present in this region. This may potentially be due to the variations in stresses between these peripheral joints, and weight bearing forces on the feet and the lack thereof in the hands. Lastly, our data for total and cortical subcortical vBMD at the dorsal region, which appears to have the highest density in both populations, agrees with the HR-US results, as

the US demonstrated that this region was least affected by erosions and therefore likely had the highest density.

Generalized osteoporosis in RA can be affected by reduced physical activity (Shibuya *et al.*, 2002). One study assessed the tibia using a pQCT scanner (XCT 3000; 50% midshaft site) in women performing varying degrees of impact sports (high-impact (e.g. high jump), odd-impact (e.g. soccer), high-magnitude (e.g. power lifting), repetitive low-impact (e.g. endurance running), repetitive nonimpact sports (e.g. swimming), and physically active non-athletic reference controls) (Rantalainen *et al.*, 2010). Bone cross-sections were divided into 4 90° sections (lateral, posterior (below), medial, anterior (top)) to determine the variation of cortical BMC. Athletes in the high-impact and odd-impact groups demonstrated significantly higher cortical BMC than the reference group at all quadrants (Rantalainen *et al.*, 2010). As well, the repetitive low-impact group also had significantly higher cortical BMC in the anterior and posterior quadrants when compared to controls (Rantalainen *et al.*, 2010). This study also measured BMC at the shaft of the fibula, but few differences were found between groups, likely because the fibula carries 6-17% of the load (Rantalainen *et al.*, 2010). Thus, regardless of the anatomical proximity of the tibia and fibula, different patterns for cortical BMC were found. In another paper by the same group with the same subjects, cortical vBMD was analyzed in tibial quadrants (Rantalainen *et al.*, 2011). The mean cortical vBMD was highest at the medial region and lowest at the anterior region (Rantalainen *et al.*, 2011). High-impact athletes and odd-impact athletes had 1.5-2.6% significantly lower cortical vBMD than the reference group at all 4 quadrants, repetitive low-impact athletics had 1.0% significantly

lower vBMD at the anterior quadrant, and the high magnitude group had 1.2% significantly lower vBMD at the lateral region (Rantalainen *et al.*, 2011). Our quadrant data is quite different from the aforementioned studies. However, this is likely because a different bone in a different population was scanned (the tibia is larger than MTPJs; athletic females were scanned), a different region was scanned (midshaft vs. epiphyseal/metaphyseal region in the present study), and the anatomical placement of the bone was different (the tibia and MTPJs are placed perpendicular to one another and have different structural properties). Participants performing impact sports had higher cortical BMC than controls, likely due to increased bone remodelling/turnover due to the increased activity. It is important to note that different trends were observed between the quadrant BMC in the tibia and fibula, regardless of close proximity, and this can potentially be applied to the differences in the quadrant vBMD in the MTPJs due to the variation in pressure and load that are placed on each toe. The studies demonstrate that physical activity indeed has an impact on bone properties and may, in part, explain differences in vBMD between patients with similar disease status.

In addition, our total density quadrant ranking data for both RA patients and controls is generally in line with the current literature, demonstrating that the dorsal region appears to have the highest density and the medial region appears to have the lowest density. These results suggest that the dorsal region is the least affected by erosions and the medial region is most affected by erosions. This is further verified with the quantitative ratio analysis across all slices, where the dorsal region consistently

displays a relative density ratio ≥1 in a majority of the cases when compared to the whole bone total density.

4.5 Association Between vBMD and Clinical and Imaging Signs of Inflammation and Bone Damage

An important objective of this study was to translate the quantitative pQCT vBMD measures into a manner that would relate them to other clinical and imaging parameters, as the comparators have established protocols which have been extensively used in RA populations.

Clinical Findings

Swollen and tender joints are important clinical markers for the severity of disease as they are incorporated in the CDAI and DAS28 scores. It is expected that if patients have a high SJC and TJC, that their disease severity is high, and if they have both, then their disease severity is even worse. As well, this suggests that the more active the patients' disease, the greater the number of erosions in that patient, and therefore the lower the vBMD. Unfortunately, our results did not demonstrate any strong patterns, as the mean total and cortical subcortical density at MTPJs 2 and 3 displayed a lot of overlap between patients who didn't have SJC/TJC, patients who had either SJC/TJC, and patients who had both. This was likely due to the small sample size.

High resolution-pQCT studies have assessed the relationship between vBMD and disease duration in RA patients. In one such study, the vBMD at the distal radius of male patients was assessed and total, trabecular and cortical vBMD were examined (Zhu *et al.*, 2014). Lower vBMD (cortical and trabecular) was associated with higher disease activity (DAS28), chronic disease (patients with longer disease duration), and greater disease severity (more deformed joints) (Zhu *et al.*, 2014). As well, patients with increased pro-

inflammatory cytokines (IL-12, TNF, IL-6, IL-1β) were associated with lower total vBMD (Zhu *et al.*, 2014). In another study, MCPJs 2 and 3 were assessed for prevalence of erosions and erosion scores at baseline and 12 months. Joints were divided into the dorsal, palmar, ulnar and radial region, and the MC heads and phalangeal bases were separated for a total of 8 analysis regions per MCPJ. Between baseline and the follow-up, the average number of erosions increased from 5.70 to 6.13, and the erosion score increased from 5.30 to 5.50 (Aschenberg *et al.*, 2013). Disease duration was the only variable that was significantly positively associated with the number of erosions (Aschenberg *et al.*, 2013). Both studies demonstrated a correlation with disease duration and bone damage. These results suggest that chronic inflammation, which may present as swollen and tender joints, are indeed related to bone loss.

In one study, the risk of bone loss in RA patients receiving standard of care at baseline and follow-up was determined. Bone measures were taken at the hip and spine by DXA. At the 2-year follow-up, patients were treated with DMARDs, corticosteroids and medications that would counteract bone loss as needed; 37% were taking antiresorptive therapy, 37% were on calcium/vitamin D only, and 48% were on prednisolone. After 2 years, mean±SD for the SJC and TJC (28 joints) changed from 7.9±6.2 to 7.6±5.3, and 6.7±6.5 to 8.4±6.7, respectively (Haugeberg *et al.*, 2002). Over the 2 years, the range for average BMD decrease was -0.29% to -0.77% (Haugeberg *et al.*, 2002). Patients who were taking antiresorptive therapy demonstrated an increase in BMD at the hip and spine, whereas those who were taking calcium and vitamin D supplements/no preventative therapy for osteoporosis displayed decreased BMD

(Haugeberg *et al.*, 2002). Similar to the aforementioned study, an open-label study with early RA patients examined progression of erosions in two groups with different drug regimens – group 1 was primarily treated with DMARDs and group 2 was treated with MTX only, and DMARDs if necessary (Yue *et al.*, 2018). At baseline and 1-year follow-up, bone erosion prevalence and BMD measures of MCPJ 2 were obtained using HR-pQCT. At baseline and 1 year, SJC and TJC (68 joints) changed from 4.5 to 0, and 8 to 1, respectively (Yue *et al.*, 2018). The mean number of erosions changed from 72 to 77 (Yue *et al.*, 2018). The mean total and cortical BMD±SD changed from 268.4±54.0 mg/cm^3 to 268.8±53.4 mg/cm^3, and from 515.2±90.5 mg/cm^3 to 513.6±89.0 mg/cm^3, respectively; mean BMD surrounding the erosion changed from 475.60±50.52 mg/cm^3 to 488.86±42.55 mg/cm^3 (Yue *et al.*, 2018). Both studies reported changes in BMD and clinical measures. Although DMARDs were used in both studies, changes for SJC/TJC were different between the studies – non-significant in the first study and significant in the second study. Although both studies did not perform correlation analyses between clinical outcomes and bone outcomes, they highlighted important factors to consider. The first paper demonstrates that changes in BMD are not only dependent on inflammation, but also external factors such as lifestyle changes, medications and supplements. The second paper emphasizes that even though patients were on therapy and there were significant improvements in SJC and TJC measures, mean total and cortical BMD did not demonstrate significant changes between baseline and follow-up. As well, the increase in the number of erosions may have been because the medications had not taken maximal effect in reducing disease activity, as patients had not gone into remission and therefore

erosion repair had not occurred. Interestingly, in the second paper, BMD surrounding the erosion demonstrated greater changes than the total and cortical density. Therefore, the absence of a negative association between clinical findings and total and cortical subcortical density in the present study are in line with these results, and are possibly because BMD differences are more effectively detected closer to the erosion region rather than at the slice level.

Ultrasound Findings

An increased thickness and greater vascularization in the synovium imply greater severity in disease. Thus, we anticipated that mean total and cortical subcortical density would be comparatively reduced in patients who had greater ST and PD scores versus patients who had lower ST and PD scores. However, our results did not demonstrate such trends as the bone density parameters did not show much variability when compared to ST and PD scores. A limitation here was that very few joints demonstrated higher PD scores.

Previous DXA studies have analyzed BMD at the MCPJs of RA patients and compared to synovitis and vascularization measures. In one study, patients with varying levels of disease (early and established (moderate activity, high activity)) were assessed in MCPJs 2-5. Synovitis was also measured at these joints using US (B-mode/PDUS; semi-quantitative scoring 0-3) and MRI (RAMRIS scoring). Patients were followed up after 1 year. At baseline, whole hand BMD in patients with early RA demonstrated a positive non-significant correlation, patients with moderate activity demonstrated no

correlation, and patients with high activity demonstrated a significant negative correlation with US synovitis (Naumann *et al.*, 2012). As well, whole hand BMD in early and moderate activity patients demonstrated no significant correlation, and high activity demonstrated a significant negative correlation with MR synovitis (Naumann *et al.*, 2012). At follow-up, the significant negative correlation between BMD and synovitis was no longer present (Naumann *et al.*, 2012). In a similar DXA study that measured BMD at MCPJs 1-5 and vascularization (using PDUS), there was a significant small negative correlation between flow patterns (increased vascularization + active inflammation) and hand BMD (Ozgocmen *et al.*, 2004). Both studies demonstrate negative correlations with PD signals and BMD. The first study demonstrated that patients with only high disease activity displayed a significant negative correlation, but not patients with low or moderate disease activity. Our findings are in line with this study, as our patients are in the early stage of disease and therefore, this may be why significant associations between BMD and US synovitis were not found. As well, it is possible that on the day the scans were performed, patients were not experiencing flare and therefore their disease activity was lower/moderate. In terms of the second study, although the results of the study are in line with what we had expected, the present study did not demonstrate such trends, likely because a majority of our patients did not have a long disease duration and because the patients were not evenly distributed between the scores for PD.

In an HR-pQCT study, RA patients with low disease activity were analyzed. The vBMD and microarchitecture at MC heads 2 and 3, and PDUS were used to determine whether patients had local inflammation or not. Those who had a Doppler positive

erosion (semi-quantitative score of 2 or 3) and those with a Doppler negative erosion (score of 0 or 1) were evaluated. Cortical density and thickness were similar between the two groups, but trabecular density and trabecular number were significantly lower in patients who had a Doppler positive erosion (Kong *et al.*, 2018). Thus, trabecular bone measures were changed in patients with active inflammation (i.e. increased discontinuity in trabeculae, lower number of trabeculae, increased trabecular separation) (Kong *et al.*, 2018). These results are consistent with what we had expected, with high inflammation/worse disease status associated with lower vBMD/weaker bone structure. Unfortunately, we could not report trabecular density, but we had expected to see a similar trend with the cortical subcortical density as this was a surrogate marker for erosion presence. However, our results did not demonstrate such a trend, as most of our patient population had a PD score of 0, thus it was difficult to elucidate any definite direction in the data.

Previous studies that have compared US with CT erosion data have found moderate sensitivity. In one study that analyzed the quadrants in MCPJs 2-5, the sensitivity and specificity of US when compared to CT as the reference method was 42% and 91%, respectively (Døhn *et al.*, 2006). However, when analyses were performed for regions that were easily accessible with US (palmar and dorsal region in MCPJs 2-5, radial region of MCPJ 2, and ulnar region of MCPJ 5), sensitivity and specificity improved to 60% and 92%, respectively (Døhn *et al.*, 2006). The sensitivity was comparable to MRI only when the accessible regions of US were considered. In a similar study that scanned MCPJs 2-5 and split the joints into quadrants, sensitivity and

specificity of US when compared to CT were 44% and 95%, respectively (Døhn *et al.*, 2011). Both studies demonstrate moderate sensitivity for bone erosion detection, thus, similar results may also be expected when comparing US synovitis and PD to vBMD measures in CT-derived modalities (e.g. pQCT). This moderate sensitivity may be one of the reasons why there is little agreement between US results and pQCT bone parameters in the present study.

Magnetic Resonance Erosions

MR is considered better than X-ray and in some cases, the gold standard, for detecting erosions due to its ability to visualize the surrounding soft tissue (Siddle *et al.*, 2014). In the present study, MR erosion data at MTPJ 2 demonstrated good agreement with pQCT total and cortical subcortical vBMD measures when compared between patients who had erosions and those who didn't. However, data at MTPJs 3 and 4 were contradictory to the expected trend. When the quadrant pQCT data was compared with quadrant MR bone erosion data, there was agreement between regions that had the lowest density in pQCT and those with bone erosions in MRI.

Past studies have shown high inter-modality agreement between MR imaging and multidetector CT scanners for measuring erosion detection at the MCPJs and wrists in RA patients (Døhn *et al.*, 2007, 2008). Both studies assessed the same RA patients and controls. In the first study, the MCPJs were assessed: CT and MRI detected 77 and 62 erosions, respectively, in RA patients; 51 of the same erosions were detected by both modalities (Døhn *et al.*, 2007). The sensitivity for erosion detection by MRI was 66%

when CT was used as the reference standard (Døhn *et al.*, 2007). Larger erosions were difficult to detect, as the border was difficult to distinguish (Døhn *et al.*, 2007). In the second study, the wrist was assessed: CT and MRI detected 166 and 119 erosions, respectively, in all participants; 92 erosions were commonly detected by both modalities (Døhn *et al.*, 2008). The sensitivity and specificity of MRI was 61% and 93%, respectively, when CT was used as a reference standard (Døhn *et al.*, 2008). The same group performed a quadrant analysis in MCPJs 2-5, and MR sensitivity and specificity for detecting bone erosions were 68% and 96%, respectively, at the quadrant level (Døhn *et al.*, 2006). A similar study that assessed quadrant level MR erosion detection in the same joints in RA patients reported similar values for sensitivity and specificity with CT as the reference method (68% and 92%, respectively) (Døhn *et al.*, 2011). All in all, the high correlation between MRI and CT reveals that MR erosions at both the MCPJs and wrist are indeed true destructions in the cortical bone. In all cases, the specificity was high and sensitivity was moderate, which may in part be the reasoning for why there is a discrepancy in the present study for average total and cortical subcortical density with the erosion status at MTPJs 3 and 4. In addition to the agreement between CT and MRI for bone erosion detection, MRI has also been shown to have predictive value for future CT erosive damage based on MR inflammation and bone oedema (Døhn *et al.*, 2011). Interestingly, quadrant sensitivity and specificity values were comparable to those of whole bone MR analyses. The moderate sensitivity may be applied to the present study, as the MTPJ quadrants with the lowest pQCT bone density parameters did not always agree with MR quadrant erosion data (patient 38, MT 2). Although, this may also be due

to the fact that pQCT density measures and MR erosion data were taken at two different times points, thus erosion status for lower grade erosions may have changed.

Several studies have explored the agreement between MRI and CT modalities in detecting bone erosions in the wrists and MCPJs of RA patients, and have shown that CT is more sensitive for detecting smaller erosions. In one such study, the wrist was scanned using MRI and CT. Both modalities detected erosions in the same carpal sites in 87% of cases; 9% of erosions were only detected by CT; 4% of erosions were only detected by MRI (Perry *et al.*, 2005). In another study, MCPJs 2-4 were scanned using MRI and HR-pQCT. Between two raters, a significantly higher number of erosions were detected on HR-pQCT than MRI (137 versus 111); 28 erosions were only detected on HR-pQCT; 2 erosions were only detected on MRI (Albrecht *et al.*, 2013). In cases where erosions were detected on MRI but not in HR-pQCT, the researchers proposed that MR pre-erosions may have been present with surrounding inflammatory tissue (Albrecht *et al.*, 2013). To add, the relation between erosion volume measured by HR-pQCT and RAMRIS erosion scoring was determined, and a strong positive relationship was found (Albrecht *et al.*, 2013). Lastly, one study assessed both the wrist and MCPJs 2 and 3 using HR-pQCT, and the wrist using MRI in patients (n=16). In 15 patients, HR-pQCT was able to detect erosions at both MCPJs and the wrist, and in 13 patients MRI was able to detect erosions at the wrist. The smallest dimension of erosions detected by HR-pQCT and MRI were 0.9 mm and 1.4 mm, respectively (Lee *et al.*, 2015). In all three studies, CT technologies were able to detect smaller erosions than MRI, likely due to the thicker MR slices (3 mm versus 2.5 mm (Perry *et al.*, 2005)) and the associated partial volume effects which make

smaller erosions difficult to visualize (specifically, those with an erosion volume <10 mm^3 (Albrecht *et al.*, 2013)), as well as due to the better spatial resolution of the CT scanners. Although partial volume effects can also be a disadvantage while using CT, erosion borders are easier to distinguish on CT due to the higher contrast between cortical bone and adjacent soft tissue (Perry *et al.*, 2005). Similar to the first study, the MR protocol in the present study also had a slice thickness of 3 mm, thus small changes in the bone may not have been detected, which can potentially be the reason for the discrepancy between the number of erosions at the joint level (MTPJs 3 and 4) and the mean total and cortical subcortical density. Alternatively, the discrepancy between erosion status and bone density parameters may have been because some of the erosions that are included in the count are not true erosions, and thus perhaps there are patients who don't have erosions being included with the average density values for those patients who truly have erosions. In the second study, the positive relation with erosion volume and erosion scoring agrees with the trend that we had anticipated for cortical subcortical density and MR erosion scores, although we could not run association studies due to the small number of erosions in the patient population. However, MR erosion status and bone density parameters at MTPJ 2 demonstrate some agreement with this.

Interestingly, contrary to most studies, one study that assessed the humeral head (shoulder) in RA patients (mean disease duration: 12 years) found that MRI and US were superior to CT for visualizing small erosions. MRI, US and CT detected 25, 24 and 20 erosions, respectively (Alasaarela *et al.*, 1998). Larger erosions were detected similarly between the three modalities. The study noted that although a high number of MR

erosions were detected, all of them may not be true erosions, as pre-erosive oedematous alterations in the subchondral bone may look like erosions, and T2- and T1-weighted images may show changes in the fat/water ratio of the bone marrow rather than the true change in bone (Alasaarela *et al.*, 1998). As well, CT likely had poor sensitivity to lesions <2 mm due to the poor resolution (1.0-1.3 mm), in comparison to US which was able to visualize structures that were 0.3-0.6 mm thick (Alasaarela *et al.*, 1998). The shoulder is anatomically different from the peripheral regions like the MCPJs and MTPJs, as the shoulder is in one of the thicker parts of the body and is difficult to access with the CT scanner. In the present study, it is possible that the number of erosions at MTPJs 3 and 4 were over-estimated, and for this reason there was no association between the erosion status and total and cortical subcortical density at these joints. Although the resolution of our pQCT protocol (0.40 mm) was fairly good, there is still a possibility that the resolution was not high enough to detect small breaks in the cortical bone. On a similar note to the aforementioned paper, if the erosions in our patient population are indeed small, then it makes sense that there is a discrepancy between the MR erosion data and pQCT vBMD data.

In a study that was similar to the present study, MR erosions were localized in quadrants of MTPJs 1-5 in RA patients; quadrants were analyzed separately for the MT head and phalangeal bases. The quadrants were assigned as follows: dorsal-medial, dorsal-lateral, plantar-medial and plantar-lateral (Siddle *et al.*, 2014). The plantar quadrants (plantar-medial and plantar-lateral) and MT heads had the highest prevalence of erosions (Siddle *et al.*, 2014). This data agrees with the present study, as the quadrants

with the lowest pQCT bone density measures and MR erosions were the plantar, medial and lateral regions. As well, our study only reported MT head MR erosions, as more erosions were present in the MT head compared to the phalangeal base. Both the aforementioned study and the present study suggest that the plantar region is most affected due to biomechanical factors at the MTPJs in RA patients (Siddle *et al.*, 2014). In contrary to these results, another study that assessed quadrant level bony changes at MTPJs 1-5 in RA patients found that erosions were most prevalent in the lateral quadrant of MTPJs 3 and 5, and the medial and plantar quadrant of MTPJ 1; the lateral quadrant in MTPJ 5 demonstrated the highest number of erosions (Boutry *et al.*, 2003). The results for this study may have been different from the first study and the present study as it measured both feet, as well as patients with early RA (median disease duration: 1 year), whereas the first study and present study only measured the most symptomatic foot and included patients with longer mean disease durations (10.6 years and 5.0 years, respectively). As well, the present study did not explore pQCT density and MR erosions at MTPJ 5 due to the poor reliability and poor clarity, respectively.

4.6 Limitations

Our study has a number of limitations. In terms of the cohort, men were under-represented in our study, as a majority of the cohort was composed of women. As well, although a sample size of n=25 was calculated with an ICC of 0.8±0.2, the sample size was too small to detect statistical differences in total and cortical subcortical densities. However, now that we have preliminary vBMD data for the MTPJs (measured with pQCT) in both RA patients and controls, we can use this to calculate a sample size for follow-up studies, which will be powered to determine a statistically significant difference between RA patients and controls.

Past studies that have assessed vBMD in RA patients have also reported markers for bone metabolism, such as hydroxyvitamin D3, osteocalcin and parathyroid hormone (Aschenberg *et al.*, 2013). It may have been beneficial to assess these markers in the present study and determine if they corresponded with the variation seen in bone density parameters.

As well, due to the cross-sectional nature of the pQCT segment of the study, the change in vBMD could not be determined in comparison to other modalities tested. This was also a limitation when comparing MRI data to the vBMD data, as the two measurements were not taken at the same time point. Thus, changes that could have taken place over the last year would not have been captured when comparing MRI data with pQCT data.

Peripheral QCT

One of the limitations of our study is that HR-pQCT was not used as the imaging modality to quantify erosions, as this imaging modality is considered the gold standard for erosion detection. However, we were limited by the cost of the modality, accessibility to the modality, and logistics of the study.

In terms of pQCT reliability for the feet, %RMSCV for test-retest reliability was poor in MTPJs 4 and 5. As previously mentioned, we are aware that our 5% benchmark for %RMSCV is conservative, however we had opted for this benchmark so that in follow-up studies that monitor the change over time, we can be confident that the change in the vBMD is due to true change and not measurement error. A tighter error threshold ensures more confidence in results. To add, since %RMSCV is a function of the difference in paired measures and the mean vBMD, lower absolute vBMD measures lead to higher values of %RMSCV and poorer precision (Martin *et al.*, 1997). The vBMD at the MTPJs is lower than that in the radius and tibia, thus, comparatively, it can be expected that variability will be higher at the toes. In addition, we expected an even lower vBMD at the MTPJs of RA patients, which likely contributed to an even poorer %RMSCV. As well, past studies have suggested that using 2 slices to represent each joint may contribute to higher variability for test-retest reliability (Perry *et al.*, 2005).

In terms of the scan protocol, one of the issues encountered during scanning patients included varying scout views between scanning trials. When the scout view scan is not accurate (due to distortion of normal anatomical landmarks in RA patients), the subsequent result is that the reference line will not be placed in the same spot each time

(Martin *et al.*, 1997). The reference line is crucial as it prescribes the location of the ROI for scanning. Any small variation from the previous scan will result in variability as the apparatus is sensitive to change. With regards to the reference lines, their placement was determined based on the most common sites for erosions in the ≥2 year follow-up. However, this is not representative of *all* the erosions found in the 25 patients, thus, this may be why the anticipated trend was not captured and why there is discrepancy between MR erosion data and pQCT vBMD data, as we may have missed some erosions. For future studies, we recommend using multiple overlapping slices at a single joint (e.g. MTPJ 2/3). Additionally, the scan time for the protocol was ~9 minutes. At times, patients had difficulty keeping their foot still (e.g. some individuals had foot spasms and others had shaking feet), which resulted in motion artefacts and misalignment between test-retest images. Thus, future studies should provide a custom cast/plate that does not affect recordings and which allows patients to sit with more comfort (our study incorporated the custom plate after we had completed scanning RA patients). When deciding on a scan protocol, a risk-benefit analysis needs to be done. It is ideal to get the most information from the scanner in the shortest period of time. However, more information requires more slice scans, slower scan speed and higher voxel resolution, and all of these require more time. Depending on the population, it is not always feasible to set up long protocols, as this may result in motion artefacts, which will distort the scan images.

Some physical barriers were also encountered during scanning. One such obstacle was the variability in foot size. The pQCT modality is not suitable for individuals of all

sizes, as those with bigger, thicker feet had difficulty fitting inside the holder. This makes it difficult to position due to the sensitivity of the machine, and because the scanner requires the peripheral joints to be centered in the gantry. To add, thicker feet often have more soft tissue, thus it was difficult to palpate feet and locate the MTPJs in participants with these conditions, which may have contributed to difficulty detecting the distal MT head in the scout view scan. Lastly, anatomically, all participants were different and this affected the slope of the MT heads. Some individuals had a larger distance between their second and fifth MT heads, making it challenging to fit MTPJs 2-5 in the short frame that was scanned during the scout view scan.

In addition, due to time constraints and logistics, patients had to be scanned twice within the same day for reproducibility measures. Previous research has shown that test-retest on the same day may underestimate the %CV values, and therefore the reproducibility (Chaplais *et al.*, 2014). Thus, there is a possibility that a type II statistical error may have occurred, where there is a true difference, but findings appear non-significant (Chaplais *et al.*, 2014). For future studies, we would suggest repeat scans on separate days.

Chapter 5.0 Conclusion

Currently, bone erosion detection in RA patients is suboptimal due to clinical and imaging limitations. To our knowledge, this is the first study to explore the use of pQCT in an RA population to quantify vBMD in MTPJs 2-5 as a surrogate marker for the presence of erosions. The present study has reliably reported vBMD at MTPJs 2 and 3, suggesting that the protocol is optimized for these two joints. As well, total and cortical subcortical density appeared to be lower in MTPJ 3 of RA patients compared to matched controls. The general agreement between quadrant level pQCT vBMD measures for total and cortical subcortical density and MR quadrant localized erosion data suggests that the reduced vBMD in RA patients are reflective of true bone damage. Thus, our results suggest that total and cortical subcortical density can indeed be used as surrogate markers for the presence of bone erosions.

This research is still in its infancy. We recommend future studies to perform a follow-up to determine whether change in vBMD correlates with a change in erosion size on MRI. As well, we recommend a larger sample size and longitudinal data so that it can be determined if vBMD measures are reproducible in the long-term. Currently pQCT is only used for research purposes, but if future studies demonstrate long-term reproducibility of results with this modality, perhaps it can be used in tandem with MRI and US to better elucidate the presence of smaller grade erosions. It is also beneficial that we now have a reference dataset to compare to. To conclude, the use of pQCT in the MTPJs as an imaging modality in clinical trials may be an additional option when assessing response to therapy.

References

Aeberli D, Eser P, Bonel H, Widmer J, Caliezi G, Varisco P, Möller B, and Villiger P (2010) Reduced trabecular bone mineral density and cortical thickness accompanied by increased outer bone circumference in metacarpal bone of rheumatoid arthritis patients: a cross-sectional study. *Arthritis Res Ther* **12**:1–10.

Alasaarela E, Suramo I, Tervonen O, Lahde S, Takalo R, and Hakala M (1998) Evaluation of humeral head erosions in rheumatoid arthritis: a comparison of ultrasonography, magnetic resonance imaging, computed tomography and plain radiography. *Br J Rheumatol* **37**:1152–1156.

Albrecht A, Finzel S, Englbrecht M, Rech J, Hueber A, Schlechtweg P, Uder M, and Schett G (2013) The structural basis of MRI bone erosions: an assessment by microCT. *Ann Rheum Dis* **72**:1351–1357.

Alenfeld FE, Diessel E, Brezger M, Sieper J, Felsenberg D, and Braun J (2000) Detailed analyses of periarticular osteoporosis in rheumatoid arthritis. *Osteoporos Int* **11**:400–407.

Aletaha D, Neogi T, Silman A, Funovits J, Felson D, Bingham C, Birnbaum N, Burmester G, Bykerk V, Cohen M, Combe B, Costenbader K, Dougados M, Emery P, Ferraccioli G, Hazes J, Hobbs K, Huizinga T, Kavanaugh A, Kay J, Kvien T, Laing T, Mease P, Menard H, Moreland L, Naden R, Pincus T, Smolen J, Stanislawska-Biernat E, Symmons D, Tak P, Upchurch K, Vencovsky J, Wolfe F, and Hawker G (2010) 2010 Rheumatoid Arthritis Classification Criteria. *Arthritis Rheum* **62**:2569–2581.

Aletaha D, and Smolen JS (2018) Diagnosis and management of rheumatoid arthritis. *J Am Med Assoc* **320**:1360–1372.

Aschenberg S, Finzel S, Schmidt S, Kraus S, Engelke K, Englbrecht M, Rech J, and Schett G (2013) Catabolic and anabolic periarticular bone changes in patients with rheumatoid arthritis: a computed tomography study on the role of age, disease duration and bone markers. *Arthritis Res Ther* **15**:R62, BioMed Central Ltd.

Barnabe C, Toepfer D, Marotte H, Hauge E-M, Scharmga A, Kocijan R, Kraus S, Boutroy S, Schett G, Keller KK, de Jong J, Stok KS, Finzel S, and SPECTRA Collaboration (2016) Definition for rheumatoid arthritis erosions imaged with high resolution peripheral quantitative computed tomography and interreader reliability for detection and measurement. *J Rheumatol* **43**:1935–1940.

Barrett-Connor E, Siris ES, Wehren LE, Miller PD, Abbott TA, Berger ML, Santora AC, and Sherwood LM (2005) Osteoporosis and fracture risk in women of different ethnic groups. *J Bone Miner Res* **20**:185–194.

Berger A (2002) How does it work?: Magnetic resonance imaging. *Br Med J* **324**:35.

Binkley TL, and Specker BL (2000) pQCT measurement of bone parameters in young children - validation of technique. *J Clin Densitom* **3**:9–14.

Boeters DM, Nieuwenhuis WP, van Steenbergen HW, Reijnierse M, Landewé RBM, and van der Helm-van Mil AHM (2018) Are MRI-detected erosions specific for RA? A large explorative cross-sectional study. *Ann Rheum Dis* **77**:861–868.

Boini S, and Guillemin F (2001) Radiographic scoring methods as outcome measures in rheumatoid arthritis: properties and advantages. *Ann Rheum Dis* **60**:817–827.

Boutroy S, Bouxsein ML, Munoz F, and Delmas PD (2005) In vivo assessment of trabecular bone microarchitecture by high-resolution peripheral quantitative computed tomography. *J Clin Endocrinol Metab* **90**:6508–6515.

Boutry N, Lardé A, Lapègue F, Solau-Gervais E, Flipo R-M, and Cotten A (2003) Magnetic resonance imaging appearance of the hands and feet in patients with early rheumatoid arthritis. *J Rheumatol* **30**:671–679.

Brigden M (1998) The erythrocyte sedimentation rate. *Postgrad Med* **103**:257–274.

Briggs AM, Perilli E, Parkinson IH, Wrigley T V, Fazzalari NL, Kantor S, and Wark JD (2010) Novel assessment of subregional bone mineral density using DXA and pQCT and subregional microarchitecture using micro-CT in whole human vertebrae: applications, methods, and correspondence between technologies. *J Clin Densitom Assess Skelet Heal* **13**:161–174, Elsevier Ltd.

Bruce B, and Fries JF (2005) The health assessment questionnaire (HAQ). *Clin Exp Rheumatol* **23**:S14–S18.

Bruce B, and Fries JF (2003) The Stanford health assessment questionnaire: a review of its history, issues, progress, and documentation. *J Rheumatol* **30**:167–178.

Brunet S, Finzel S, Engelke K, Boyd S, Barnabe C, and Manske S (2019) Bone changes assessed by high-resolution peripheral quantitative computed tomography (HR-pQCT) in early inflammatory arthritis: a 12-month cohort study. *Ann Rheum Dis* 1–30.

Burghardt AJ, Lee CH, Kuo D, Majumdar S, Imboden JB, Link TM, and Li X (2013) Quantitative in vivo HR-pQCT imaging of 3D wrist and metacarpophalangeal joint space width in rheumatoid arthritis. *Ann Biomed Eng* **41**:2553–2564.

Burmester GR, and Pope JE (2017) Targeted treatments for rheumatoid arthritis 2 - novel treatment strategies in rheumatoid arthritis. *Lancet* **389**:2338–2348.

Cate DF Ten, Luime JJ, Swen N, Gerards AH, De Jager MH, Basoski NM, Hazes JM, Haagsma CJ, and Jacobs JW (2013) Role of ultrasonography in diagnosing early rheumatoid arthritis and remission of rheumatoid arthritis - a systematic review of the literature. *Arthritis Res Ther* **15**:1–9, BioMed Central Ltd.

Chaplais E, Greene D, Hood A, Telfer S, du Toit V, Singh-Grewal D, Burns J, Rome K, Schiferl DJ, and Hendry GJ (2014) Reproducibility of a peripheral quantitative computed tomography scan protocol to measure the material properties of the second metatarsal. *BMC Musculoskelet Disord* **15**:1–6.

Cheung AM, Adachi JD, Hanley D, Kendler D, Davison K, Josse R, Brown J, Ste-Marie L, Kremer R, Erlandson MC, Dian L, Burghardt AJ, and Boyd SK (2013) High-resolution peripheral quantitative computed tomography for the assessment of bone strength and structure: a review by the Canadian Bone Strength Working Group. *Curr Osteoporos Rep* **11**:136–146.

Chirchir H (2016) Limited trabecular bone density heterogeneity in the human skeleton. *Anat Res Int* **2016**:1–7, Hindawi Publishing Corporation.

Choy E, and Panayi G (2001) Cytokine pathways and joint inflammation in rheumatoid arthritis. *N Engl J Med* **344**:907–917.

Colebatch AN, Edwards CJ, Østergaard M, van der Heijde D, Balint P V, D'Agostino M-A, Forslind K, Grassi W, Haavardsholm EA, Haugeberg G, Jurik A-G, Landewé

RBM, Naredo E, O'Connor PJ, Ostendorf B, Potocki K, Schmidt WA, Smolen JS, Sokolovic S, Watt I, and Conaghan PG (2013) EULAR recommendations for the use of imaging of the joints in the clinical management of rheumatoid arthritis. *Ann Rheum Dis* **72**:804–814.

Conaghan P, Bird P, Ejbjerg B, O'Connor P, Peterfy C, McQueen F, Lassere M, Emery P, Shnier R, Edmonds J, and Østergaard M (2005) The EULAR-OMERACT rheumatoid arthritis MRI reference image atlas: the metacarpophalangeal joints. *Ann Rheum Dis* **64**:11–21.

Conaghan PG, O'Connor P, McGonagle D, Astin P, Wakefield RJ, Gibbon WW, Quinn M, Karim Z, Green MJ, Proudman S, Isaacs J, and Emery P (2003) Elucidation of the relationship between synovitis and bone damage - a randomized magnetic resonance imaging study of individual joints in patients with early rheumatoid arthritis. *Arthritis Rheum* **48**:64–71.

Curtis E, Litwic A, Cooper C, and Dennison E (2015) Determinants of muscle and bone aging. *J Cell Physiol* **230**:2618–2625.

D'Agostino MA, Terslev L, Aegerter P, Backhaus M, Balint P, Bruyn GA, Filippucci E, Grassi W, Iagnocco A, Jousse-Joulin S, Kane D, Naredo E, Schmidt W, Szkudlarek M, Conaghan PG, and Wakefield RJ (2017) Scoring ultrasound synovitis in rheumatoid arthritis: A EULAR-OMERACT ultrasound taskforce - part 1: definition and development of a standardised, consensus-based scoring system. *RMD Open* **3**:1–9.

Daly RM, Rosengren BE, Alwis G, Ahlborg HG, Sernbo I, and Karlsson MK (2013) Gender specific age-related changes in bone density, muscle strength and functional performance in the elderly: a-10 year prospective population-based study. *BMC Geriatr* **13**:2–9, BMC Geriatrics.

Daragon A, Krzanowska K, Vittecoq O, Ménard J-F, Hau I, Jouen-Beades F, Lesage C, Bertho J-M, Tron F, and Le Loët X (2001) Prospective X-ray densitometry and ultrasonography study of the hand bones of patients with rheumatoid arthritis of recent onset. *Jt Bone Spine* **68**:34–42.

Demontiero O, Vidal C, and Duque G (2012) Aging and bone loss: new insights for the clinician. *Ther Adv Musculoskelet Dis* **4**:61–76.

Deodhar AA, Brabyn J, Jones PW, Davis MJ, and Woolf AD (1995) Longitudinal study of hand bone densitometry in rheumatoid arthritis. *Arthritis Rheum* **38**:1204–1210.

Department of Health and Human Services (2004) *Bone Health and Osteoporosis: A Report of the Surgeon General*, Rockville.

Devlin J, Lilley J, Gough A, Huissoon A, Holder R, Reece R, Perkins P, and Emery P (1996) Clinical associations of dual-energy X-ray absorptiometry measurement of hand bone mass in rheumatoid arthritis. *Br J Rheumatol* **35**:1256–1262.

Dill T (2008) Contraindications to magnetic resonance imaging. *Heart* **94**:943–948.

do Prado AD, Staub HL, Bisi MC, da Silveira IG, Mendonça JA, Polido-Pereira J, and Fonseca JE (2018) Ultrasound and its clinical use in rheumatoid arthritis: where do we stand? *Adv Rheumatol* **58**:1–10, Advances in Rheumatology.

Døhn UM, Ejbjerg B, Boonen A, Hetland ML, Hansen MS, Knudsen LS, Hansen A, Madsen OR, Hasselquist M, Møller JM, and Østergaard M (2011) No overall

progression and occasional repair of erosions despite persistent inflammation in adalimumab-treated rheumatoid arthritis patients: results from a longitudinal comparative MRI, ultrasonography, CT and radiography study. *Ann Rheum Dis* **70**:252–258.

Døhn UM, Ejbjerg BJ, Court-Payen M, Hasselquist M, Narvestad E, Szkudlarek M, Møller JM, Thomsen HS, and Østergaard M (2006) Are bone erosions detected by magnetic resonance imaging and ultrasonography true erosions? A comparison with computed tomography in rheumatoid arthritis metacarpophalangeal joints. *Arthritis Res Ther* **8**:1–9.

Døhn UM, Ejbjerg BJ, Hasselquist M, Narvestad E, Court-Payen M, Szkudlarek M, Møller J, Thomsen HS, and Østergaard M (2007) Rheumatoid arthritis bone erosion volumes on CT and MRI: reliability and correlations with erosion scores on CT, MRI and radiography. *Ann Rheum Dis* **66**:1388–1392.

Døhn UM, Ejbjerg BJ, Hasselquist M, Narvestad E, Møller J, Thomsen HS, and Østergaard M (2008) Detection of bone erosions in rheumatoid arthritis wrist joints with magnetic resonance imaging, computed tomography and radiography. *Arthritis Res Ther* **10**:1–8.

Duff WRD, Björkman KM, Kawalilak CE, Kehrig AM, Wiebe S, and Kontulainen S (2017) Precision of pQCT-measured total, trabecular and cortical bone area , content, density and estimated bone strength in children. *J Musculoskelet Neuronal Interact* **17**:59–68.

Egerer K, Feist E, and Burmester G (2009) The serological diagnosis of rheumatoid arthritis. *Dtsch Arztebl Int* **106**:159–163.

Felder M, and Ruegsegger P (1991) Bone loss in patients with rheumatoid arthritis - effect of steroids measured by low dose quantitative computed tomography. *Rheumatol Int* **11**:41–44.

Finzel S, Ohrndorf S, Englbrecht M, Stach C, Messerschmidt J, Schett G, and Backhaus M (2011) A detailed comparative study of high-resolution ultrasound and micro–computed tomography for detection of arthritic bone erosions. *Arthritis Rheum* **63**:1231–1236.

Firestein GS, and Mcinnes IB (2017) Immunopathogenesis of rheumatoid arthritis. *Immun Rev* **46**:183–196, Elsevier Inc.

Fonseca A, Gordon CL, and Barr RD (2013) Peripheral quantitative computed tomography (pQCT) to assess bone health in children, adolescents, and young adults: A review of normative data. *J Pediatr Hematol Oncol* **35**:581–589.

Fouque-Aubert A, Boutroy S, Marotte H, Vilayphiou N, Bacchetta J, Miossec P, Delmas PD, and Chapurlat RD (2010) Assessment of hand bone loss in rheumatoid arthritis by high-resolution peripheral quantitative CT. *Ann Rheum Dis* **69**:1671–1676.

Fujii Y, Miyauchi A, Takagi Y, Goto B, and Fujita T (1995) Fixed ratio between radial cortical volume and density measured by peripheral quantitative computed tomography (pQCT) regardless of age and sex. *Calcif Tissue Int* **56**:586–588.

Fuller JT, Archer J, Buckley JD, Tsiros MD, and Thewlis D (2016) The reliability of dual-energy X-ray absorptiometry measurements of bone mineral density in the metatarsals. *Skeletal Radiol* **45**:135–140.

Geusens P, and van den Bergh J (2014) Bone erosions in rheumatoid arthritis. *Rheumatology* **53**:4–5.

Gluer C, Blake G, Lu Y, Blunt B, Jergas M, and Genant H (1995) Accurate assessment of precision errors: how to measure the reproducibility of bone densitometry techniques. *Osteoporos Int* **5**:262–270.

Goldring SR (2003) Pathogenesis of bone and cartilage destruction in rheumatoid arthritis. *Rheumatology* **42**:ii11–ii16.

Gonzalez J, and Gottlieb A (2016) Review of the health assessment questionnaire use in psoriatic arthritis. *J Psoriasis Psoriatic Arthritis* **1**:74–79.

Hammer HB, Bolton-King P, Bakkeheim V, Berg TH, Sundt E, Kongtorp AK, and Haavardsholm EA (2011) Examination of intra and interrater reliability with a new ultrasonographic reference atlas for scoring of synovitis in patients with rheumatoid arthritis. *Ann Rheum Dis* **70**:1–4.

Harvey C, and Blomley M (2005) Principles and precautions of conventional radiography. *Surg* **23**:158–161.

Haugeberg G, Green MJ, Quinn MA, Marzo-Ortega H, Proudman S, Karim Z, Wakefield RJ, Conaghan PG, Stewart S, and Emery P (2006) Hand bone loss in early undifferentiated arthritis: evaluating bone mineral density loss before the development of rheumatoid arthritis. *Ann Rheum Dis* **65**:736–740.

Haugeberg G, Ørstavik RE, Uhlig T, Falch JA, Halse JI, and Kvien TK (2002) Bone loss in patients with rheumatoid arthritis - results from a population-based cohort of 366 patients followed up for two years. *Arthritis Rheum* **46**:1720–1728.

Helliwell P, Reay N, Gilworth G, Redmond A, Slade A, Tennant A, and Woodburn J (2005) Development of a foot impact scale for rheumatoid arthritis. *Arthritis Rheum* **53**:418–422.

Hoff M, and Haugeberg G (2010) Using hand bone mass measurements to assess progression of rheumatoid arthritis. *Ther Adv Musculoskelet Dis* **2**:79–87.

Hoff M, Haugeberg G, and Kvien TK (2007) Hand bone loss as an outcome measure in established rheumatoid arthritis: 2-year observational study comparing cortical and total bone loss. *Arthritis Res Ther* **9**:1–8.

Ingegnoli F, Castelli R, and Gualtierotti R (2013) Rheumatoid factors: clinical applications. *Dis Markers* **35**:727–734.

Jensen T, Hansen M, Jensen KE, Pødenphant J, Hansen TM, and Hyldstrup L (2005) Comparison of dual X-ray absorptiometry (DXA), digital X-ray radiogrammetry (DXR), and conventional radiographs in the evaluation of osteoporosis and bone erosions in patients with rheumatoid arthritis. *Scand J Rheumatol* **34**:27–33.

Jensen T, Klarlund M, Hansen M, Jensen K, Podenphant J, Hansen T, Skjodt H, Hyldstrup L, and TIRA group (2004) Bone loss in unclassified polyarthritis and early rheumatoid arthritis is better detected by digital x ray radiogrammetry than dual x ray absorptiometry: relationship with disease activity and radiographic outcome. *Ann Rheum Dis* **63**:15–22.

Jimenez-Boj E, Nobauer-Huhmann I, Hanslik-Schnabel B, Dorotka R, Wanivenhaus A-H, Kainberger F, Trattnig S, Axmann R, Tsuji W, Hermann S, Smolen J, and Schett G (2007) Bone erosions and bone marrow edema as defined by magnetic resonance

imaging reflect true bone marrow inflammation in rheumatoid arthritis. *Arthritis Rheum* **56**:1118–1124.

Joshua F, Edmonds J, and Lassere M (2006) Power Doppler ultrasound in musculoskeletal disease: a systematic review. *Semin Arthritis Rheum* **36**:99–108.

Juhász B, Gulyás K, Horváth Á, Petho Z, Bhattoa HP, Vancsa A, Szekanecz E, Horváth C, Kocsis J, Horváth Z, Hodosi K, Szanto S, Szucs G, and Szekanecz Z (2017) Comparison of peripheral quantitative computed tomography forearm bone density versus DXA in rheumatoid arthritis patients and controls. *Osteoporos Int* **28**:1271–1277.

Katti G, Ara SA, and Shireen A (2011) Magnetic resonance imaging (MRI) – a review. *Int J Dent Clin* **3**:65–70.

Kawashiri S, Suzuki T, Nakashima Y, Horai Y, Okada A, Iwamoto N, Ichinose K, Tamai M, Arima K, Nakamura H, Origuchi T, Uetani M, Aoyagi K, Eguchi K, and Kawakami A (2014) Ultrasonographic examination of rheumatoid arthritis patients who are free of physical synovitis: power Doppler subclinical synovitis is associated with bone erosion. *Rheumatology* **53**:562–569.

Kay J, and Upchurch KS (2015) ACR/EULAR 2010 rheumatoid arthritis classification criteria. *Rheumatology* **51**:vi5–vi9.

Kim K-W, Kim B-M, Moon H-W, Lee S-H, and Kim H-R (2015) Role of C-reactive protein in osteoclastogenesis in rheumatoid arthritis. *Arthritis Res Ther* **17**:1–12.

Kim TK (2015) T test as a parametric statistic. *Korean J Anesthesiol* **68**:540–546.

Kocijan R, Finzel S, Englbrecht M, Engelke K, Rech J, and Schett G (2014) Decreased quantity and quality of the periarticular and nonperiarticular bone in patients with rheumatoid arthritis: a cross-sectional HR-pQCT study. *J Bone Miner Res* **29**:1005–1014.

Kong S, Locrelle H, Amouzougan A, Denarie D, Collet P, Pallot-Prades B, Thomas T, and Marotte H (2018) Remaining local subclinical joint inflammation is associated with deteriorated metacarpeal head bone microarchitecture in rheumatoid arthritis patients low disease activity. *Jt Bone Spine* **85**:569–572.

Koo TK, and Li MY (2016) A guideline of selecting and reporting intraclass correlation coefficients for reliability research. *J Chiropr Med* **15**:155–163, Elsevier B.V.

Kothari M, Keaveny TM, Lin JC, Newitt DC, Genant HK, and Majumdar S (1998) Impact of spatial resolution on the prediction of trabecular architecture parameters. *Bone* **22**:437–443.

Kushdilian M, Ladd L, and Gunderman R (2016) Radiology in the study of bone physiology. *Acad Radiol* **23**:1298–1308, Elsevier Inc.

Landewé R, and van der Heijde D (2005) Radiographic progression in rheumatoid arthritis. *Clin Exp Rheumatol* **23**:S63–S68.

Ledingham J, Snowden N, and Ide Z (2017) Diagnosis and early management of inflammatory arthritis. *Br Med J* **358**:1–8.

Lee CH, Srikhum W, Burghardt AJ, Virayavanich W, Imboden JB, Link TM, and Li X (2015) Correlation of structural abnormalities of the wrist and metacarpophalangeal joints evaluated by high-resolution peripheral quantitative computed tomography, 3 Tesla magnetic resonance imaging and conventional radiographs in rheumatoid

arthritis. *Int J Rheum Dis* **18**:628–639.
Li SC, and Liebling MS (2009) The use of Doppler ultrasound to evaluate lesions of localized scleroderma. *Curr Rheumatol Rep* **11**:205–211.
Litao MKS, and Kamat D (2014) Erythrocyte sedimentation rate and C-reactive protein: How best to use them in clinical practice. *Pediatr Ann* **43**:417–420.
Looker AC, Melton III LJ, Harris T, Borrud L, Shepherd J, and McGowan J (2009) Age, gender, and race/ethnic differences in total body and subregional bone density. *Osteoporos Int* **20**:1141–1149.
Maetzel A, Li L, Pencharz J, Tomlinson G, Bombardier C, and Team CH and APS (2004) The economic burden associated with osteoarthritis, rheumatoid arthritis, and hypertension: a comparative study. *Ann Rheum Dis* **63**:395–401.
Majithia V, and Geraci SA (2007) Rheumatoid arthritis: diagnosis and management. *Am J Med* **120**:936–939.
Malm K, Bergman S, Andersson MLE, Bremander A, and Larsson I (2017) Quality of life in patients with established rheumatoid arthritis: a phenomenographic study. *SAGE Open Med* **5**:1–8.
Manhard MK, Nyman JS, and Does MD (2017) In-depth review of biology and treatment of bone disorders. *Transl Res* **181**:1–14, Elsevier Inc.
Maricic M (2014) Use of DXA-based technology for detection and assessment of risk of vertebral fracture in rheumatology practice. *Curr Rheumatol Rep* **16**:1–7.
Martin JC, Munro R, Campbell MK, and Reid DM (1997) Effects of disease and corticosteroids on appendicular bone mass in postmenopausal women with rheumatoid arthritis: comparison with axial measurements. *Br J Rheumatol* **36**:43–49.
Mateen S, Zafar A, Moin S, Khan AQ, and Zubair S (2016) Understanding the role of cytokines in the pathogenesis of rheumatoid arthritis. *Clin Chim Acta* **455**:161–171, Elsevier B.V.
McGonagle D, Tan AL, Døhn UM, Østergaard M, and Benjamin M (2009) Microanatomic studies to define predictive factors for the topography of periarticular erosion formation in inflammatory arthritis. *Arthritis Rheum* **60**:1042–1051.
Mcinnes IB, Buckley CD, and Isaacs JD (2015) Cytokines in rheumatoid arthritis - shaping the immunological landscape. *Nat Rev Rheumatol* **12**:63–68, Nature Publishing Group.
McMahon K, Cowin G, and Galloway G (2011) Magnetic resonance imaging: the underlying principles. *J Orthop Sport Phys Ther* **41**:806–819.
McQueen FM (2000) Magnetic resonance imaging in early inflammatory arthritis: What is its role? *Rheumatology* **39**:700–706.
McQueen FM, Stewart N, Crabbe J, Robinson E, Yeoman S, Tan PLJ, and McLean L (1998) Magnetic resonance imaging of the wrist in early rheumatoid arthritis reveals a high prevalence of erosions at four months after symptom onset. *Ann Rheum Dis* **57**:350–356.
Mukaka MM (2012) Statistics corner: a guide to appropriate use of correlation coefficient in medical research. *Malawi Med J* **24**:69–71.
Muradin I, and van der Heide HJL (2016) The foot function index is more sensitive to

change than the Leeds Foot Impact Scale for evaluating rheumatoid arthritis patients after forefoot or hindfoot reconstruction. *Int Orthop* **40**:745–749.

Naredo E, D'Agostino MA, Wakefield RJ, Möller I, Balint P V, Filippucci E, Iagnocco A, Karim Z, Terslev L, Bong DA, Garrido J, Martínez-Hernández D, Bruyn GAW, and Force OUT (2013) Reliability of a consensus-based ultrasound score for tenosynovitis in rheumatoid arthritis. *Ann Rheum Dis* **72**:1328–1334.

Naumann L, Hermann K, Huscher D, Lenz K, Burmester G, Backhaus M, and Buttgereit F (2012) Quantification of periarticular demineralization and synovialitis of the hand in rheumatoid arthritis patients. *Osteoporos Int* **23**:2671–2679.

Nikander R, Sievänen H, Uusi-Rasi K, Heinonen A, and Kannus P (2006) Loading modalities and bone structures at nonweight-bearing upper extremity and weight-bearing lower extremity: a pQCT study of adult female athletes. *Bone* **39**:886–894.

Nilas L, and Christiansen C (1988) Rates of bone loss in normal women: evidence of accelerated trabecular bone loss after the menopause. *Eur J Clin Invest* **18**:529–534.

Norman D, Mills C, Brant-Zawadzki M, Yeates A, Crooks L, and Kaufman L (1983) Magnetic resonance imaging of the spinal cord and canal: potentials and limitations. *Am J Roentgenol* **141**:1147–1152.

Ory PA (2003) Interpreting radiographic data in rheumatoid arthritis. *Ann Rheum Dis* **62**:597–604.

Østergaard M, Hansen M, Stoltenberg M, Gideon P, Klarlund M, Jensen KE, and Lorenzen I (1999) Magnetic resonance imaging-determined synovial membrane volume as a marker of disease activity and a predictor of progressive joint destruction in the wrists of patients with rheumatoid arthritis. *Arthritis Rheum* **42**:918–929.

Østergaard M, Pedersen SJ, and Dohn UM (2008) Imaging in rheumatoid arthritis – status and recent advances for magnetic resonance imaging, ultrasonography, computed tomography and conventional radiography. *Best Pract Res Clin Rheumatol* **22**:1019–1044, Elsevier Ltd.

Ostergaard M, Peterfy C, Conaghan P, McQueen F, Bird P, Ejbjerg B, Shnier R, O'Connor P, Klarlund M, Emery P, Genant H, Lassere M, and Edmonds J (2003) OMERACT rheumatoid arthritis magnetic resonance imaging studies. Core set of MRI acquisitions, joint pathology defintions, and the OMERACT RA-MRI scoring system. *J Rheumatol* **30**:1385–1386.

Østergaard M, Peterfy CG, Bird P, Gandjbakhch F, Glinatsi D, Eshed I, Haavardsholm EA, Lillegraven S, Bøyesen P, Ejbjerg B, Foltz V, Emery P, Genant HK, and Conaghan PG (2017) The OMERACT rheumatoid arthritis magnetic resonance imaging (MRI) scoring system: updated recommendations by the OMERACT MRI in arthritis working group. *J Rheumatol* **44**:1706–1712.

Østergaard M, and Wiell C (2004) Ultrasonography in rheumatoid arthritis: a very promising method still needing more validation. *Curr Opin Rheumatol* **16**:223–230.

Otter SJ, Lucas K, Springett K, Moore A, Davies K, Cheek L, Young A, and Walker-Bone K (2010) Foot pain in rheumatoid arthritis prevalence, risk factors and management: An epidemiological study. *Clin Rheumatol* **29**:255–271.

Ozgocmen S, Kiris A, Kocakoc E, Ardicoglu O, and Kamanli A (2004) Evaluation of

metacarpophalangeal joint synovitis in rheumatoid arthritis by power Doppler technique: relationship between synovial vascularization and periarticular bone mineral density. *Jt Bone Spine* **71**:384–388.

Papaioannou A, Kennedy C, Cranney A, Hawker G, Brown J, Kaiser S, Leslie W, O'Brien C, Sawka A, Khan A, Siminoski K, Tarulli G, Webster D, McGowan J, and Adachi J (2009) Risk factors for low BMD in healthy men age 50 years or older: a systematic review. *Osteoporos Int* **20**:507–518.

Perry D, Stewart N, Benton N, Robinson E, Yeoman S, Crabbe J, and McQueen F (2005) Detection of erosions in the rheumatoid hand; a comparative study of multidetector computerized tomography versus magnetic resonance scanning. *J Rheumatol* **32**:256–267.

Peters M, van den Bergh J, Geusens P, Scharmga A, Loeffen D, Weijers R, van Rietbergen B, and van Tubergen A (2019) Prospective follow-up of cortical interruptions, bone density, and micro-structure detected on HR-pQCT: a study in patients with rheumatoid arthritis and healthy subjects. *Calcif Tissue Int* **104**:571–581, Springer US.

Polidoulis I, Beyene J, and Cheung A (2012) The effect of exercise on pQCT parameters of bone structure and strength in postmenopausal women - a systematic review and meta-analysis of randomized controlled trials. *Osteoporos Int* **23**:39–51.

Porter D, Gadsby K, Thompson P, White J, McClinton C, and Oliver S (2011) DAS28 and rheumatoid arthritis: the need for standardization. *Musculoskeletal Care* **9**:222–227.

Rantalainen T, Nikander R, Daly RM, Heinonen A, and Sievänen H (2011) Exercise loading and cortical bone distribution at the tibial shaft. *Bone* **48**:786–791.

Rantalainen T, Nikander R, Heinonen A, Suominen H, and Sievanen H (2010) Direction-specific diaphyseal geometry and mineral mass distribution of tibia and fibula: a pQCT study of female athletes representing different exercise loading types. *Calcif Tissue Int* **86**:447–454.

Raymond KN, and Pierre VC (2005) Next generation, high relaxivity gadolinium MRI agents. *Bioconjug Chem* **16**:3–8.

Regensburger A, Rech J, Englbrecht M, Finzel S, Kraus S, Hecht K, Kleyer A, Haschka J, Hueber AJ, Cavallaro A, Schett G, and Faustini F (2015) A comparative analysis of magnetic resonance imaging and high-resolution peripheral quantitative computed tomography of the hand for the detection of erosion repair in rheumatoid arthritis. *Rheumatology* **54**:1573–1581.

Roschger P, Gupta H, Berzlanovich A, Ittner G, Dempster D, Fratzl P, Cosman F, Parisien M, Lindsay R, Nieves J, and Klaushofer K (2003) Constant mineralization density distribution in cancellous human bone. *Bone* **32**:316–323.

Rowbotham EL, and Grainger AJ (2011) Rheumatoid arthritis: ultrasound versus MRI. *Am J Roentgenol* **197**:541–546.

Scharmga A, Peters M, van den Bergh JP, Geusens P, Loeffen D, van Rietbergen B, Schoonbrood T, Vosse D, Weijers R, and van Tubergen A (2018) Development of a scoring method to visually score cortical interruptions on high-resolution peripheral quantitative computed tomography in rheumatoid arthritis and healthy controls.

PLoS One **13**:1–13.

Schett G, and Gravallese E (2012) Bone erosion in rheumatoid arthritis: mechanisms, diagnosis and treatment. *Nat Rev Rheumatol* **8**:656–664.

Shibuya K, Hagino H, Morio Y, and Teshima R (2002) Cross-sectional and longitudinal study of osteoporosis in patients with rheumatoid arthritis. *Clin Rheumatol* **21**:150–158.

Shields RK, Dudley-Javoroski S, Boaldin KM, Corey T, Fog DB, and Ruen JM (2006) Peripheral quantitative computed tomography: measurement sensitivity in persons with and without spinal cord injury. *Arch Phys Med Rehabil* **87**:1376–1381.

Shimizu S, Shiozawa S, Shiozawa K, Imura S, and Fujita T (1985) Quantitative histologic studies on the pathogenesis of periarticular osteoporosis in rheumatoid arthritis. *Arthritis Rheum* **28**:25–31.

Siddle HJ, Hensor EMA, Hodgson RJ, Grainger AJ, Redmond AC, Wakefield RJ, and Helliwell PS (2014) Anatomical location of erosions at the metatarsophalangeal joints in patients with rheumatoid arthritis. *Rheumatology* **53**:932–936.

Sievanen H, Koskue V, Rauhio A, Kannus P, Heinonen A, and Vuori I (1998) Peripheral quantitative computed tomography in human long bones: evaluation of in vitro and in vivo precision. *J Bone Miner Res* **13**:871–882.

Singh H, Kumar H, Handa R, Talapatra P, Ray S, and Gupta V (2011) Use of clinical disease activity index score for assessment of disease activity in rheumatoid arthritis patients: an Indian experience. *Arthritis* **2011**:1–5.

Siu W, Qin L, and Leung K (2003) pQCT bone strength index may serve as a better predictor than bone mineral density for long bone breaking strength. *J Bone Miner Metab* **21**:316–322.

Sornay-Rendu E, Boutroy S, Munoz F, and Delmas PD (2007) Alterations of cortical and trabecular architecture are associated with fractures in postmenopausal women, partially independent of decreased BMD measured by DXA: The OFELY study. *J Bone Miner Res* **22**:425–433.

Srikhum W, Virayavanich W, Burghardt AJ, Yu A, Link TM, Imboden JB, and Li X (2013) Quantitative and semiquantitative bone erosion assessment on high-resolution peripheral quantitative computed tomography in rheumatoid arthritis. *J Rheumatol* **40**:408–416.

Stach CM, Bauerle M, Englbrecht M, Kronke G, Engelke K, Manger B, and Schett G (2010) Periarticular bone structure in rheumatoid arthritis patients and healthy individuals assessed by high-resolution computed tomography. *Arthritis Rheum* **62**:330–339.

Stagi S, Cavalli L, Cavalli T, de Martino M, and Brandi ML (2016) Peripheral quantitative computed tomography (pQCT) for the assessment of bone strength in most of bone affecting conditions in developmental age: a review. *Ital J Pediatr* **42**:1–20.

Stathopoulos K, Zoubos A, Papaioannou N, Mastrokalos D, Galanos A, Papagelopoulos P, and Skarantavos G (2016) Differences of bone mineral mass, volumetric bone mineral density, geometrical and structural parameters and derived strength of the tibia between premenopausal and postmenopausal women of different age groups: a

peripheral quantitative computed tomograph. *J Musculoskelet Neuronal Interact* **16**:113–121.

Statistics Canada (2006) Musculoskeletal diseases: rheumatoid arthritis.

Szabo KA, Webber CE, Gordon C, Adachi JD, Tozer R, and Papaioannou A (2011) Reproducibility of peripheral quantitative computed tomography measurements at the radius and tibia in healthy pre- and postmenopausal women. *Can Assoc Radiol J* **62**:183–189.

Szekanecz Z, Soós L, Szabó Z, Fekete A, Kapitány A, Végvári A, Sipka S, Szücs G, Szántó S, and Lakos G (2008) Anti-citrullinated protein antibodies in rheumatoid arthritis: As good as it gets? *Clin Rev Allergy Immunol* **34**:26–31.

Szkudlarek M, Court-Payen M, Jacobsen S, Klarlund M, Thomsen HS, and Østergaard M (2003) Interobserver agreement in ultrasonography of the finger and toe joints in rheumatoid arthritis. *Arthritis Rheum* **48**:955–962.

Szkudlarek M, Klarlund M, Narvestad E, Court-Payen M, Strandberg C, Jensen K, Thomsen H, and Ostergaard M (2006) Ultrasonography of the metacarpophalangeal and proximal interphalangeal joints in rheumatoid arthritis: a comparison with magnetic resonance imaging, conventional radiography and clinical examination. *Arthritis Res Ther* **8**:1–11.

Szkudlarek M, Narvestad E, Klarlund M, Court-Payen M, Thomsen HS, and Østergaard M (2004) Ultrasonography of the metatarsophalangeal joints in rheumatoid arthritis - Comparison with magnetic resonance imaging, conventional radiography, and clinical examination. *Arthritis Rheum* **50**:2103–2112.

Taber K, Herrick R, Weathers S, Kumar A, Schomer D, and Hayman L (1998) Pitfalls and artifacts encountered in clinical MR imaging of the spine. *Radiographics* **18**:1499–1521.

Tan YK, and Conaghan PG (2011) Imaging in rheumatoid arthritis. *Best Pract Res Clin Rheumatol* **25**:569–584, Elsevier Ltd.

Topp T, Müller T, Huss S, Kann PH, Weihe E, Ruchholtz S, and Zettl RP (2012) Embalmed and fresh frozen human bones in orthopedic cadaveric studies: which bone is authentic and feasible? *Acta Orthop* **83**:543–547.

Towheed T, Gupta S, Glustein S, and Sahai V (2016) Quantifying the arthritis pyramid for Ontario by using comprehensive community health data. *J Heal Res Rev* **3**:86–91.

van der Woude D, Syversen SW, van der Voort EIH, Verpoort KN, Goll GL, van der Linden MPM, van der Helm-van Mil AHM, van der Heijde DMFM, Huizinga TWJ, Kvien TK, and Toes REM (2010) The ACPA isotype profile reflects long-term radiographic progression in rheumatoid arthritis. *Ann Rheum Dis* **69**:1110–1116.

van Riel PLCM, and Renskers L (2016) The disease activity score (DAS) and the disease activity score using 28 joint counts (DAS28) in the management of rheumatoid arthritis. *Clin Exp Rheumatol* **34**:S40–S44.

van Venrooij WJ, Hazes JM, and Visser H (2002) Anticitrullinated protein/peptide antibody and its role in the diagnosis and prognosis of early rheumatoid arthritis. *Neth J Med* **60**:383–388.

Veitch SW, Findlay SC, Ingle BM, Ibbotson CJ, Barrington A, Hamer AJ, and Eastell R

(2004) Accuracy and precision of peripheral quantitative computed tomography measurements at the tibial metaphysis. *J Clin Densitom* **7**:209–217.

Venables H (2011) How does ultrasound work? *Ultrasound* **19**:44–49.

Vlok J, Simm PJ, Lycett K, Clifford SA, Grobler AC, Lange K, Ismail N, Osborn W, and Wake M (2019) pQCT bone geometry and strength: population epidemiology and concordance in Australian children aged 11-12 years and their parents. *Br Med J Open* **9**:63–74.

Voshaar MAHO, ten Klooster PM, Glas CAW, Vonkeman HE, Taal E, Krishnan E, Moens HJB, Boers M, Terwee CB, van Riel PLCM, and van de Laar MAFJ (2015) Validity and measurement precision of the PROMIS physical function item bank and a content validity-driven 20-item short form in rheumatoid arthritis compared with traditional measures. *Rheumatology* **54**:2221–2229.

Vyas S, Bhalla AS, Ranjan P, Kumar S, Kumar U, and Gupta AK (2016) Rheumatoid arthritis revisited – advanced imaging review. *Polish J Radiol* **81**:629–635.

Wakefield RJ, Balint P V, Szkudlarek M, Filippucci E, Backhaus M, D'Agostino M-A, Sanchez EN, Iagnocco A, Schmidt WA, Bruyn GAW, Bruyn G, Kane D, O'Connor PJ, Manger B, Joshua F, Koski J, Grassi W, Lassere MND, Swen N, Kainberger F, Klauser A, Ostergaard M, Brown AK, Machold KP, and Conaghan PG (2005) Musculoskeletal ultrasound including definitions for ultrasonographic pathology. *J Rheumatol* **32**:2485–2487.

Weatherholt AM, Avin KG, Hurd AL, Cox JL, Marberry ST, Santoni BG, and Warden SJ (2016) Peripheral quantitative computed tomography (pQCT) predicts humeral diaphysis torsional mechanical properties with good short-term precision. *J Clin Densitom* **18**:551–559.

Weidekamm C, Koller M, Weber M, and Kainberger F (2003) Diagnostic value of high-resolution B-mode and Doppler sonography for imaging of hand and finger joints in rheumatoid arthritis. *Arthritis Rheum* **48**:325–333.

Widdifield J, Bernatsky S, Bombardier C, and Paterson JM (2015) Rheumatoid arthritis surveillance in Ontario: monitoring the burden, quality of care and patient outcomes through linkage of administrative health data. *Healthc Q* **18**:7–10.

Widdifield J, Bernatsky S, Paterson JM, Tomlinson G, Tu K, Kuriya B, Thorne JC, Pope JE, Hollands S, and Bombardier C (2015) Trends in excess mortality among patients with rheumatoid arthritis in Ontario, Canada. *Arthritis Care Res (Hoboken)* **67**:1047–1053.

Wilson O, Hewlett S, Woodburn J, Pollock J, and Kirwan J (2017) Prevalence, impact and care of foot problems in people with rheumatoid arthritis: Results from a United Kingdom based cross-sectional survey. *J Foot Ankle Res* **10**:1–11, Journal of Foot and Ankle Research.

Wong A (2016) A comparison of peripheral imaging technologies for bone and muscle quantification: a technical review of image acquisition. *J Musculoskelet Neuronal Interact* **16**:265–282.

Wong A, Beattie K, Min K, Gordon C, Pickard L, Papaioannou A, Adachi J, and Canadian Multicentre Osteoporosis Study (CaMos) Research Group (2014) Peripheral quantitative computed tomography-derived muscle density and peripheral

magnetic resonance imaging-derived muscle adiposity: precision and associations with fragility fractures in women. *J Musculoskelet Neuronal Interact* **14**:401–410.

Yang H, Yu A, Burghardt AJ, Virayavanich W, Link TM, Imboden JB, and Li X (2017) Quantitative characterization of metacarpal and radial bone in rheumatoid arthritis using high resolution- peripheral quantitative computed tomography. *Int J Rheum Dis* **20**:353–362.

Yazdani-Biuki B, Stadlmaier E, Mulabecirovic A, Brezinschek R, Tilz G, Demel U, Mueller T, Brickmann K, Graninger WB, and Brezinschek H-P (2005) Blockade of tumour necrosis factor alpha significantly alters the serum level of IgG- and IgA-rheumatoid factor in patients with rheumatoid arthritis. *Ann Rheum Dis* **64**:1224–1226.

Yue J, Griffith JF, Xu J, Xiao F, Shi L, Wang D, Wong PCH, Li EK, Li M, Li TK, Mak WY, Zhu TY, Hung VW, Qin L, and Tam L-S (2018) Effect of treat-to-target strategies on bone erosion progression in early rheumatoid arthritis: an HR-pQCT study. *Semin Arthritis Rheum* **48**:374–383.

Zengin A, Prentice A, and Ward KA (2015) Ethnic differences in bone health. *Front Endocrinol (Lausanne)* **6**:1–6.

Zhu TY, Griffith JF, Qin L, Hung VW, Fong TN, Au SK, Li M, Lam YY-O, Wong CK, Kwok AW, Leung PC, Li EK, and Tam LS (2014) Alterations of bone density, microstructure, and strength of the distal radius in male patients with rheumatoid arthritis: a case-control study with HR-pQCT. *J Bone Miner Res* **29**:2118–2129.

Zhu TY, Griffith JF, Qin L, Hung VWY, Fong TN, Kwok AW, Leung PC, Li EK, and Tam LS (2012) Bone density and microarchitecture: relationship between hand, peripheral, and axial skeletal sites assessed by HR-pQCT and DXA in rheumatoid arthritis. *Calcif Tissue Int* **91**:343–355.

Appendix

Appendix A1. 2010 ACR/EULAR Classification Criteria

Domain	Category	Point score
A	Joint involvement (0–5 points)[a]	
	1 large joint	0
	2–10 large joints	1
	1–3 small joints (large joints not counted)	2
	4–10 small joints (large joints not counted)	3
	>10 joints including at least one small joint	5
B	Serology (at least one test needed for classification; 0–3 points)[b]	
	Negative RF and negative ACPA	0
	Low positive RF or low positive ACPA	2
	High positive RF or high positive ACPA	3
C	Acute-phase reactants (at least one test needed for classification; 0–1 point)[c]	
	Normal CRP and normal ESR	0
	Abnormal CRP or abnormal ESR	1
D	Duration of symptoms[d]	
	<6 weeks	0
	⩾6 weeks	1

The points from each of domains A through D are added and the sum is considered to be the total score. A total score of ⩾6 is needed to classify a patient as having definite RA. [a]Joint involvement refers to any swollen or tender joint on examination, which may be confirmed by imaging evidence of synovitis. DIP joints, first CMC joints and first MTP joints are excluded from assessment. Large joints refers to shoulders, elbows, hips, knees and ankles. Small joints refers to MCP joints, PIP joints, second through fifth MTP joints, thumb IP joints and wrists. [b]Negative means less than or equal to the upper limit of normal (ULN); low positive means >ULN; high positive means >3× ULN. [c]Normal and abnormal are determined by local laboratory standards. [d]Duration of symptoms as per patient's self-report. Table adapted from Ref. [5] with permission of John Wiley and Sons Ltd.

Appendix A2. Standard Operating Procedure (SOP) for pQCT MTPJ protocol

Jessica Amin

Acknowledgements: Thank you to Dr. Andy Kin On Wong for helping to set up the protocol and Dr. Chris Gordon for letting us use the pQCT scanner.

This protocol is for the Stratec XCT 2000 (image below). The machine is located in 25 Charlton Ave, in suite 610. The thickness of each slice produced by the device is 2.3 mm. For the purposes of this protocol, each scan slice releases 1 μSv of radiation.

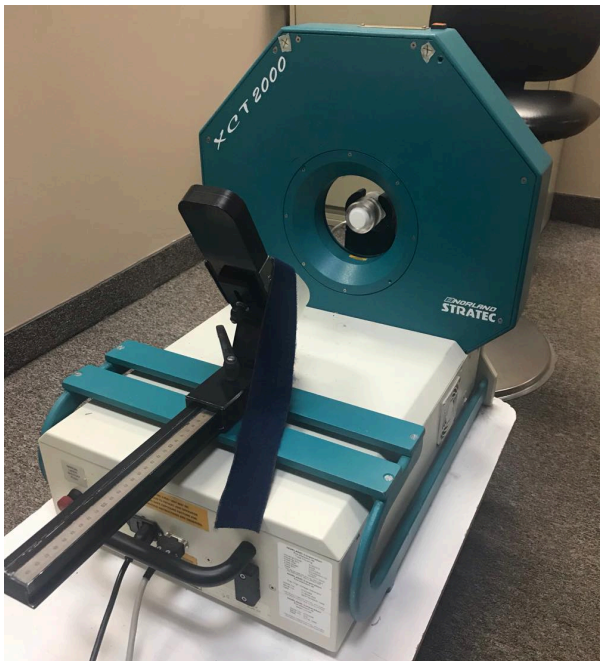

To begin:

1. Open “Start C_XCT” from the Desktop.
2. When asked “Create license entry?”, press “No”.
3. User ID: 9999, Password: service
4. Press “Esc” three times to reach the main menu.
5. Ensure that the phantom is placed in the holder and is centered in the gantry (refer to image below for front (left) and back (right) view).

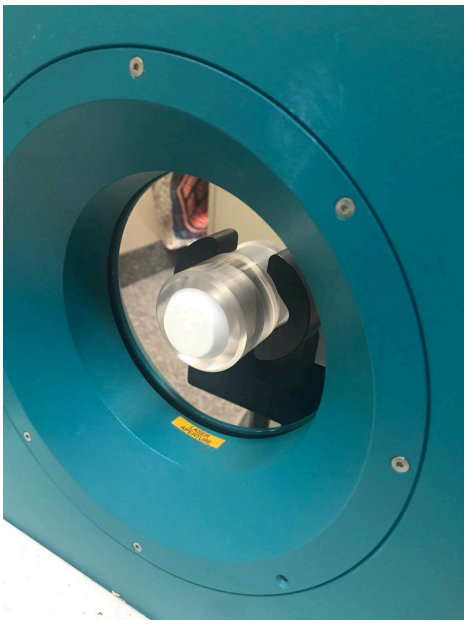

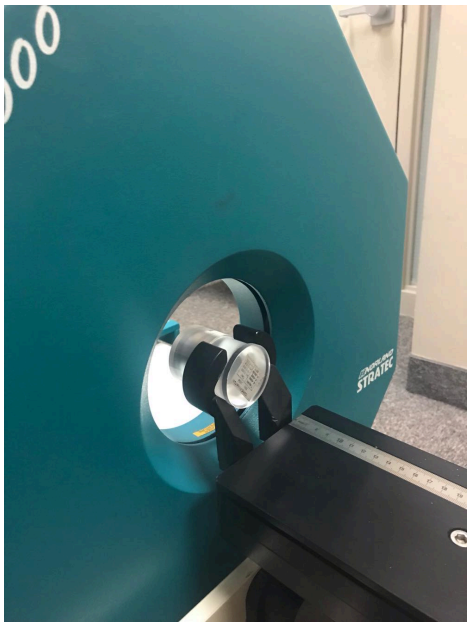

6. Select “QA-Scan” > “Select phantom”.

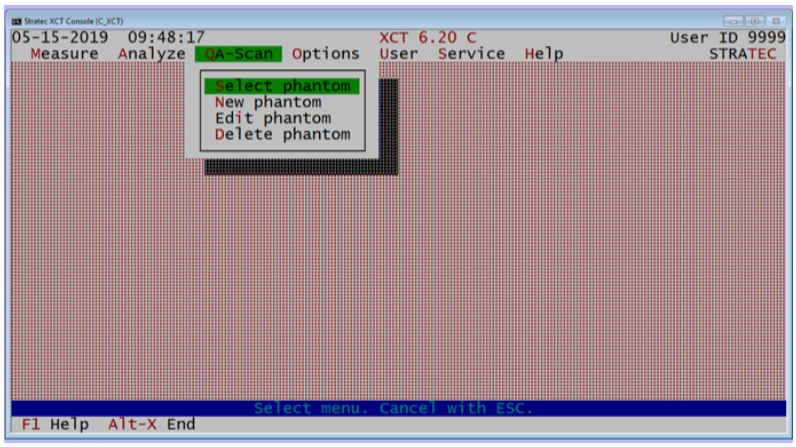

7. Then select “CONE PHANTOM”.

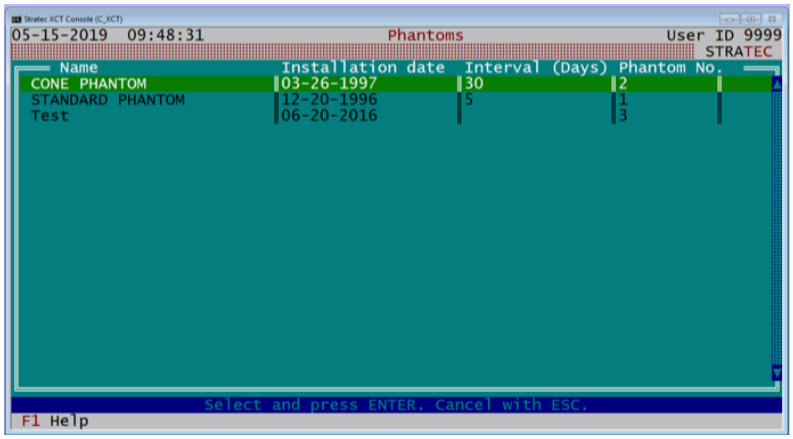

8. Press “F4” to save and proceed. Perform the rest of the Quality Assurance (QA) scan as stated in *pQCT Daily QC*, written by Dr. Andy Kin On Wong. A QA scan MUST be performed before beginning scans for each day. After completing a successful QA test, copy down the given values from the left-hand column into the yellow folder titled “pQCT quality assurance log”. The cone phantom can now be removed.

Marking the patient

1. Ask the participant to remove their shoes and socks from the most symptomatic/dominant foot and mark metatarsophalangeal joints (MTPJs) 2-5 with a washable marker. (Hint: Ask the participant to curl their toes and then detect the bumps, but in cases when this does not work, ask them to move their toes so that you can feel the end of the joint.)

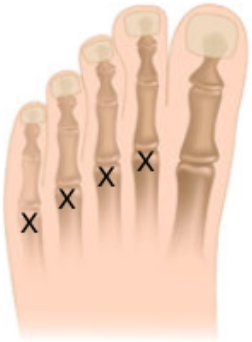

To begin scanning

1. Go to "Measure" > "New Patient".

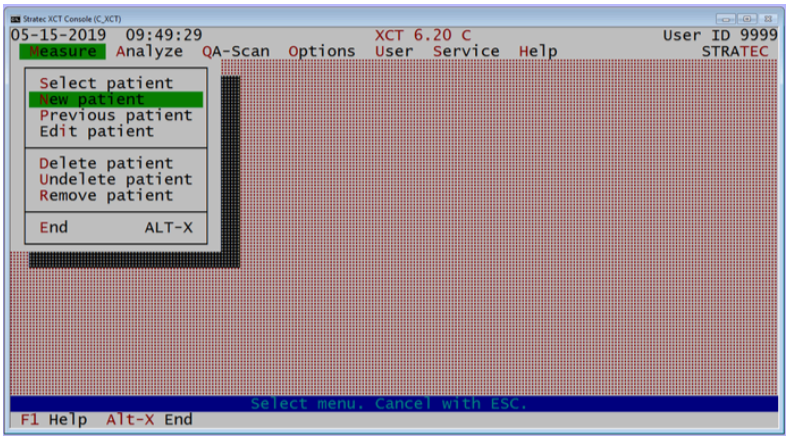

2. The "Patient data" screen will appear. Enter their name (first initial, last initial, FIS#; e.g. Jennifer Smith FIS 20 would be JS20), first name (set to "FIS19"), birth date (use only the month and year, day can be 01 for all participants), and gender (1=female, 2=male). Then, press "F4".

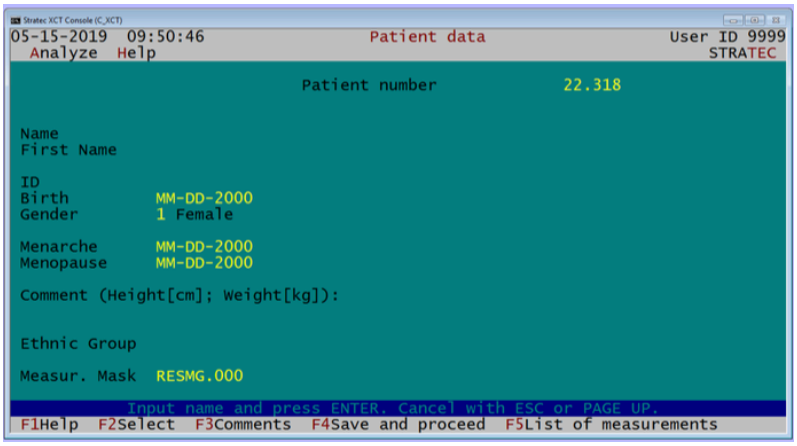

3. This will take you to the “Measurement” screen, where the protocol can be selected.

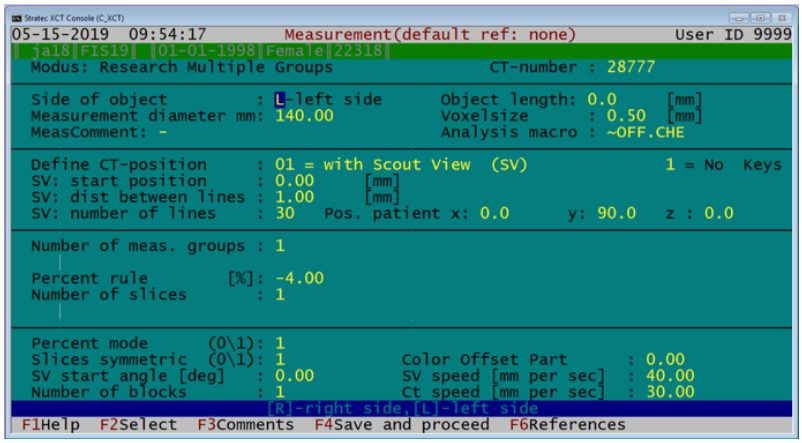

4. Click “F6”, then select “Measure without reference”.

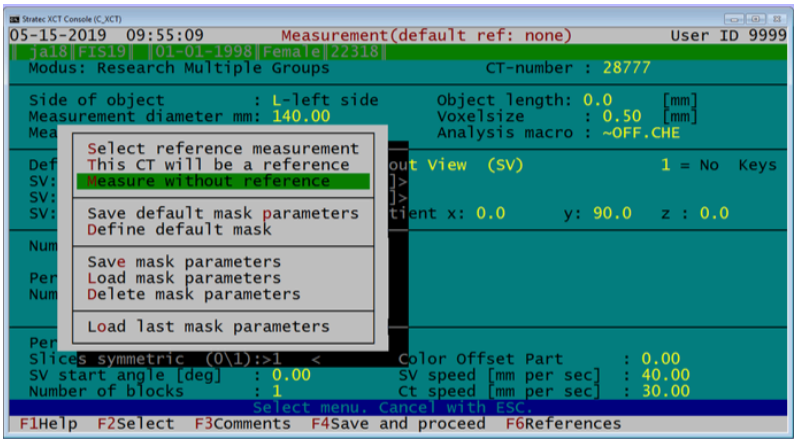

5. Click “F6” again, then “Load mask parameters”.

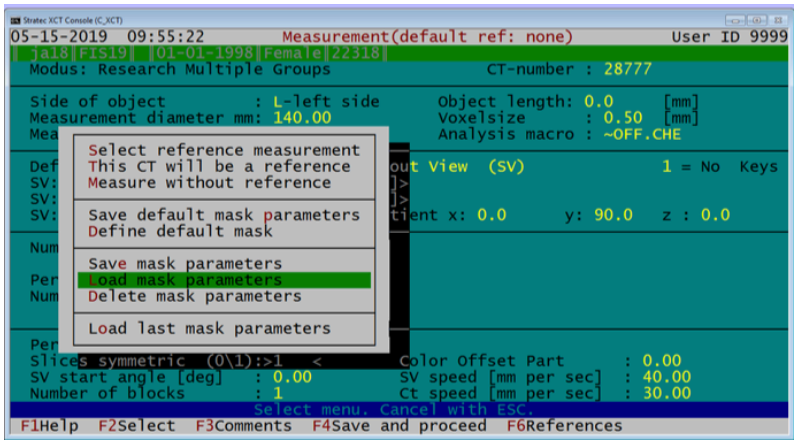

6. Select the protocol “MTP2-5 3.5-5”.

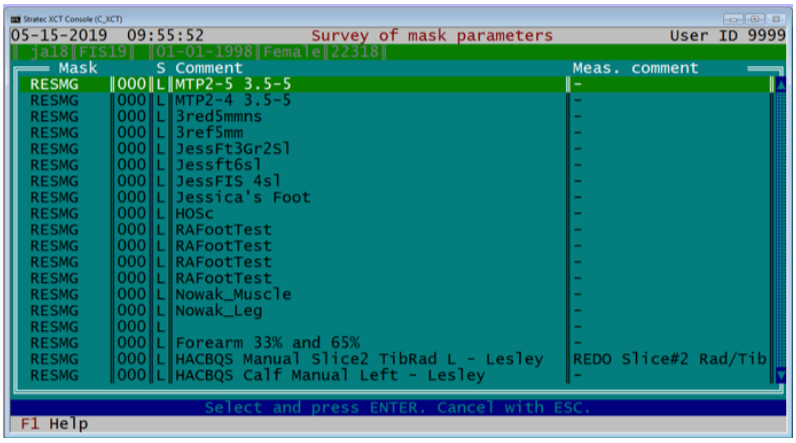

7. The following protocol will load on screen (shown below). The protocol is set for 8 scan slices, 2 per MTPJ. For each MTPJ, transaxial scans at 3.50 mm and 5.00 mm from the reference line will be taken.

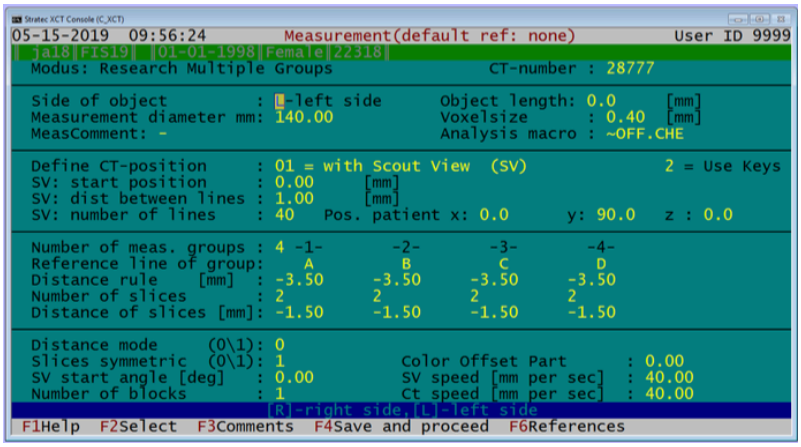

8. In the “MeasComment” row, type a comment on the foot you are scanning (right/left) and whether the scan is test/retest. Press “F4”

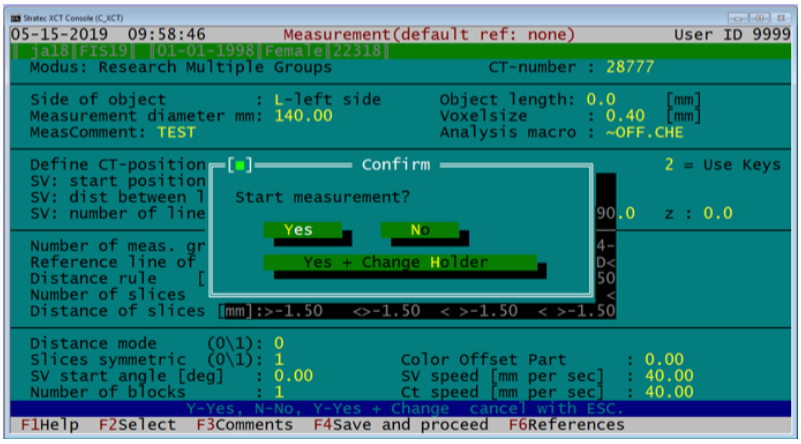

9. To start measurement, press “Y” on your keyboard. If the holder needs to be changed, press “H”. Then press “Enter”.
10. Below is an image of the modality without any additions (A). Prior to use, attach the custom foot plate to the plank (B). The plate has two Velcro straps that are used to secure the plate to the plank. Seat the patient on the black hydraulic pump chair and ask them to place their heel at the end of the holder (C). Place a stool under the foot that is not being scanned so that the patient is comfortable. Once the patient is comfortably seated, secure their forefoot with the Velcro strap.

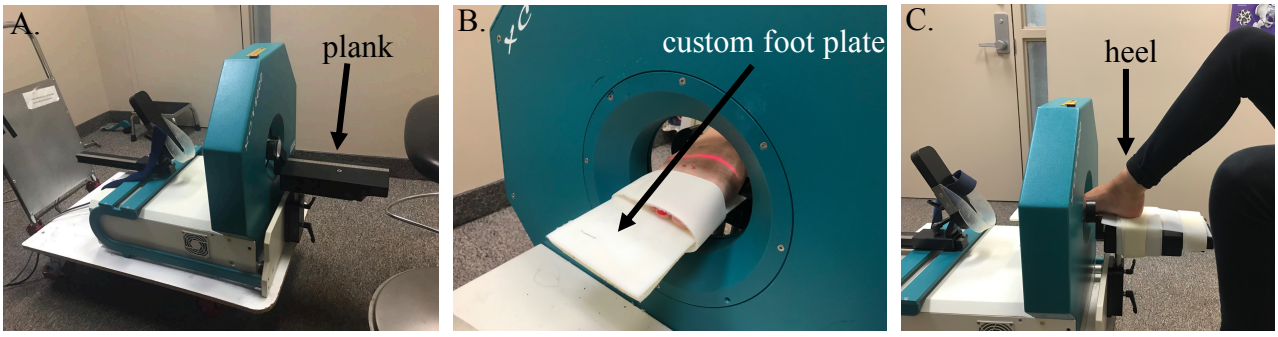

11. Next, a scout view scan needs to be performed in order for the scanner to determine where the foot is positioned in the gantry. Press the right “Shift” button on your keyboard to move the scanner away from the patient, and the left “Shift” button to move the scanner toward the patient (A).
    **Note you will have to move the red laser a certain distance away from the patient in order for the “Start SV” button to become functional (B).

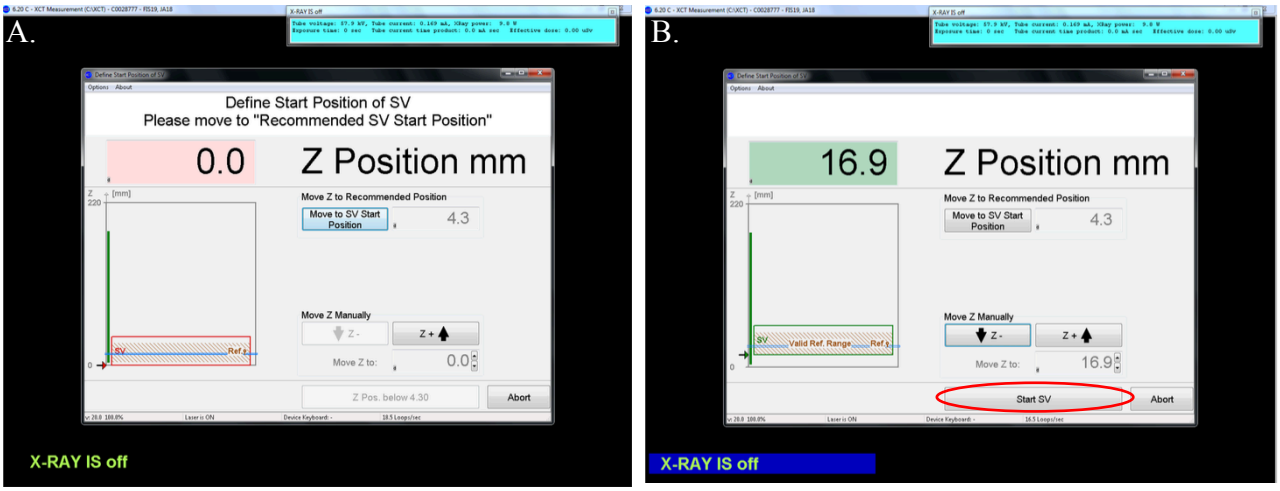

12. Once the red laser is placed at the 5th MTPJ, you are ready to begin the scout view scan. The protocol is set up so that the scanner will move away from the patient, i.e. the red line will move from the proximal foot to the distal foot (shown below). When you have let the patient know that they will have to stay still from now on, you can press the "Start SV" button.

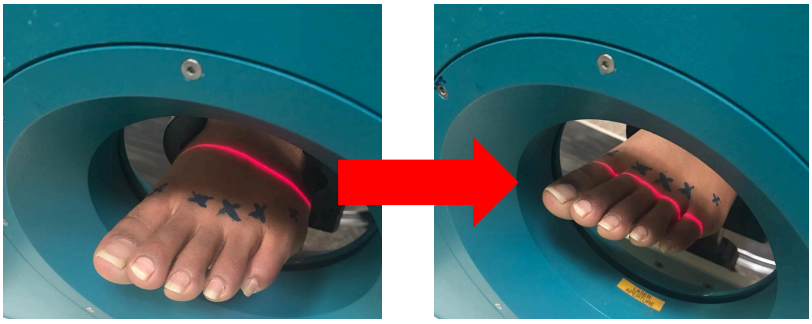

13. After the scout view scan is completed, click "Pos" and move the respective reference lines to the end of MT heads 2-5 (shown below). You can navigate between reference lines by pressing the "Tab" button on your keyboard.

Examples for reference line placement:

RA corresponds to MT head 2.

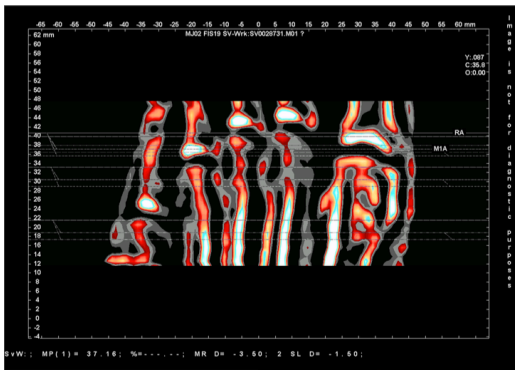

RC corresponds to MT head 4.

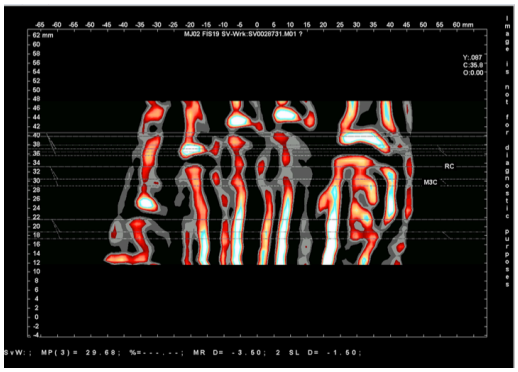

RB corresponds to MT head 3.

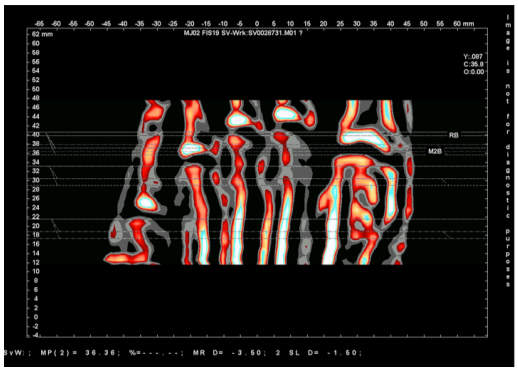

RD corresponds to MT head 5.

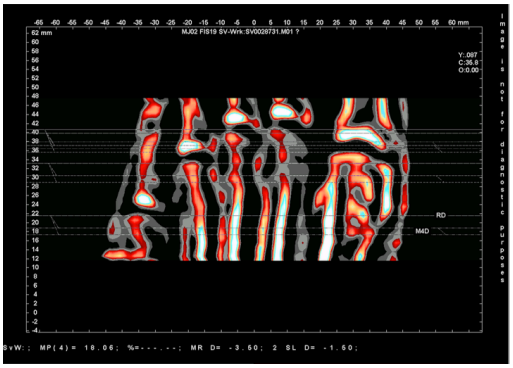

14. After setting the reference lines, press “Start CT”. The scan protocol will begin. The protocol takes ~9 minutes to complete.
15. When the scan is complete, a screen will appear with all 8 images (shown below). To navigate between slices, click “Page Up” and “Page Down” on your keyboard.

16. Remove the patient from the scanner.
17. To leave this screen, press “Esc”, then select “END”. You will return to the main menu.
18. To exit the program, go to “Measure” > press “E” (End) > End program?: press “Y” (Yes). Then press “Esc”.

Appendix A3. Standard Operating Procedure (SOP) for pQCT MTPJ analysis
Jessica Amin

1. Open Stratec XCT application, input username and password (9999, service, respectively)
2. Go to "Analyze" > "Select Patient" > in the "Name" section, type the respective patient/control ID, then click "Enter"
3. A list of scans will be presented, select the one with the corresponding first name – "FIS19". This will lead to the patient data screen:

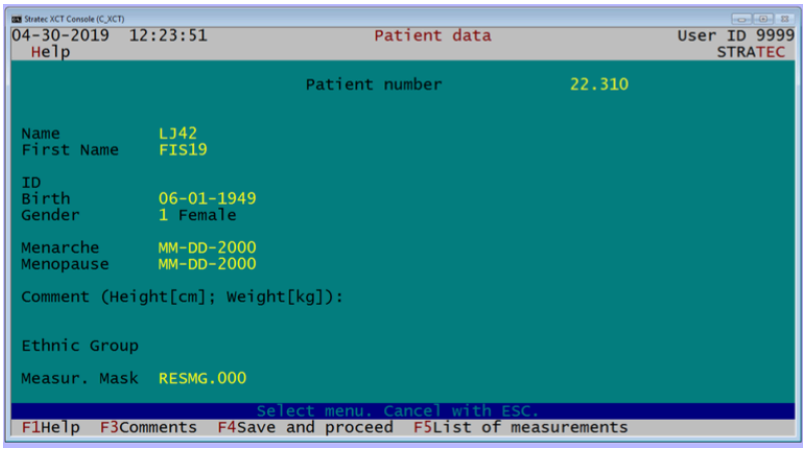

4. Press F5 to continue to the list of measurements:

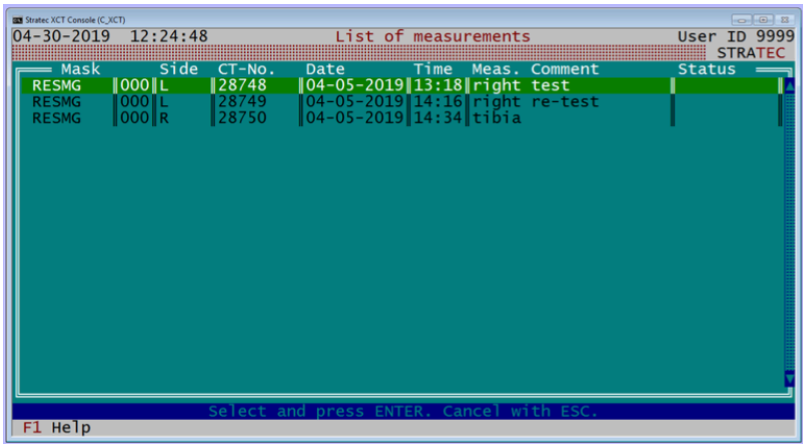

5. Select the test you wish to analyze, then press "Enter".

6. The next screen will give an overview of the slices that were scanned for the respective protocol:

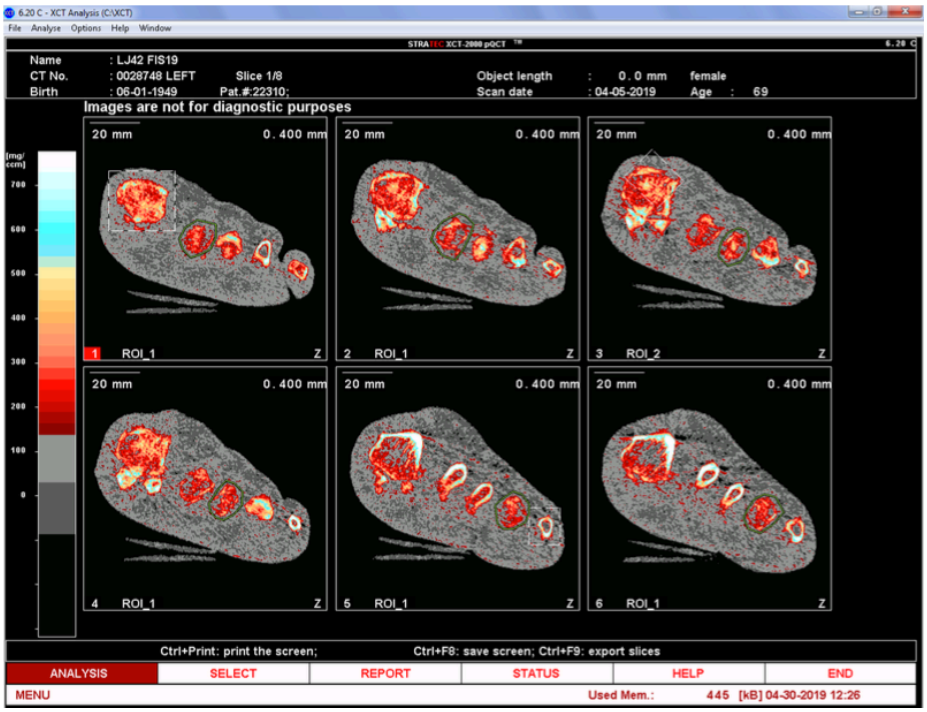

7. Select the first slice and begin analysis (click “Page Up” or “Page Down” to navigate between slices, the slice number is on the bottom left corner of each image)

Analyzing manually:

8. Go to “ROI”, then “CALCBD”.

9. Input a "Threshold" value, "Trab. area" %, "Contour mode", and "Peel mode" value:

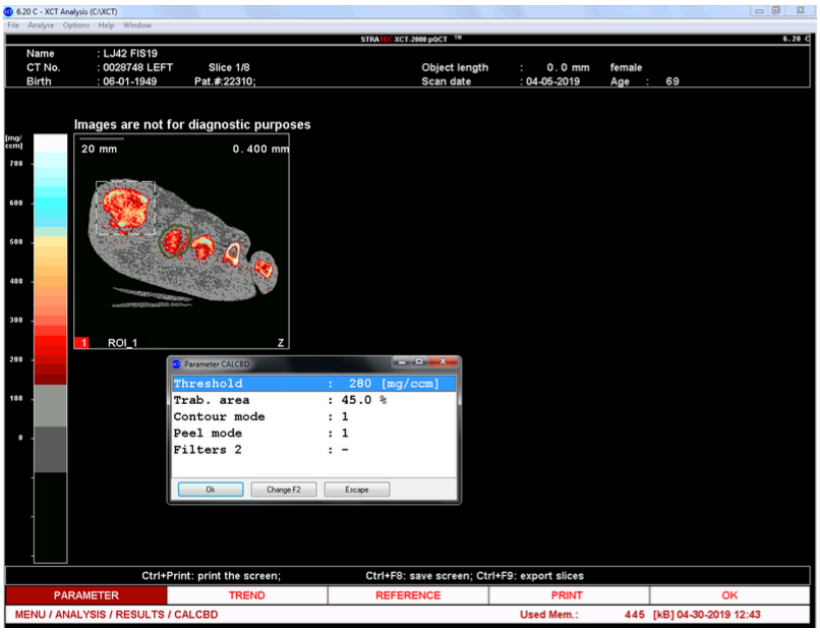

10. Press "OK", and the following screen will appear with all bone mineral density and area measurements:

Analyzing using a Loop (pre-determined analysis):

11. After selecting a slice image, click "Results", then select "ROI", then "NEW". This will take you to an enlarged screen with the image:

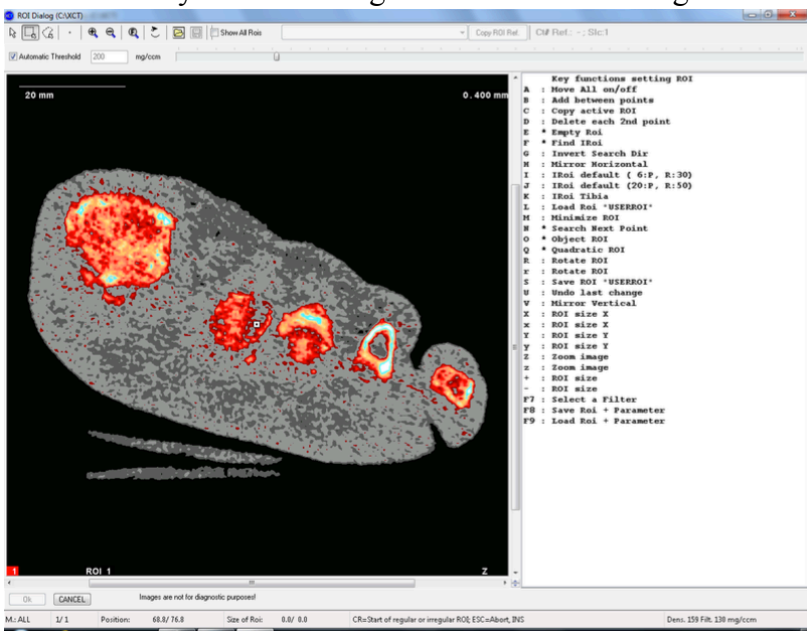

12. Click the "Set rectangular ROI" button for a rectangle shape (A), or the "Set irregular ROI" button for a custom ROI (B). The type of ROI varies based on each joint, thus, choose according to which would be best suited (case by case basis).

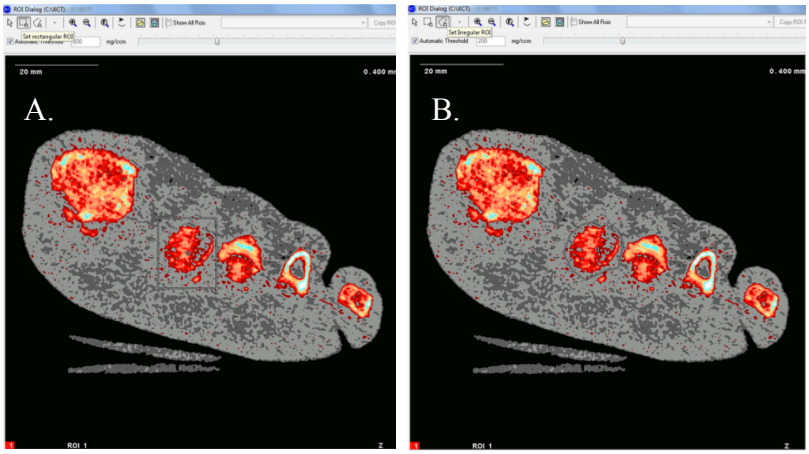

13. After selecting the ROI, press "OK".
14. Navigate to "Loop", then press "Enter", then "Select" > "Jessica_Loop", "Enter", then "start "Jessica_Loop"". Below is an example of 6 loops that will run with the selected ROI, with the pre-set values for each parameter:

	Analysis 1	Analysis 2	Analysis 3	Analysis 4	Analysis 5	Analysis 6
***ThBd mg/ccm**	180.0	200.0	180.0	200.0	220.0	220.0
ThBd2 mg/ccm	400.0	400.0	400.0	400.0	400.0	400.0
***Trab. Area %**	45.0	45.0	60.0	60.0	45.0	60.0
Contour mode	1	1	1	1	1	1
***Peel mode**	1	1	1	1	1	1
ThCort mg/ccm	710.0	710.0	710.0	710.0	710.0	710.0

*ThBd indicates the threshold of bone that will be considered in analysis, the higher the threshold, the lower the error

*Trab. area % indicates the amount that is left on the trabecular region after peeling the exterior. For instance, trab. area 60% indicates that 40% of the exterior is peeled off.

*Peel mode changes the proportion of cortical and trabecular bone

15. To edit the loop, go to "Edit" and adjust as needed.
16. Complete the loop analyses for all required scan slices.
17. To exit, press "OK", then "OK" again, then "OK" again, then "END". This will bring you back to the main screen.

To access the analyzed Loops:

1. Open the Windows C: drive.

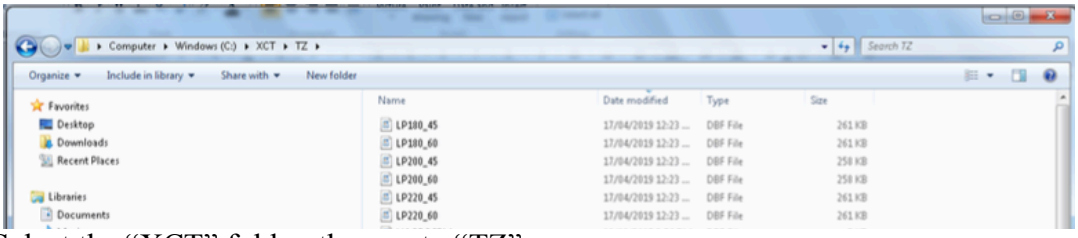

2. Select the "XCT" folder, then go to "TZ"
3. Select the .dbf files and copy to your USB key: e.g. LP180_45, LP180_60.
4. The measures from the .dbf files can then be copied and pasted to an Excel document and are ready for statistical analyses.

Various cases of pQCT images

Bad/Unclear Images

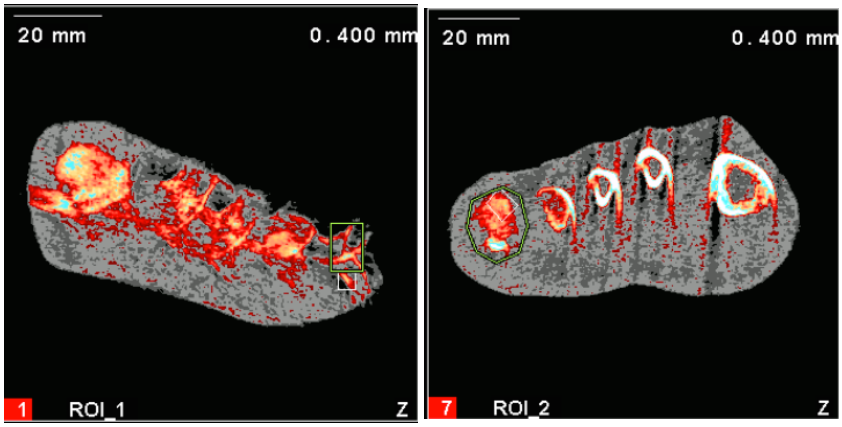

ROI drawing standardization

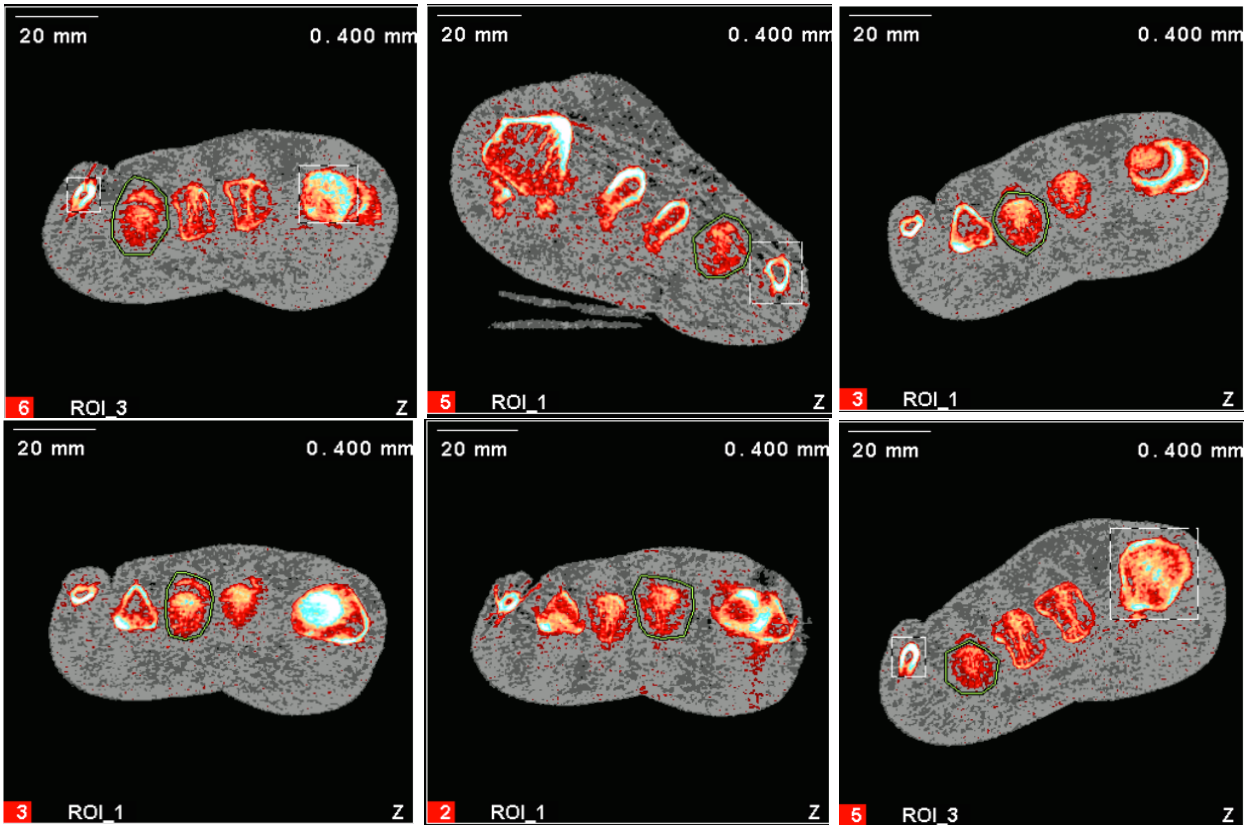

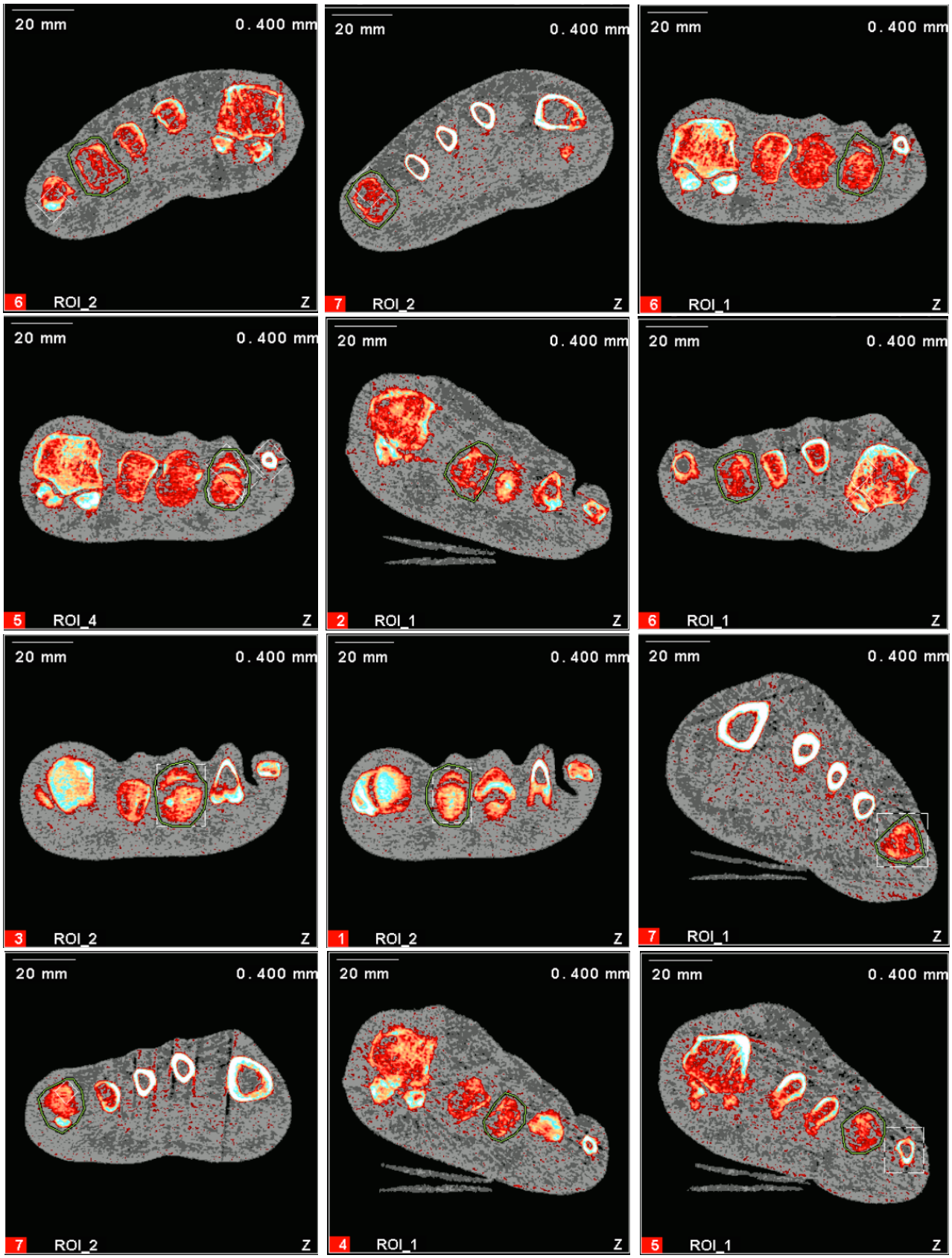
20 mm
0.400 mm
6 ROI_2 Z
20 mm
0.400 mm
7 ROI_2 Z
20 mm
0.400 mm
6 ROI_1 Z
20 mm
0.400 mm
5 ROI_4 Z
20 mm
0.400 mm
2 ROI_1 Z
20 mm
0.400 mm
6 ROI_1 Z
20 mm
0.400 mm
3 ROI_2 Z
20 mm
0.400 mm
1 ROI_2 Z
20 mm
0.400 mm
7 ROI_1 Z
20 mm
0.400 mm
7 ROI_2 Z
20 mm
0.400 mm
4 ROI_1 Z
20 mm
0.400 mm
5 ROI_1 Z

Appendix A4. Correlation coefficients between average vBMD and questionnaire parameters

Questionnaire parameters	Total density			Cortical subcortical density		
	Correlation Coefficient		Significance	Correlation Coefficient		Significance
	Pearson	Spearman		Pearson	Spearman	
LFIS total		-0.061	0.772		0.013	0.952
LFIS IS	0.057		0.786	0.114		0.587
LFIS PA		-0.139	0.508		-0.047	0.824
HAQ		-0.068	0.745		-0.012	0.953
PAIN		0.001	0.997		0.113	0.592
FT		0.177	0.397		0.194	0.353
GL		0.032	0.880		0.106	0.613
Morning stiffness		0.183	0.382		0.159	0.448